STRUCTURAL DNA ORIGAMI: ENGINEERING SUPERMOLECULAR SELF-ASSEMBLY FOR NANODEVICE FABRICATION

by

Craig Marshal Onodera

A thesis

submitted in partial fulfillment

of the requirements for the degree of

Master of Science in Materials Science and Engineering

Boise State University

May 2012

BOISE STATE UNIVERSITY GRADUATE COLLEGE

DEFENSE COMMITTEE AND FINAL READING APPROVALS

of the thesis submitted by

Craig Marshal Onodera

Thesis Title: Structural DNA Origami: Engineering Supermolecular Self-Assembly for Nanodevice Fabrication

Date of Final Oral Examination: 09 March 2012

The following individuals read and discussed the thesis submitted by student Craig Marshal Onodera, and they evaluated his presentation and response to questions during the final oral examination. They found that the student passed the final oral examination.

William L. Hughes, Ph.D.	Chair, Supervisory Committee
William B. Knowlton, Ph.D.	Member, Supervisory Committee
Bernard Yurke, Ph.D.	Member, Supervisory Committee

The final reading approval of the thesis was granted by William L. Hughes, Ph.D., Chair of the Supervisory Committee. The thesis was approved for the Graduate College by John R. Pelton, Ph.D., Dean of the Graduate College.

ACKNOWLEDGEMENTS

It has been over 35 years since an innocent ‘bring your child to work’ event at a Phoenix wafer fab led to what is turning out to be a lifetime of hard work trying to understand the physics and chemistry behind all of life’s mysteries. For this, I credit—and some days blame—my father, George, for passively leading me down this path by his daily demonstrations of knowledge of just about everything. I also would like to thank my mother, Rosalind, for providing the needed balance and a safe home in which to grow and develop.

Since my undergraduate years, I had considered an advanced engineering degree as impossibility. My undergraduate career was unremarkable and I was marked as an average student for chemical engineering. Ten years after merely surviving my undergraduate experience I faced a choice: move across country to stay employed or go back to school full time to get an advanced degree. Reluctantly, I chose the latter and ended up at Boise State University not knowing a soul. My first graduate level class at this school was Biomaterials. I worked hard and did well. This led the instructor, Dr. William Hughes to recruit me for his research group. For this I am grateful and would like to thank Dr. Hughes for being my adviser and allowing me the opportunity to work at a level that would not have been possible looking at my transcripts alone.

My acceptance to the research group was not immediate. However, after interviewing with the students already working in what was then called The Knowlton

Research Group, I quickly accepted the offer. The students were among the best and brightest I have known and I benefited greatly from interacting with them. For this, I would like to thank the group members past and present. I would also like to thank Dr. Bill Knowlton for allowing me to join his research group and for providing the environment for the aforementioned students to develop.

I would like to thank Dr. Bernard Yurke, Dr. Elton Graugnard and Dr. Jeunghoon Lee for their help these last three years. Dr. Yurke and Dr. Lee provided much needed expertise and were always inspiring due to their positive attitudes. Dr. Graugnard was there from the beginning trying to learn about the unfamiliar field of DNA nanotechnology with me. I think after this many years we may have finally scratched the surface.

A special thanks goes to Hieu Bui, whose footsteps I followed and Sadao Takabayashi who will follow me. Hieu has been a pleasure to work with and learn from and Sadao has helped tremendously in the final months of my research, allowing me to focus on writing this thesis.

ABSTRACT

Two challenges encountered in nanotechnology are the ability to create nanostructures inexpensively and the ability to arrange nanomaterials with a precision commensurate with their size. In nature, nanostructures are created using a bottom-up approach, whereby molecules hierarchically self-assemble into larger systems. Similarly, structural DNA nanotechnology harnesses the programmability, specificity, and structural integrity of DNA to engineer synthetic, self-assembled materials. For example, during scaffolded DNA origami, a long single stranded DNA polymer is artificially folded into nanostructures using short oligonucleotides. Once folded, two- and three-dimensional nanostructures may be decorated with proteins, metallic nanoparticles, and semiconductor quantum dots. Using gold nanoparticles and semiconductor quantum dots, scaffolded DNA origami was explored for future nanoelectronic and nanophotonic applications. Nanostructure design, synthesis, and characterization focused on increasing the site-specificity and attachment efficiency between nanoparticle arrays and the DNA origami scaffold. Results have established improved design rules to fabricate future devices.

TABLE OF CONTENTS

LIST OF TABLES

LIST OF FIGURES

LIST OF ABBREVIATIONS

4HB…….....…Four-Helix Bundle Chiral Nanoparticle Array

A……...Adenine

AFM……..Atomic force microscopy

AgNP……...Silver nanoparticle

AuNP…….Gold nanoparticle

A AuNP……....A gold nanoparticle (AuNP with strand A oligonucleotide)

B AuNP……....B gold nanoparticle (AuNP with strand B oligonucleotide)

C AuNP……....C gold nanoparticle (AuNP with strand C oligonucleotide)

AuNPAx……Gold nanoparticle array x nanoparticle binding sites

AuNPA29……..…Gold nanoparticle array 29 nanoparticle binding sites

AuNPA15……..…Gold nanoparticle array 15 nanoparticle binding sites

AuNPA9……..Gold nanoparticle array 9 nanoparticle binding sites

AuNPA5……..Gold nanoparticle array 5 nanoparticle binding sites

AuNPAxDSE……AuNP array x nanoparticle binding sites, dual sticky ends

AuNPA29DSE……AuNP array 29 nanoparticle binding sites, dual sticky ends

AuNPA15DSE……AuNP array 15 nanoparticle binding sites, dual sticky ends

AuNPA29ABC…….AuNP array 29 nanoparticle binding sites, dual sticky ends, for A, B, and C AuNPs

C…….……..……Cytosine

CD……..……..……Circular dichrosim

cSA…….……..……..…Complementary strand to strand A

cSB……..Complementary strand to strand B

cSC……..Complementary strand to strand C

DNA…….Deoxyribonucleic Acid

G…….....…Guanine

HNPA29……Heterogeneous nanoparticle array 29 nanoparticle binding sites

MFE……...Mean free energy

mer……...Monomer, repeating unit in polymer

p……...*p* value, probability of attachment

T……...Thymine

QD…….Quantum dot

QDAx……..Quantum dot array x nanoparticle binding sites

QDA29……..…Quantum dot array 29 nanoparticle binding sites

QDA15……..…Quantum dot array 15 nanoparticle binding sites

QDA9……..Quantum dot array 9 nanoparticle binding sites

QDA5……..Quantum dot array 5 nanoparticle binding sites

SA…….Strand A, oligonucleotide for A AuNPs

SB……..Strand B, oligonucleotide for B AuNPs

SC……..…Strand C, oligonucleotide for C AuNPs

CHAPTER 1: INTRODUCTION

Two challenges are often encountered in nanotechnology: the ability to make structures at the nanoscale inexpensively and the ability to arrange nanomaterials with a precision commensurate with their dimensions. Construction of synthetic nanoscale structures typically uses a top-down approach where excess material is deposited and then selectively removed to form nanostructures. This approach necessitates multistep processes that waste raw material and require extensive resources to control [1]. In comparison, a bottom-up approach is commonly used in nature where individual components self-assemble to form larger systems.

DNA (deoxyribose nucleic acid) is a biological material that naturally self-assembles into hierarchically organized structures in living organisms. A human cell contains approximately 2 meters of double stranded DNA (dsDNA). This long structure, 2 nm in diameter, is condensed into micrometer size chromosomes by hierarchal folding controlled by proteins called histones, termed H1, H2A, H2B, H3, and H4. Pairs of H2A, H2B, H3, and H4 form a histone octamer core, about which sections of the double helix wrap approximately 1.7 times in a left-hand spiral consuming approximately 147 base pairs (paired nucleotides). This protein and DNA structure is called a nucleosome and is approximately 11 nm in diameter. Nucleosomes are separated from each other by linker DNA of up to 80 base pairs to form a structure called chromatin. The addition of the H1 histone further compacts the structure into a 30 nm chromatin fiber by controlled folding

of the linker section of DNA. The 30 nm fiber is directed by non-histone proteins to form loops approximately 300 nm in diameter, which are then further compacted into chromosomes [2].

Chromosomes are biologically self-assembled nanomaterials. The resolution, information density, structural integrity, and programmability of the DNA used to organize chromosomes are applicable to engineered self-assembly of device scaffolds. The use of DNA was proposed to construct a bio-memory chip decades ago, but the electrical properties of DNA are not compatible with electrical circuitry [3, 4]. Engineered self-assembly thus necessitates electrically active materials for device applications. Many functional nanoparticles are available with desirable electrical, optical, and magnetic properties but there is lack of a means to self-assemble in a precise manner to create functional devices. The growing field of DNA nanotechnology uses the predictability and extraordinary selectivity of DNA to create synthetic structures from the bottom up and is showing promise with its ability to arrange nanoparticles with great precision [5].

Structural DNA nanotechnology was catalyzed by Ned Seeman beginning in the 1980's with the idea to create a three-dimensional DNA scaffold to arrange proteins into crystals for x-ray analysis [6]. The immobilization of the Holliday junction [7] and the antiparallel DNA double crossover [8] accelerated progress in the field. In 2009, members of Ned Seeman's laboratory used the technology he inspired to create a three-dimensional DNA crystal capable of x-ray analysis and large enough to be imaged via optical microscopy [9].

Compositional DNA nanotechnology uses the properties of DNA as ‘smart-glue’ to direct assembly of materials into three-dimensional arrays without control over the final form of the structure [10]. Gold nanoparticles (AuNPs) were the first nanoparticles to be organized by DNA into close packed [11, 12] structures. Later programmed DNA oligonucleotides were able to arrange AuNPs with greater control over the final form to form a crystal [13] and a hexagon [14]. Recently semiconductor quantum dots (QDs) were arranged into designed arrays by carefully controlled complementary DNA ‘sticky ends’—single stranded DNA domains designed to find a targeted complement [15]. These techniques were important in refining the ability to functionalize inorganic nanoparticles with organic DNA.

Discrete motifs such as octahedra [16, 17], tetrahedra [18, 19], prisms [20-22], and a six-helix bundle [23] have been created, demonstrating the ability to form arbitrary shapes not found in nature in a programmed manner. In 1998, DNA nanostructures called ‘tiles’ were designed by Erik Winfree to self-assemble with other tiles by use of complementary sticky ends in order to form a two-dimensional crystal [24]. The tiles were based on antiparallel double-crossover molecules with 36 or 47 nucleotides each and dimensions of approximately 2 nm x 2 nm x 13 nm and 2 nm x 2 nm x 16 nm, respectively. The sticky ends were programed such that the tiles formed either a repeating AB or ABCD pattern. The method came to be known as tiling and has been used for algorithmic self-assembly of two-dimensional sheets [5, 25-45], three-dimensional crystals [9], and nanotubes [46-52]. Tiled arrays have also been used to arrange AuNPs [5, 33-37], QDs [45], proteins [38-43], and peptides [44] into arrays. Tiling demonstrated that nucleotides could be assembled into nanoscale building blocks,

which then could be programmed to assemble into even larger structures. These structures could then be used to arrange a variety of nanoparticles with great precision. Drawbacks to tiling include the small size of the tiles limiting space available for functionalization with nanoparticles and the lack of control over the size of the macromolecular array. In 2005, Liu *et al.* addressed the control issue by programming tiles to arrange in a self-terminating motif approximately 110 nm x 110 nm [31]. However, the cross-like pattern of the tiles left large cavities in the final structure that could otherwise have been utilized for nanoparticle arrangement.

A milestone for DNA nanotechnology was the introduction of a long single stranded DNA (ssDNA) polymer called a scaffold strand to guide the assembly of other DNA molecules. The first use of a scaffold strand by Hao Yan occurred in 2003 to make a nanobarcode [53]. Here synthetic 327-mer and 267-mer single ssDNA scaffolds were used to direct the arrangement of rectangular tiles aperiodically. The next year a synthetic 1669 nucleotide scaffold was used to create an octahedron by directed folding using five, 40-mer oligonucleotides [54]. An event taking the idea of a scaffold strand dramatically further came in 2006 with the introduction of scaffolded DNA origami by Paul Rothemund [55]. This method used the naturally occurring, ssDNA circular plasmid from the bacteriophage m13mp18 as a scaffold. Hundreds of short, programmed, synthetic DNA oligonucleotides called ‘staple strands’ were then used to fold the scaffold into two-dimensional shapes such as triangles, rectangles, and smiley faces. Other researchers later made a dolphin [56] and a map of China [57] using Rothemund’s method, demonstrating that the technique was robust and adaptable to new systems and structures. The m13mp18 plasmid contains 7249 nucleotides making significantly larger

structures than anything created in the past possible. Moreover, harvesting naturally occurring DNA is significantly less expensive than synthesizing long chains, thus reducing the cost of scaffold strands and the known but random sequence allows precise placement of each of the staple strands negating the need to closely control stoichiometry [55].

The quantum leap in addressable surface area provided by scaffolded DNA origami nanostructures made them ideal platforms for use in other studies. Geometric shapes were used by other researchers as seeds to organize smaller tiles in a programmed manner [58, 59]. Two-dimensional arrays were organized by controlled hybridization of uniform DNA origami tiles [60-62] and asymmetric origami tiles were fit together like puzzle pieces [63-66]. This demonstrated that tiling could be scaled up while maintaining the resolution inherent in DNA and that shape could be used to direct self-assembly rather than relying solely on sticky ends.

Three-dimensional structures such as a tetrahedron [67], a prism [68], and boxes [69, 70] were created with single m13mp18 scaffold strands by forming the two-dimensional faces before folding them into the final shapes with staple strands. One of the boxes was designed with a lid that could open or close using ssDNA 'keys' [69]. Devices such as these may be used as cages to encapsulate nanocargos such as enzymes, ribosomes [69], and drugs.

Semi-solid three-dimensional structures were created with double helices filling the interior to form a hexagonal cross-section similar to a honeycomb. Shapes as simple as rectangles to very intricate structures such as a railed bridge and interpenetrating crosses were created with this method [71, 72]. A square cross-section was later

developed [73]. This introduced a new method for forming three-dimensional structures that were rigid and robust. The computer-aided design program caDNAno was developed along with the new methodology, enabling researchers to design complex designs without *de novo* programming of their own [71].

These nanostructures, it was discovered, could be twisted into various shapes by programmed insertion and deletion of base pairs to create spirals, horseshoe shapes with a radius of curvature as little as 6 nm, and even geared wheels [74]. A sphere and a nanoflask were later created in what are possibly the most intricate structures to date [75]. Nanostructures such as these introduced a new method of shaping more structurally rigid DNA origami and demonstrated the ability to manipulate the double helix to extents never before accomplished.

Two-dimensional DNA origami has been used to arrange AuNPs [76-78], proteins [79-83], virus capsids [84], carbon nanotubes [85], and dendrimers [86]. Triangular origami structures developed by Rothemund were adopted as platforms for AuNP arrays and silver nanoparticle (AgNP) arrays [76, 86]. The triangular AuNP array was the first to deliberately use unique DNA sequencing to direct nanoparticles of differing size to specific sites. The AgNP array became the first heterogeneous nanoparticle structure created on DNA origami when both an AuNP and an AgNP were deposited on the same DNA origami structure [86].

Douglas *et al.* [87] used the concept of the six-helix bundle created by Mathieu *et al*. [23] and applied the scaffolded DNA origami method using the m13mp18 scaffold to create a nanotube that was over 400 nm long. By dimerization, Douglas *et al.* was able to double the length. Unlike most of the origami structures, which were created to

demonstrate the capability of programming and shaping of DNA molecules, the six-helix nanotube was designed to perform a task. It was successfully used to align membrane proteins to aid nuclear magnetic resonance spectroscopy [87]. Stearns *et al.* used the nanotube developed by Douglas *et al.* and included ssDNA designed to hybridize with peptide modified complementary strands [88]. The peptides served as nucleation sites for gold nanoparticle growth. Bui *et al.* incorporated biotin molecules into a modified version of the Douglas *et al.* six-helix DNA origami nanotube then attached streptavidin conjugated QDs in a controlled periodic fashion [89]. These studies indicate that the size, precision, and programmability of scaffolded DNA origami nanostructures may ultimately allow select nanoparticles to be arranged into a functional device. Three-dimensional origami devices may allow increased device complexity by allowing the nanoparticles to be arranged on multiple planes.

Successful nanophotonic and nanoelectronic devices will require precise and site-specific arrangement of optically and electrically active nanoparticles while maintaining a robust process and low cost. Three-dimensional DNA origami is a promising platform that can be used as a nanobreadboard for the arrangement of nanoparticles to create such devices. Here, progress is presented towards the creation of scaffolded DNA origami nanodevices.

In this study, the primary DNA origami nanostructure used was the six-helix nanotube developed by Bui *et al.* [89]. This structure was modified to arrange QDs and AuNPs into precise arrays. Chapter 2 provides a background on DNA and DNA origami and explains in detail the design and synthesis of this nanotube. Like the nanotubes created by Douglas *et al.* [87], there was the possibility that the six-helix nanotubes

would be too short for some devices, thus methods of dimerization were explored. Chapter 3 discusses these methods and the experimental results. Chapter 4 details functionalization of the six-helix DNA origami nanotubes with semiconductor QDs and AuNPs. In Chapter 5, the results of the design and synthesis of two purpose built nanophotonic devices, including a completely new DNA origami nanostructure, and a theoretical nanoelectric device are discussed.

CHAPTER 2: DNA ORIGAMI

2.1: DNA Structure

DNA stands for deoxyribonucleic acid. The building blocks of DNA are called nucleotides. Each nucleotide is composed of a deoxyribose sugar, a phosphate subgroup, and a base. The nucleotide is determined by which one of four bases it contains: adenine, thymine, guanine, or cytosine. These are written short hand as A, T, G, and C, respectively. The bases can be either polycyclic aromatic purines, A and G, or monocyclic aromatic pyrimidines, T and C. Figure 2.1 illustrates the components of the nucleotide [90].

The five carbon sugar β-D-2-deoxyribose is the central molecule of the nucleotide. The carbon atoms of the sugar are numbered from 1' to 5', whereas the atoms of the aromatic base rings are numbered without the prime (') designator, as shown in Figure 2.1. A nucleotide is formed when a base bonds to the 1' carbon of the sugar via either the number 9 nitrogen (purines) or the number 1 nitrogen (pyrimidines) and a phosphate bonds to the 5' carbon of the sugar. Nucleotides polymerize by joining the 3' carbon of one sugar to the 5' carbon of an adjacent nucleotide sugar through the phosphate side group. This bond is called a 3'-5' phosphodiester bond and creates a polar (directional) polymer with a 3' hydroxyl end and a 5' phosphate end as shown in Figure 2.2. Single stranded DNA is chemically polar with a net negative charge due to the oxygen molecules on the phosphate group [90].

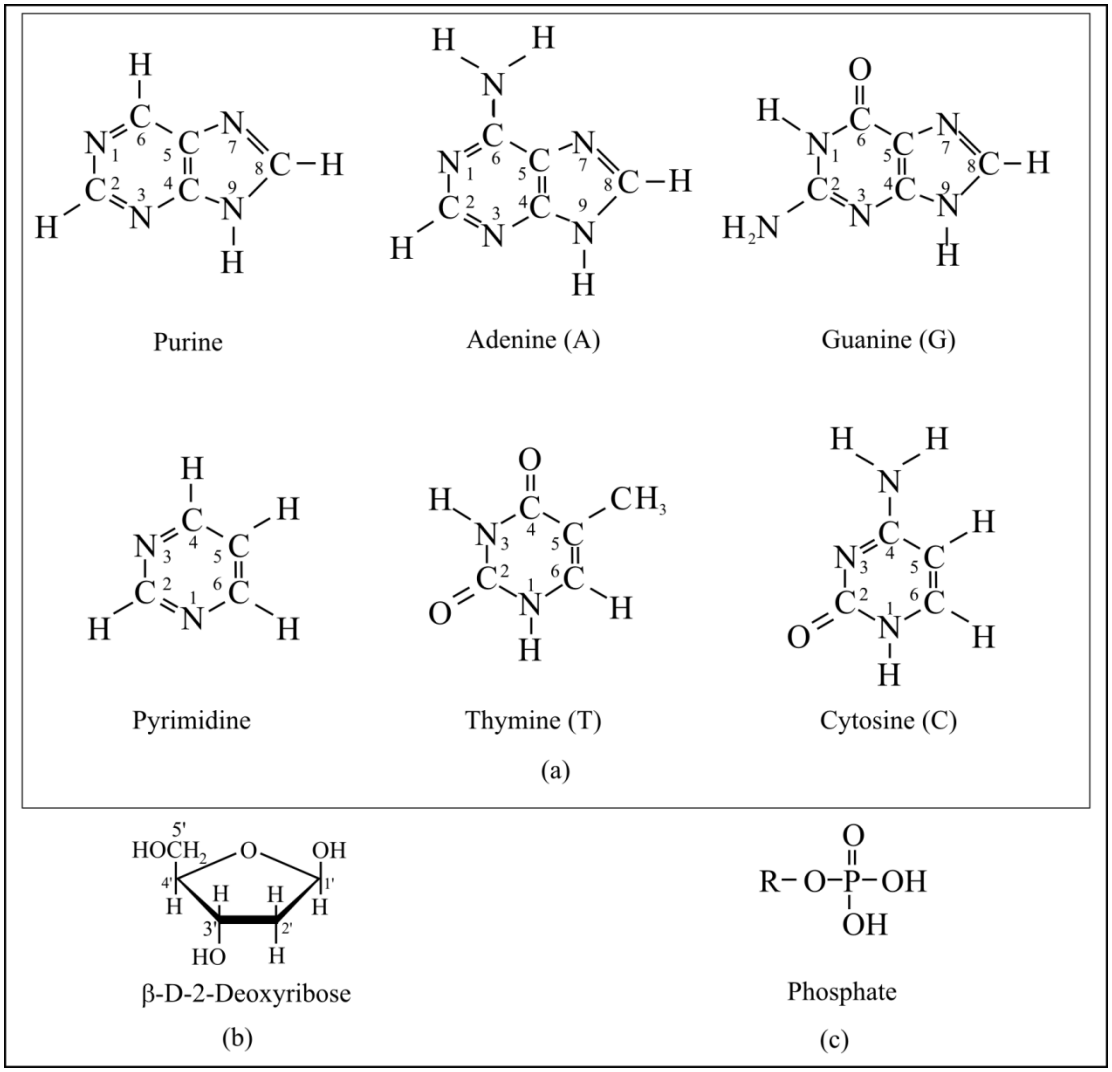

Figure 2.1: DNA nucleotides are composed of a (a) nitrogenous base, (b) a deoxyribose sugar, and (c) a phosphate group. There are four bases: adenine (A), guanine (G), thymine (T), and cytosine (C) in DNA. Bases are classified as either polycyclic aromatic purines (A and G) or monocyclic aromatic pyrimidines (T and C). The complementarity of DNA is between a purine and a pyrimidine; A bonds with T and G bonds with C. Note that the sugar carbon atoms are numbered with a prime (') designator whereas the base ring atoms are numbered without the designation (a). A nucleotide is formed when a base bonds to the 1' carbon via either the number 9 nitrogen (purines) or the number 1 nitrogen (pyrimidines), and the phosphate bonds to the 5' carbon of the sugar. Adopted from ref. [90].

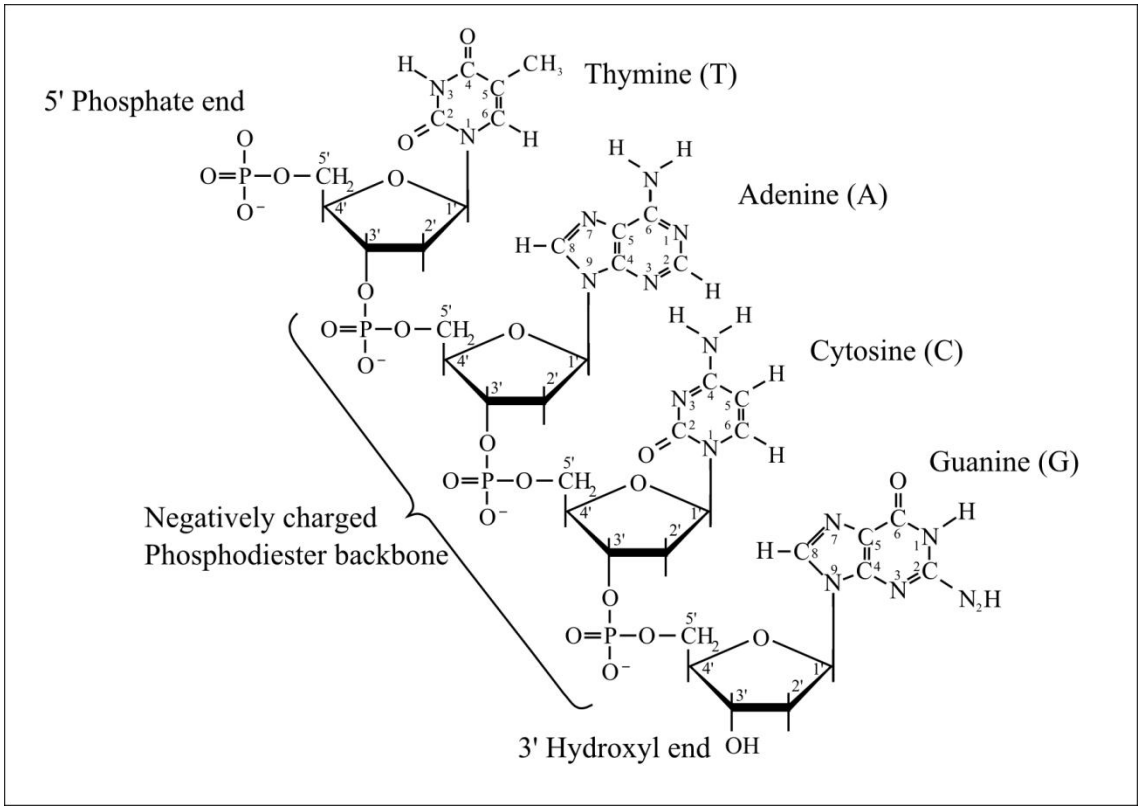

Figure 2.2: Nucleotides are connected into a single stranded DNA polymer by bonding of the 3' carbon of one nucleotide to the 5' carbon of an adjacent nucleotide through the phosphate. The resulting bond is called a 3'-5' phosphodiester bond. The DNA strand is polar (directional), designated by which functional group is terminal. In this image, upper left is the 5', phosphate end, whereas the 3', hydroxyl end is at the bottom. ssDNA is written by convention 5' to 3', thus the base sequence for this oligonucleotide is written TACG. The complimentary strand is written CGTA, noting that hybridization occurs in an antiparallel orientation. DNA is hydrophilic (chemically polar) due to the negative charge of the phosphate oxygen molecules in solution. Image not to scale. Adopted from ref. [90].

The sequence of the ssDNA polymer strand is the primary structure and can be any combination of nucleotides and in any order. Thus, if there are *N* nucleotide monomers, there are 4^N possible combinations for the primary structure. By convention, the shorthand letter abbreviation of the nucleotide base is used and written from 5' to 3'. For example, the oligonucleotide illustrated in Figure 2.2 is written as TACG.

The base pairs (A-T and G-C) will secondary bond with one another when aligned in an antiparallel direction. These bases are said to be complementary and the action of secondary bonding is called hybridization. The secondary structure formed via hybridization is the DNA double helix. Nucleation is the rate-limiting step of hybridization and begins when complementary strands first make intimate contact [90]. The complementary strand to the oligonucleotide in Figure 2.2 is CGTA.

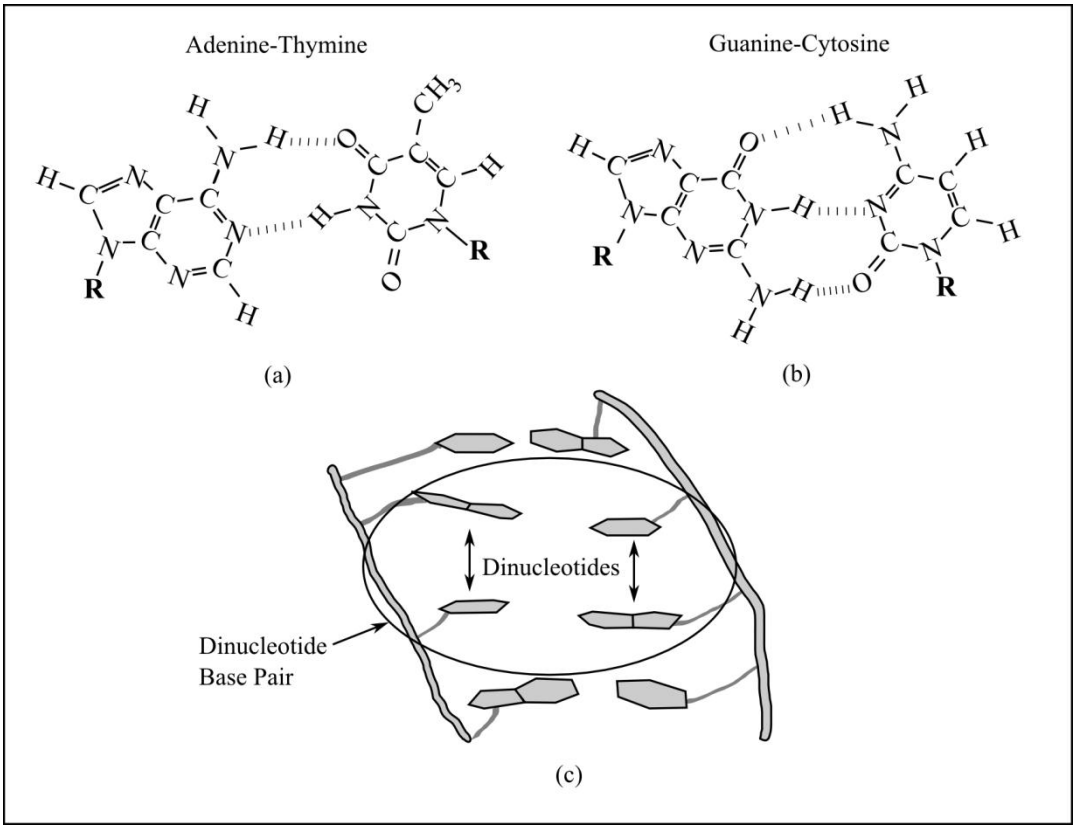

Figure 2.3: The energy for hybridization comes from hydrogen bonding, (a)-(b), and base stacking (c). H-bond energies in DNA are in the 2-3 kcal/mol range and are specific between base pair A and T, which form 2 bonds (a) and base pair G and C, which form 3 bonds (b). The planar, aromatic nature of the bases allows non-specific base stacking. Bond energy is derived from van der Waals forces, π–π interaction, and hydrophobic interaction and is measured for dinucleotide base pairs. Base stacking bond energies are more sequence dependent and often exceed those of hydrogen bonds. Adopted from ref. [90, 91]. Stacking image adopted from http://www.atdbio.com/content/1/Ultraviolet-absorbance-of-oligonucleotides#figure-base-stacking

The reduction in energy due to hybridization comes from a combination of hydrogen bonding and base stacking, with base stacking often providing the majority of the bond energy. Hydrogen bonding is specific and directional. Two hydrogen bonds (H-bonds) occur between A and T whereas C and G have three H-bonds. The energy for an H-bond in a double helix is in the 2-3 kcal/mol per base pair range [90]. Base stacking, also called aromatic-aromatic interaction, occurs between the planar, aromatic bases of adjacent dinucleotide base pairs. The mechanisms for base stacking include hydrophobic interactions, $\pi-\pi$ interactions, and van der Waals forces (dipole-induced dipole and induced dipole-induced dipole) [92, 93]. Bond energy due to base stacking varies greatly, depending on sequence, and is in the range of 4-15 kcal/mol per dinucleotide base pair. Stacking energies for nearest neighbor dinucleotide base pairs are listed in tab 2.1. Hydrogen bonding sites and base stacking are shown in Figure 2.3 [90].

DNA is known to form three types of double helices; A, B, and Z. However, the B-form is the most prevalent form found in cells [91] and is the form of interest in these studies. The B-form has a right-hand sense and forms a major and minor groove. The average diameter of a double helix is 2 nm and there are on average between 10.4-10.5 base pairs per full helical turn. In this study, designs were based on 10.5 nucleotides per turn. The average pitch length is 3.57 nm per full helical turn. The axial rise (the distance between adjacent base pairs) is approximately 0.34 nm. The twist angle translated per dinucleotide base pair varies from 27.7º between (AG) and (CT), to 40.0º between (GC) and (GC), depending not just on the base pair and the nearest neighbor base pairs, but the sequencing of extended region adjacent to nearest neighbor base pairs

and surrounding aqueous environment. Thus, the twist angle can vary even between identical nearest neighbor dinucleotide base pairs. The average angle per base pair is around 34.3º, and is the value used in this study for design purposes. The double helix physical data is illustrated in Figure 2.4. Twist angles for all dinucleotide base pair combinations are shown in Table 2.1 [90].

Table 2.1: Stacking energies and twist angles for all possible dinucleotide pairs. Stacking energy is often the predominant bonding force for hybridization but varies considerably by sequence. Twist angle also is sequence dependent and varies by adjacent dinucleotide pairs as well. In this study, an average twist angle of 34.6º per base pair was used.

Dinucleotide Base Pairs	Stacking Energies (kcal/mol)[b]	Twist Angle (deg)[a]
(GC)-(GC)	**-14.59**	**40.0 ± 1.2**
(CA)-(TG)	**-10.51**	**34.5 ± 0.9**
(GA)-(TC)	**-9.81**	**36.9 ± 0.9**
(CG)-(CG)	**-9.69**	**29.8 ± 1.1**
(CC)-(GG)	**-8.26**	**33.7 ± 0.1**
(AG)-(CT)	**-6.78**	**27.7 ± 1.5**
(AC)-(GT)	**-6.57**	**34.4 ± 1.3**
(AT)-(AT)	**-6.57**	**31.5 ± 1.1**
(AA)-(TT)	**-5.37**	**35.6 ± 0.1**
(TA)-(TA)	**-3.82**	**36.0 ± 1.0**

[a]Data from Kabsch *et al.* (1982) [94].

[b]Data from Ornstein *et al.* (1978) [95]

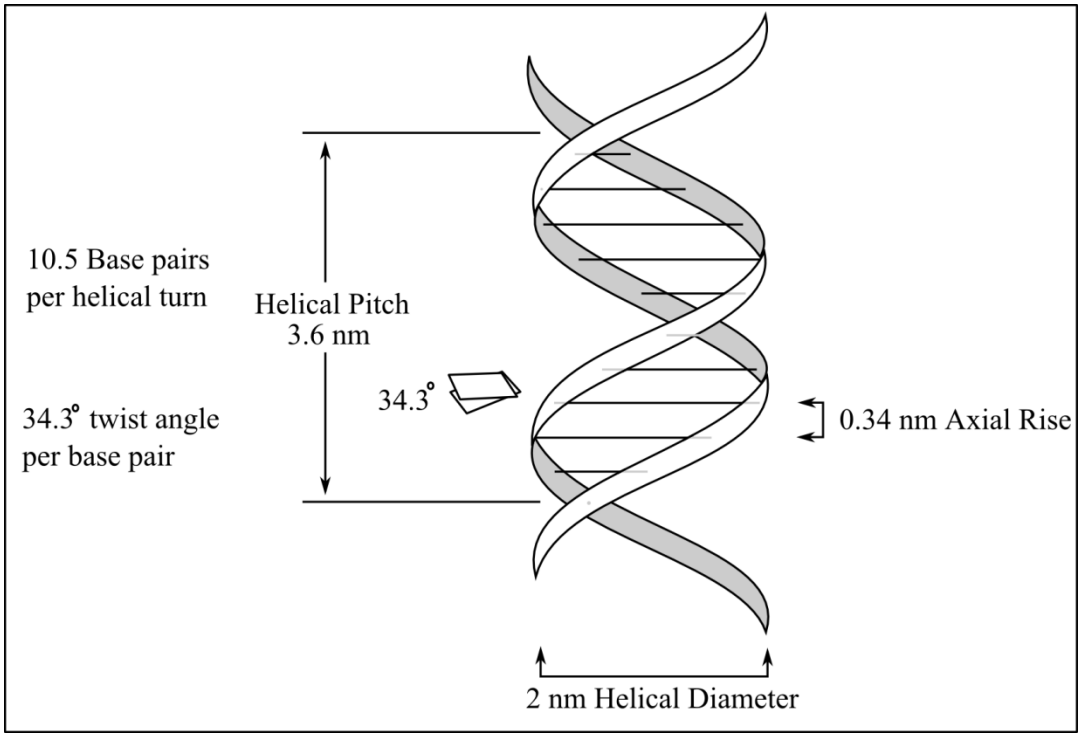

Figure 2.4: Physical characteristics of the B-form of a DNA double helix. There are three known forms of DNA double helices: A, B, and Z. DNA origami is designed around the physical characteristics of the B-form. The DNA origami described henceforth in this text assumes: 34.3° twist angle, 2 nm diameter helix, 0.34 nm axial rise, and 10.5 base pairs per helical rotation. Adopted from ref. [90].

2.2: DNA Origami Overview

2.2.1: Immobile Holliday Junction and Antiparallel Crossover

During genetic replication in living systems, strands of identical double stranded DNA form four-arm branched junctions consisting of interconnected identical double helices. Figure 2.5 (i) shows two double helices composed of strands *a* (blue) and *b* (red). Note that one of the double helices has been drawn in dashed lines for clarity and that by convention arrows representing ssDNA point from 5' to 3'. If a section of the dashed red strand hybridizes with the solid blue strand in the place of the solid red strand, the dashed ssDNA strand is said to have 'crossed over.' In similar fashion, the solid red

strand can cross over the dashed blue strand. The point of intersection, where single stranded DNA cross between helices, is called a Holliday junction [96] and is illustrated in Figure 2.5 (ii). Since the strands of DNA involved are homologous, the junction can move in a process called branch migration [97]. To create useful synthetic structures, the mobility of the junction must be reduced or eliminated [6]. This was accomplished by disrupting the sequence symmetry about the junction creating an immobile Holliday junction as shown in Figure 2.5 (iii) [7]. Here the ssDNA strands creating the double helices are not identical pairs. Rather the ssDNA were designed to create complementary domains, which manifest as branched double helical arms. One domain is indicated in the dotted circle, and was created by designed complementarity of the 3' end of strand *c* (navy) with the 5' end of strand *e* (orange). The other ends of these two strands are not complementary to each other, but rather are complementary to 5' end of strand *d* (maroon) and the 3' end of strand *f* (green), respectively, creating two more double helical arms. The final domain was created by the complementarity of the 3' end of *f* with the 5' end of *d*. The lack of sequence symmetry about the junction prevents the junction from migrating.

The Holliday junction and immobile Holliday junction use parallel crossovers where the strand that crosses over hybridizes with the same polarity (direction) as before. It was discovered that reversing the polarity of the ssDNA after crossing over, forming an antiparallel double helix, creates a more stable structure in small molecules (Figure 2.5 (d)). This became known as the antiparallel double crossover where the double refers to the fact that two helices are connected by the crossover strand [8]. The antiparallel crossover, for reasons to be shown, is the most common type of crossover for scaffolded

DNA origami.

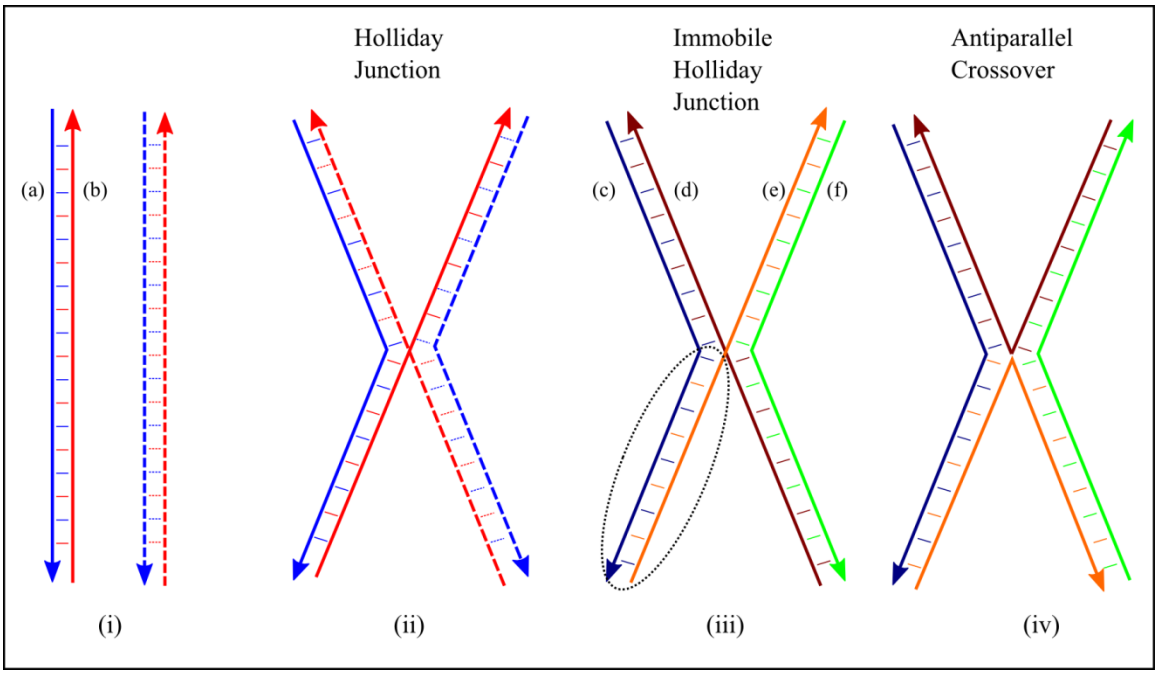

Figure 2.5: In (i), there are two equivalent double helices with an *a* strand (blue) and a *b* strand (red)—the dashed lines are drawn to enable the reader to track the strands. Recall that the arrow representation of ssDNA points from 5' to 3' by convention. In (ii), the solid red strand is hybridized with part of the dashed blue strand and the dashed red strand is hybridized with part of the solid blue strand. The intersection of these strands is called a Holliday junction. The strands that exchanged locations are said to have 'crossed over', thus the junction is also called a crossover. Homologous sequencing between the two strands allows this junction to slide up and down in a process referred to as branch migration. The immobile Holliday junction (iii) is created by disrupting the sequence symmetry of the Holliday junction, preventing branch migration, thus locking the junction in place. Here there are four unique ssDNA strands that create four complementary domains arranged as branched double helical arms. An example of one domain and thus one branched arm is shown in the dotted circle. This domain was created by designing the sequence of the 3' end of strand *c* (navy) to be complementary to the 5' end of strand *e* (orange). The other end of *c* is not complementary to the remainder of *e*, but rather to the 3' end of *d* (maroon). These domains combine to create the double helix branched arm in the upper-left quadrant. The remaining two domains are created in a similar manner. Reversing the polarity of strand *f* from (iii) yields the structure in (iv). This is referred to as an antiparallel double crossover, which is used extensively in scaffolded DNA origami.

2.2.2: Two-Dimensional Scaffolded DNA Origami

Two-dimensional scaffolded DNA origami developed by Paul Rothemund [55] laid the foundation for scaling up DNA nanostructures while maintaining the inherent resolution by using the inexpensive, naturally occurring bacteriophage m13mp18 plasmid as a scaffold strand. It is presented in detail here to introduce the reader to this particular method, but more importantly to introduce the reader to DNA as an engineering material.

In scaffolded DNA origami, a long strand of ssDNA with quasi-random but known sequencing is folded into a designed tertiary structure by reaction with synthetic oligonucleotides called staple strands. The staple strands are complementary to different sections of the scaffold, thus when the staple strand is fully hybridized the scaffold sections are brought into close proximity to each other. Since the sequence of the scaffold is quasi-random, the staple strands can be programmed uniquely, negating the need to closely control stoichiometry. In an action similar to folding a length of rope by hand and holding it in place with twine, hundreds of staple strands were able to form the 7249 nucleotide m13mp18 ssDNA strand into planar shapes such as rectangles and smiley faces in the 100 nm x 100 nm size range. Figure 2.6 illustrates the folding mechanism.

A desired shape is created to begin a scaffolded DNA origami design. The physical dimensions of the DNA double helix are conceptualized as cylinders 3.6 nm long in the *x* direction and 2 nm tall in the *y* direction representing one full helical turn of double stranded DNA. As illustrated in Figure 2.7, the shape is filled with paired cylinders representing two double helices stacked one atop the other in the *y* direction. As will be demonstrated, the cylinders must be paired as a consequence of the raster

pattern of the scaffold strand. An integer number of paired cylinders are added to fit the shape in the *x* and *y* directions. In Figure 2.7 (a), the desired shape is a rectangular base with a trapezoid on top (red). The cylinders representing double helices are shown in gray with tick marks indicating full helical rotations. As drawn, the base is 32.4 nm wide and narrows to 10.8 nm. The nominal height is 24 nm.

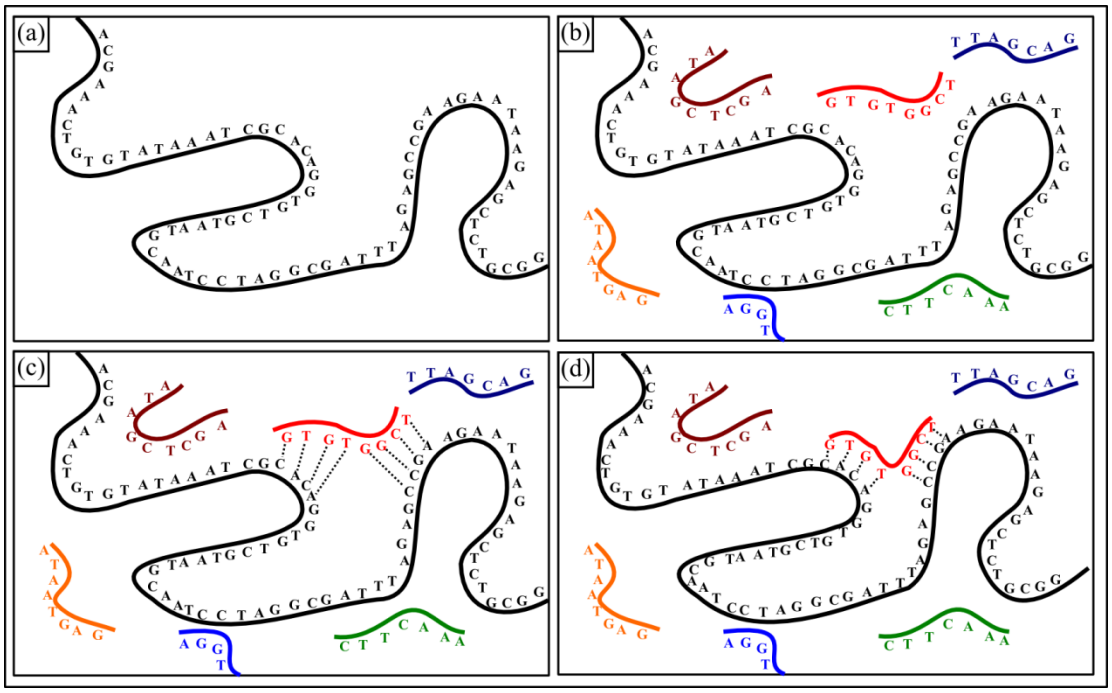

Figure 2.6: Scaffolded DNA origami mechanism. (a) A single stranded scaffold strand with known but random sequence is identified. (b) Short oligonucleotides with domains complementary to specific locations on the scaffold strand are added to the solution containing the scaffold. (c) The complementary domains on the staple strands and scaffold strand find each other in solution, discriminating against all other sequences. (d) After hybridization, sections of the scaffold strand that were many nucleotides away on the backbone of the polymer and free to rotate in space are now tightly bound in close proximity. (Adapted from http://www.ted.com/talks/paul_rothemund_details_dna_folding.html)

Staple crossover points are identified after the design space is filled with the aforementioned cylinders. Staple crossovers can only be added at locations where helices to be joined are co-planar. For planar (two-dimensional) DNA origami, crossover points

are allowed at integer multiples of 1/2 helical rotations where the nucleotides of a staple strand are 180^{o} from its start position. Since a full helical turn takes a non-integer number of nucleotides to complete, Rothemund used the approximation of 16 base pairs equaling 1.5 helical turns. (Using the estimate of 10.5 base pairs per helical turn, the actual rotation deviates from ideal and is closer to 1.52 helical turns.) In Figure 2.7 (a), the locations for the crossovers are shown in blue. The inset illustrates the crossover pattern created by 16 base pairs.

The scaffold strand is drawn in a raster pattern over the network of cylinders to identify the actual locations where the DNA scaffold strand will physically lay. In Figure 2.7 (b), the scaffold is shown in black. Here it can be seen how the raster pattern of the scaffold strand necessitated that paired cylinders to be used to fill the design space. This pattern also shows why scaffolded DNA origami staple strands use antiparallel crossovers. Locations where the scaffold strand changes direction are referred to as scaffold crossovers and are marked in red on the cylinders. Calculation of the twist angle of each nucleotide was performed via a computer program taking into account the average rotation per base pair and the number of base pairs. Here the deviation from the ideal rotation angle, by using the 16 base pair equating to 1.5 helical turns approximation, was accounted for. Scaffold crossover points with large angular deviations from the co-planar requirement were adjusted by addition or deletion of base pairs on an individual basis. Once the bases were adjusted, the sequences of the staple strands were determined using the sequence of the actual scaffold strand. In this example, the staple strands were short, in the 16 nucleotide range, as shown in Figure 2.7 (c).

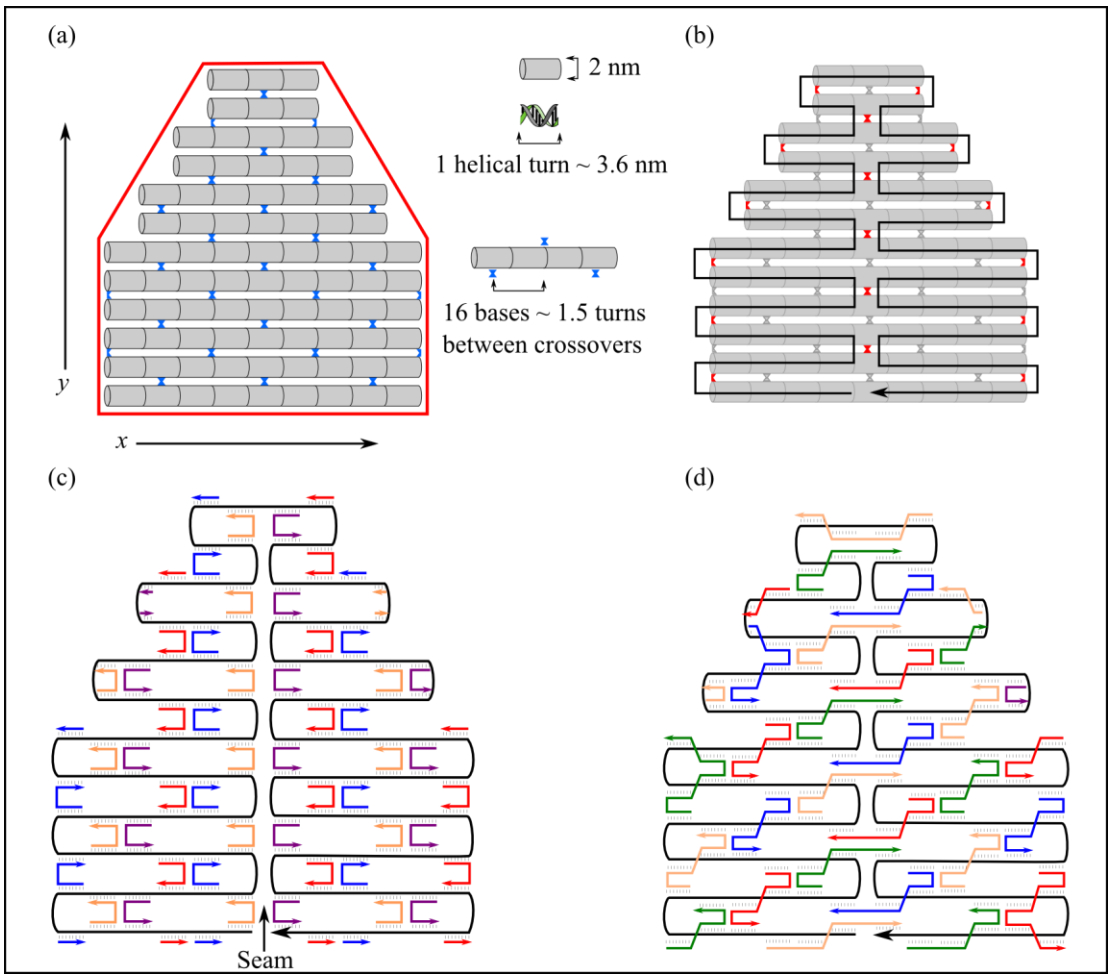

Figure 2.7: The method of two-dimensional scaffolded DNA origami. (a) A desired shape to create is shown in red. An integer number of pairs of cylinders representing parallel double helices with dimensions of 3.6 nm in the *x* direction by 4 nm in the *y* direction are added until the shape is filled. Staple crossovers are added at various locations (blue hourglass shapes) using the estimate of 16 base pairs equaling 1.5 helical turns. (b) The scaffold strand (black) is woven through the network of cylinders from the previous step. Locations of scaffold crossovers are marked on the cylinders in red. The scaffold sequence is input to into a computer program to determine the twist angle corresponding to each scaffold crossover. Bases are added or subtracted until the minimum angular deviation from co-planar is achieved. (c) After optimizing the scaffold raster pattern to achieve minimum stress, another computer program determines the sequences of the staple strands from the known sequence of the scaffold strand. The area in the center of the structure between scaffold crossovers is called the 'seam'. (d) Staple strands binding domains are lengthened via computer, thus increasing their stability (more bonds per strand). During this process, the seam is reinforced by designing the staple strands to bridge opposite sides of the seam. A computer program assigns the sequence for the final, lengthened staple strands. Adapted from ref. [55].

The final step in the design phase was to lengthen the binding domains of the staple strands by strategically combining two or more of the shorter strands via a computer program. Simultaneously, the 'seam' was reinforced. The seam represents the area down the center of the structure where the scaffold strand crosses over repeatedly. The seam was reinforced by eliminating the staple crossover points that were coincident with the scaffold crossovers and extending adjacent staples to bridge the seam as shown in Figure 2.7 (d). In this example, the average final length of a staple strand was 32 nucleotides. The sequences of the individual staple strands were then ready to be synthesized by a commercial manufacturer.

To synthesize the structures, staple strands were added in 100:1 ratio, each, to bacteriophage m13mp18 strands in a buffer solution. All secondary structure was removed by thermal denaturing the DNA at 95ºC. The solution was then slowly cooled to 20ºC with a total cycle time of approximately 2 hours. During the cooling process, staple strands located their addressed locations on the scaffold and hybridized via self-assembly. The slow temperature ramp down favored the lowest energy structures (full hybridization) while allowing time for displacement of less favorable structures such as partially matched sequences, or ssDNA fragments.

Rothemund's method of scaffolded DNA origami provided a quantum leap in the scale of DNA origami nanostructures while maintaining the precision inherent to DNA. The use of a naturally occurring plasmid ssDNA scaffold helped reduce cost greatly as well. Many of his original structures were borrowed and modified by other researchers, while others used the principles developed in his study to demonstrate the robustness of the method to form unique two-dimensional nanostructures. It was not long before

researchers applied the same method to extend scaffolded DNA origami into three dimensions.

2.3: Six-Helix DNA Origami Nanotube

2.3.1: Background

The first published account of a three-dimensional DNA origami nanostructure was by Douglas *et al.* in 2006 when they applied the technique of scaffolded DNA origami to create a six-helix nanotube [87]. The inspiration for the architecture was the pre-scaffolded DNA origami six-helix bundle made by Mathieu *et al.* in 2005 [23]. Mathieu *et al.* recognized that a seven base pair sequence created a perfect 2/3 of a rotation. This allowed the construction of double helices connected with 120º dihedral angles when viewed on end. Mathieu *et al.* constructed a six-helix bundle by combining 16 synthetic oligonucleotides with a total count of 504 base pairs. The number of base pairs between crossovers was asymmetric, but was in multiples of 14. The final structure had nominal dimensions of 6 nm in diameter by 20.7 nm in length with a 2 nm hole down the axis.

The intent of Douglas *et al.* was to create two unique 0.4 μm monomers six-helix nanotubes and dimerize them using dove-tailing ends and linking staple strands to create a single 0.8 μm structure. The 14 base pairs between crossovers was borrowed from Mathieu *et al.* but the raster pattern was made symmetric: each staple strand would be 42 base pairs long and crossover two times connecting (while simultaneously creating) three double helices. Two of these staple strands created two halves of a nanotube (this is shown in detail in Section 2.3.2). The structure was said to have 120º screw

pseudosymmetry. Two screw operations created what was described as a pseudorepeat unit. Each pseudorepeat unit was 42 base pairs in length, axially, and there were 28 per nanotube monomer creating a nominal 400 nm section of the nanotube. The ends of the nanotubes were asymmetric with unspecified variation in the lengths of the individual helices. The reported total length of each end was 14 nm. Two different monomers were created that were structurally identical, but sequentially unique. This was accomplished by simply changing the location on the scaffold where a computer program determined the staple strand sequences [87].

Douglas *et al.* used a modified 7308 base pair variant of the m13mp18 bacteriophage plasmid ssDNA as a scaffold. Nanotube monomers were synthesized by heat denaturation at 80ºC for 7 minutes, followed by a slow ramp down to 20ºC over the course of two hours. Monomers were dimerized by reaction of equimolar aliquots of each at 37ºC for two hours. The dimerized nanotubes measured 813 nm ± 9 nm and were successfully used as a liquid crystal agent to aid nuclear magnetic resonance spectroscopy of membrane proteins as was intended [87].

Bui *et al.* made slight modifications to the Douglas *et al.* design with the intent of creating a three-dimensional vehicle for nanoparticle arrangement [89]. The nanotubes created by Bui *et al.* used the same pseudorepeat units as Douglas *et al.*, but which were referred to as a staple motif. Bui *et al.* blunted the ends of the nanotubes to prevent unwanted dimerization and used the nucleotides that would have gone to the dovetailing end structures to add another 1/3 of a staple motif. One end of the nanotube had a 14 base pair long, axially, section without staple strands to be used for attachment experiments. Finally, the Bui *et al.* nanotubes were only of one sequence (there were not

two monomers) and the scaffold strand was an unmodified version of the m13mp18 bacteriophage plasmid DNA. The studies presented here were based on the Bui *et al.* modified nanotube, thus the design and synthesis is summarized in great detail in Section 2.3.2.

2.3.2: Design of the Bui *et al.* DNA Origami Nanotube

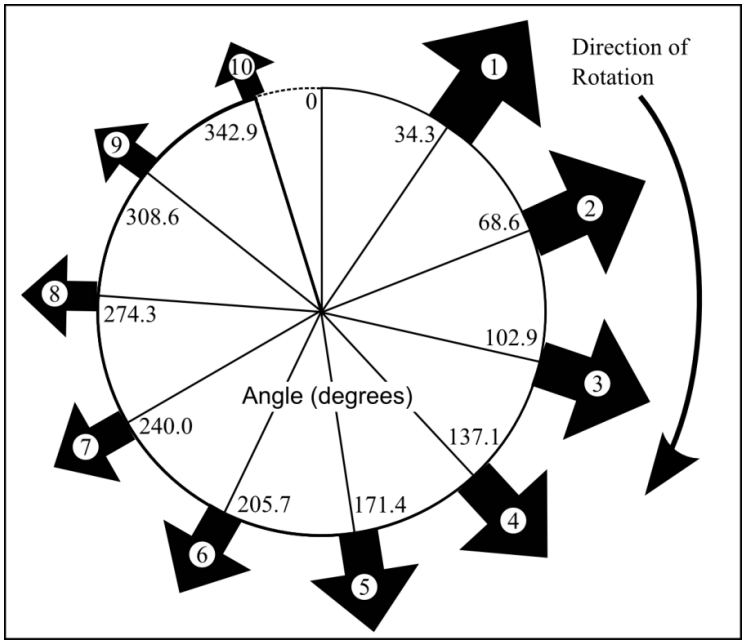

Figure 2.8: Degree of twist per base pair is idealized as 360º divided by 10.5 base pairs per helical turn. The arrows represent tangent points of the i^{th} nucleotide. The B-form double helix has a right-hand pitch, thus looking down a helix from the 5' end of the staple strand nucleotides are moving into the page. Seven base pairs create a perfect 240º, or 2/3 of a rotation. This will become the basis for the number of nucleotides between crossovers for the six-helix nanotube.

Recall that a DNA double helix requires ~10.5 nucleotides to make a full rotation. As shown in Figure 2.8, the average number of degrees rotated per base pair can be approximated by dividing 360^{o} by 10.5, which gives 34.3º. The arrows drawn in perspective represent the tangent point of the i^{th} nucleotide. The arrows get smaller as the number increases to represent translation into the page as the helix propagates away from

the reader. Nucleotide number 7 creates a perfect 240^{o} angle; the same as 2/3 of a full rotation. The nanotube used in these experiments utilized 14 base pairs or 4/3 of a full rotation between crossovers.

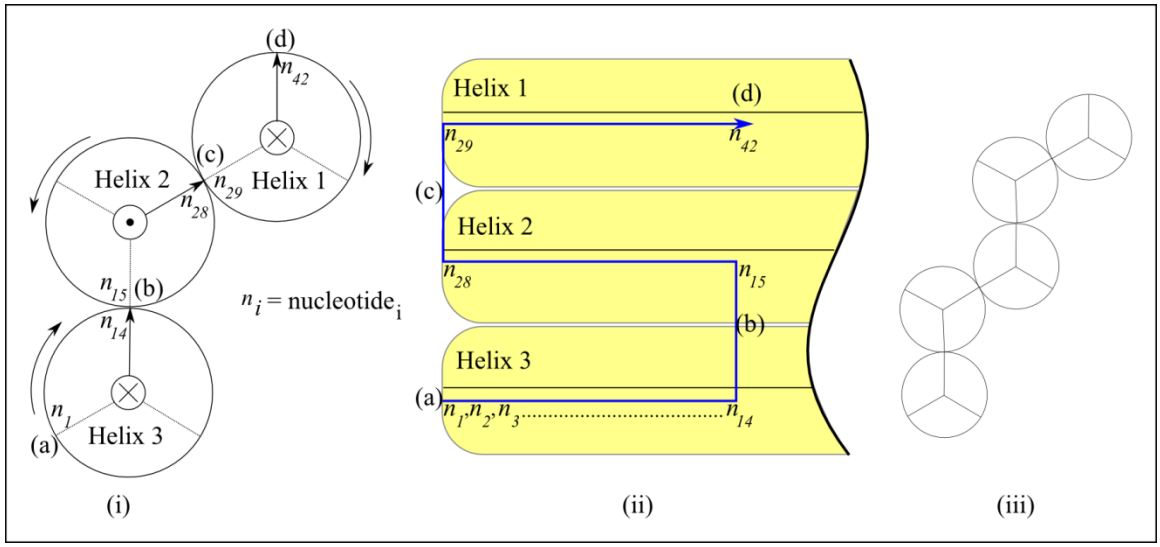

Figure 2.9: Six-helix nanotube staple strand raster pattern: axial view (i), unrolled side view (ii), axial view of pleated repeat pattern (iii). For demonstration purposes assume that the scaffold strand is present wherever a staple strand is placed and that its orientation is antiparallel. All descriptions are therefore relative to the staple strand. (i) Let the symbol '×' indicate a helix rotating into the page and the "·" (dot) to symbolize a helix rotating out of the page. Forward direction is from 5' to 3', thus the symbol '×' means the nucleotide closest to the reader is 5' and the 3' end extends into the page. The "·" symbol indicates the 3' end coming towards the viewer. Both directions are in a right-handed screw pattern and relative to the direction of the staple strand. For clarification, the arrows outside of the circles indicate direction of rotation and the arrows inside the circles point to the crossover location. Starting at point (a) (nucleotide 1 → n_1) and translating 14 base pairs into the page, the helical pattern rotates clockwise and completes 4/3 of a rotation. Nucleotide 14 (n_{14}) is tangent to helix 2 at point (b). Crossing over to helix 2 the direction of hybridization is now out of the page with a counterclockwise rotation. Translating 14 base pairs from point (b) places nucleotide 28 (n_{28}) at point (c) where the staple strand crosses over to helix 1. After translating another 14 base pairs into the page, nucleotide 42 (n_{42}) comes to rest at point (d). (ii) Two-dimensional representation of (i) with the view closest to the reader at left. Note that there are no nucleotides between the helices despite the lines at points (b) and (c) as noted by the nucleotide numbering. These are drawn to expand the image for better viewing. The arrow in this image is making use of the 5' to 3' convention. (iii) The number of crossovers is limited to 2, otherwise a pleated sheet will form.

Figure 2.9 illustrates the raster pattern of a staple in axial view (i) and plan view (ii). In Figure 2.9 (i), circles represent an axial (end-on) view of DNA helices with the direction of the staple strand indicated by '×' for a staple strand extending from 5' to 3' into the page, or by '·' (dot) indicating the 3' end coming out of the page. B-DNA hybridizes in a right-hand screw, thus curved arrows indicate direction of helical rotation. Each helix is divided into thirds so the reader can track 4/3 of a rotation per 14 base pairs. Starting with nucleotide 1 (n_1) at point (a) on helix 3, rotating clockwise and translating 14 base pairs into the page, nucleotide 14 (n_{14}) will be tangent at point (b). Crossing over to an antiparallel segment of scaffold strand located at point (b), the staple strand will now rotate counterclockwise out of the page. Translating 14 base pairs along helix 2, nucleotide 28 (n_{28}) will be located 4/3 of a turn from point (b) at point (c). Crossing over to another section of antiparallel scaffold at point (c), and extending another 14 nucleotides, the number 42 nucleotide (n_{42}) will be tangent to helix 1 at point (d). The result of these 2 periodic crossovers is a central helix, helix 2, bounded by helix 1 and helix 3 with a dihedral angle of 120º. Continuing this pattern would yield a pleated sheet as illustrated in Figure 2.9 (iii), thus the number of crossovers is limited to two.

Structurally, not taking into account the unique sequencing, what was described in Figure 2.9 (i) is one half of a DNA origami nanotube pseudo unit cell. The term 'pseudo' is used to indicate that symmetry is structural only, and not sequential. The other half is created by a pseudo rotoinversion operation—a rotation about an axis followed by reflection through the perpendicular plane—of the first half, yielding a six-helix annulus. At this point, the unit cell halves are not attached, but a pseudo screw operation—a rotation operation along an axis combined with a translation—ensures that the helices

become interconnected traveling along the axis. Structurally, the unit cell has three-fold symmetry and the staple strand pseudo motif is created with two 1/3 rotations with one unit cell length translation each, as illustrated in Figure 2.10.

The design space was explored to determine how to best organize the motif into the full nanotube once the staple motif was determined. As an analogue to Rothemund's two-dimensional origami, the motif would represent the cylinders used to fill the desired shape but with the added goal of consuming the maximum number of available nucleotides to create the longest possible structure. The m13mp18 bacteriophage scaffold strand contains 7249 nucleotides. Since there are 6 helices, the maximum number of bases per helix is 1208 with one remainder. Each motif had a length of 42 nucleotides, thus 28 motifs plus two unit cells could be created with 25 unused nucleotides. The first staple strand motif was moved back one unit cell, leaving the first 14 nucleotides of each helix unbound—an unbound unit cell. This served to provide single stranded DNA loops to allow for attachment of nanoparticles, as well as to relieve possible stress. The end opposite the unbound unit cell had 4 unbound nucleotides on helices 1-5, and 5 unbound nucleotides on helix 6. These nucleotides were the remainders that did not fit in the repeating structure and were included at the end to relieve stress.

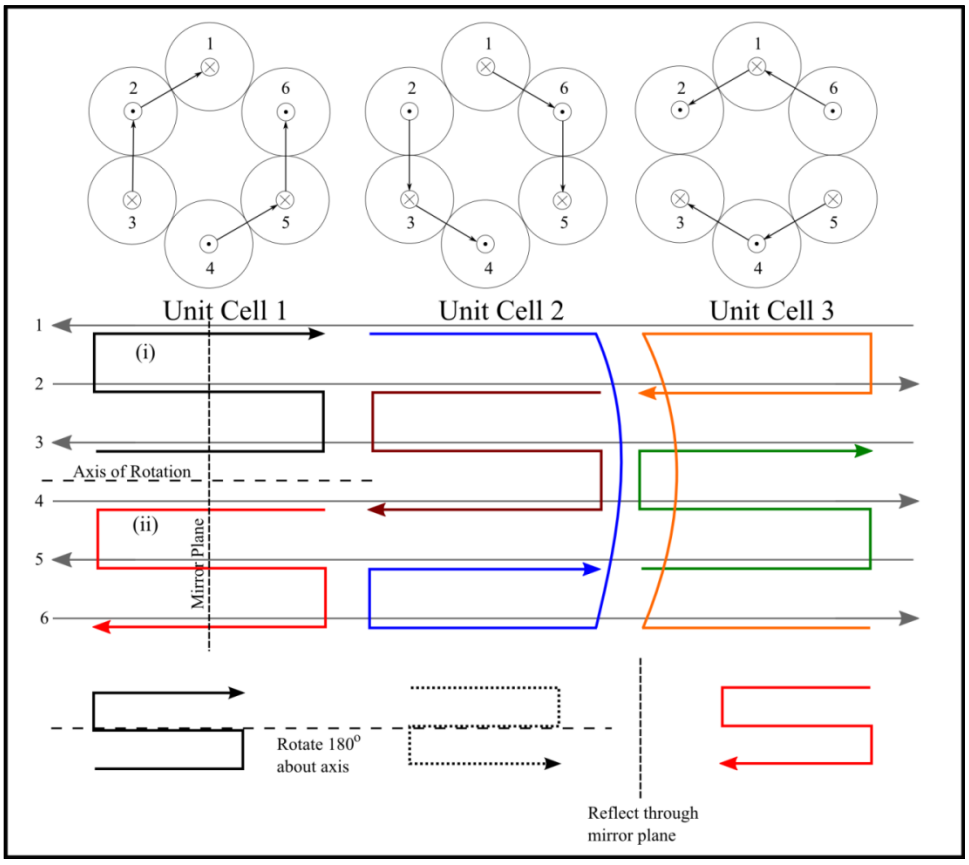

Figure 2.10: Pseudo staple motif. The gray arrows represent the scaffold strand while the colored, raster arrows indicate staple strands. The space between staples is drawn for clarity, but in the actual structure, there are no gaps between adjacent staple strands or between helices at crossover points. The pseudo unit cell is created by a pseudo rotoinversion operation of helices 1, 2, and 3. This operation is easiest to see in the unrolled side view. There is an axis of rotation down the annulus of the nanotube, indicated by the dashed line between helices 3 and 4, and a mirror plane perpendicular to the axis of rotation. As shown at the bottom of the figure, operating on the black strand (i), rotating 180º about the axis of rotation yields the intermediate, dotted staple strand. Reflection through the mirror plane yields the red strand (ii). Two more unit cells are created by screw operations of two 1/3 rotations translating one unit cell each. For example, taking unit cell 1 as seen from the axial view and rotating right 120º the staple pattern for unit cell 2 is created. This unit cell is placed at the bottom of unit cell one. The three unit cells combine to create the staple motif. The two-dimensional representation of the motif shows that the halves of each unit cell are not connected. For example, in unit cell 1, helix 1 is not connected to helix 6, and helix 3 is not connected to helix 4. However, these helices are connected in unit cells 2 and 3. Likewise, the unconnected helices in unit cell 2 are connected in unit cells 1 and 3, and so forth. This mutual support ultimately holds the structure together. Each staple strand is 42 nucleotides long, but only extends 14 nucleotides down the axis giving the motif a 42 nucleotide length along the axis.

The final DNA origami nanotube design required 170, 42-mer staple strands arranged in 85 unit cells. To determine the sequencing of the staple strands, the scaffold was woven through the structure to determine start and end points and scaffold crossover locations. Figure 2.11 (a) shows the scaffold raster pattern with the m13mp18 nucleotide count at the start, end, and each scaffold crossover location. The break shown in the figure is for clarity, as bacteriophage m13mp18 was to be folded in uncut form.

In Figure 2.11 (b)-(d) the unit cells are represented as columns and are numbered from left to right as drawn starting with 0 and ending at 85. Column 0 is the unbound unit cell. The remainder nucleotides, at the far right end of Figure 2.11 (d), were not counted as a column. Helices are numbered from 1 to 6, top to bottom. The naming convention for the staple strands was developed as a two alphanumeric character system with the helix number preceded by a capital 'H' and the column number proceeded by a capital 'C'. Helices are determined by the location of the 5' end of the strand. For example, the uppermost staple strand on the left in Figure 2.11 (c) would be H3 C37. The scaffold strand nucleotide numbering begins and ends in column 43. Scaffold crossovers were located in column 41 between columns 2 and 4, and column 39 between helices 4 and 5.

Once synthesized, the nominal dimension for the unit cell was 4.76 nm axially by 6 nm in diameter. The nominal length is 412.3 nm including the unbound scaffold nucleotides at each end. The nanotube in Figure 2.11 (e) is drawn to scale to show the final aspect ratio.

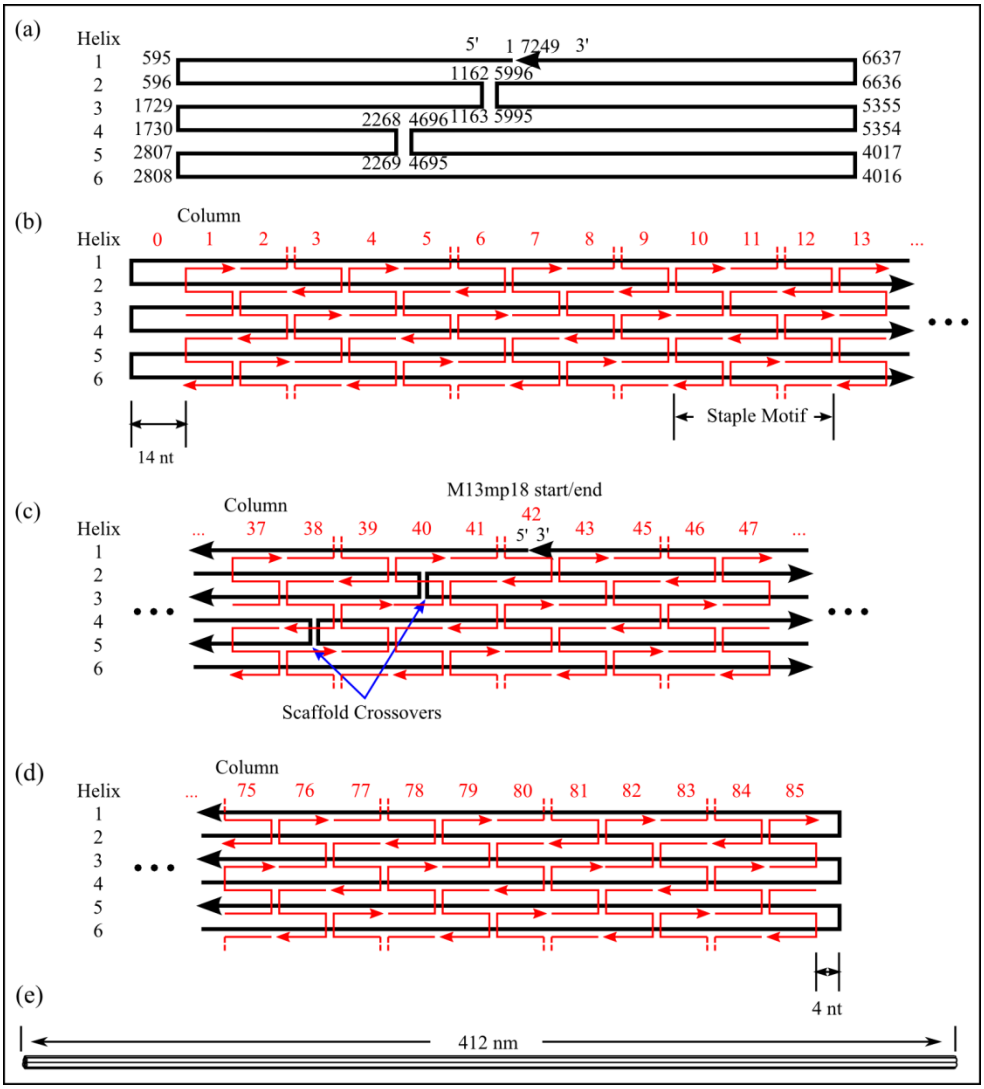

Figure 2.11: Six-helix nanotube scaffold and staple layout. (a) Scaffold strand layout for 6 helix nanotube using m13mp18. Five of the six helices were laid out to contain 1208 nucleotides, with helix 6 containing 1209. The scaffold break is shown for clarity, as the plasmid of m13mp18 bacteriophage was to be used uncut. The nucleotides at each crossover are shown numbered. (b) Beginning of the DNA origami nanotube. The black lines represent the scaffold while the red lines are staple strands. The unit cells are represented as columns, starting with column 0, the unbound unit cell. (c) The center of the nanotube contains scaffold crossovers in columns 38 and 40, and the start/end in column 42. Note that the staple strands bridge the seams of the scaffold crossovers. Staple strand naming convention is a two character alphanumeric system with the helix where the 5' end of the strand begins, preceded by an 'H' and the column where the strand resides, preceded by a 'C'. For example, the upper-left strand in (c) would be H3 C37. (d) The end of the DNA origami nanotube. Unbound remainder nucleotides are at the end to relieve stress. Helix 6 has 5 unbound nucleotides, not the 4 shown. (e) The six-helix nanotube drawn to scale. Adapted from ref. [89].

2.3.3: Synthesis

The m13mp18 bacteriophage strands were purchased from New England Biolabs with a concentration of 52.5 nM in nuclease free water. Staple strands were purchased from Integrated DNA Technologies with a specified concentration of 100 μM in nuclease free water. A staple strand solution was created by transferring a 5 μL aliquot of each of the 170 staple strands into a single test tube. By simple dilution, the final concentration of the i^{th} oligo, C_i, in the staple strand solution was determined to be (100 μM /170) = 0.588 μM or 588 nM.

It was desired to react each staple strand in a 10:1 ratio with the m13mp18 bacteriophage. The volume of the m13mp18 bacteriophage, V_{m13}, was used as the independent variable and the volume of the staple strand solution, $V_{staple\ strand}$, was calculated based on that value using the following equation:

$$V_{staple\ strand} = 10 \cdot V_{m13} C_{m13} / C_i \tag{2.1}$$

where the C_{m13} is the previously reported concentration of m13mp18 ssDNA. Thus, for 100 μL of m13mp18 solution 89.3 μL of oligo solution was required.

Since ssDNA in solution is negatively charged, buffer solution containing the divalent cation Mg^{++} was added to shield this charge and allow nucleation. It was desired to bring the total solution to a 1x TAE Mg^{++} concentration (40 mM tris, 20 mM acetic acid, 2 mM ethylenediaminetetracetic acid [EDTA], and 12.5 mM magnesium acetate; pH 8.0). TAE, magnesium acetate tetrahydrate, and laboratory grade water [Milli-Q Water, Millipore] were purchased from Sigma Aldrich. This was accomplished by using a 10x TAE Mg^{++} solution and adding in a 1:9 by volume ratio with the staple

strand/scaffold DNA solution. For the example given above, the volume of 10x TAE Mg^{++} is (100 μL + 89.3 μL) / 9 = 21.03 μL.

The final reaction solution was annealed by heating to 90ºC and denaturing for 20 min., followed by a ramp down to room temperature over a 2-hour period using a thermal cycler (Eppendorf Mastercycler Personal). Denaturing is used to 'melt' the double stranded DNA, while the slow ramp down allows intermediate structures that may be metastable to be replaced by the lowest energy configuration. Rothemund [98] developed this technique for scaffolded DNA origami with inspiration gained from the concept of strand displacement developed by Yurke *et al.* [99]. This thermal cycle program was dictated to Bui *et al.* [89] directly from Dr. Yurke.

The denaturing temperature, T_d, is based on the melting temperature of double stranded DNA. The melting temperature is defined as the temperature at which 50% of a DNA oligonucleotide in solution with its perfect complement is in duplex (double stranded) form. The simplest form of melting temperature formula, in this case T_d, is the Wallace Rule [100]:

$$T_d = 2°C(A+T) + 4°C(G+C) \tag{2.2}$$

Here *A*, *T*, *G*, and *C* refer to the number of those respective bases in the single stranded oligonucleotide. The experiments on which this equation is based considered base pairs alone, and did not take into account nearest neighbor interactions. Moreover, the oligonucleotides were short, no more than 17 nucleotides. For example, the staple strand ACCGCTTCTGGTGCACCACACCCGCCGCAACAGGAAAAACGC used in the six-helix DNA origami nanotube designed by Bui *et al.* would have a melting

temperature of 136ºC based on Equation 2.2, however the manufacturer (Integrated DNA Technologies) calculated a melting temperature of 74ºC. The governing melting temperature equation, which was used to determine the latter value was developed by SantaLucia *et al.* and is based on nearest neighbor interaction in dinucleotide pairs [101]:

$$T_M(^oC) = \frac{\Delta H^o}{\Delta S^o + R\ln[oligo]} - 273.15 \tag{2.3}$$

T_M is the melting temperature, R is the ideal gas constant and [*oligo*] is the molarity of the oligonucleotide. Enthalpy (ΔH^o) and entropy (ΔS^o) are thermodynamic parameters that were determined by SantaLucia *et al.* and published along with that report.

The melting temperature data from Equation 2.3 was based on a solution with only monovalent sodium ions. However, as noted, this experiment uses divalent magnesium ions. Integrated DNA Technologies (idtdna.com) allows users to vary the concentrations of both cations and adjust for interactions using an online application. This application compensates for salt concentrations using equations developed by Owczarzy *et al.* [102]. These equations are beyond the scope of this introduction but can be viewed from the manufacturer's site (www.idtdna.com). Adjusting for no Na^+ ions and 12.5 mM Mg^{++} ions, the melting temperature for the example oligo was 81.8ºC. Using this value, the 90ºC denaturing temperature was warranted.

Excess staple strands were removed using Amicon Ultra 100k centrifuge filters (Millipore). Enough filters were used to keep the volume of DNA solution in the 50-100 μL range per filter to prevent filter loading. For the example above, three filters would have been used. Buffer was added to each filter until a total volume of 500 μL was

reached in each filter. Filter apparatuses were centrifuged for 10 minutes at 14,000 relative centrifugal force (rcf), and then reversed into a fresh test tube and the sample recovered by centrifugation for 3 minutes at 1,000 rcf.

The concentration of nanotube solution was determined via UV absorbance at 260 nm. Recovered DNA concentrations were too high to measure directly due to not enough light being able to transmit to the detector through the sample. Moreover, recovered DNA sample solution volumes were often less than the minimum 50 μL required by the spectrophotometer. A 50:1 dilution with 1x TAE Mg^{++} was used to mitigate these problems and to save sample. An Eppendorf Biophotometer was set to use a wavelength of 260 nm and zeroed using a disposable cuvette (Eppendorf Uvette) and 98 μL of 1x TAE Mg^{++} buffer. Two microliters of sample were added directly to the buffer used to zero the system without removing it from the cuvette. The sample was mixed using a pipette and the absorbance measured 5 times and averaged.

The Beer Lambert Law was used to determine the concentration from the absorbance:

$$A = C \cdot \varepsilon_{260\,nm} \cdot l \tag{2.4}$$

where A is the absorbance, C is the concentration, $\varepsilon_{260\,nm}$ is the extinction coefficient at 260 nm and l is the path length. l was known from the cuvette (either 1 cm or 0.2 cm, depending on which path was used), A was measured and $\varepsilon_{260\,nm}$ estimated by summing the individual extinction coefficients for each of the 170 staple strands in double helix form. The value of $\varepsilon_{260\,nm}$ used for the DNA origami nanotube was 1.15×10^8 $M^{-1}cm^{-1}$. Concentration was given in moles and was multiplied by the dilution factor. Thus, the

concentration in nM was determined by:

$$C = 50 \cdot (A/\varepsilon_{260\,nm} \cdot l) \cdot (10^9)\ nM \tag{2.5}$$

The duplex DNA extinction coefficient at 260 nm, ε_D, for each staple strand was determined using the manufacturer's interactive website. Those values were determined using [103]:

$$\varepsilon_D = (1 - h_{260nm})(\varepsilon_{s1} - \varepsilon_{s2}) \tag{2.6}$$

where:

$$h_{260nm} = 0.287\, f_{AT} + 0.059\, f_{GC} \tag{2.7}$$

In these equations, ε_{s1} and ε_{s2} are the single stranded extinction coefficients of strand 1 and strand 2, respectively, at 260 nm where the strands are perfect complements. The variables f_{AT} and f_{GC} are the fractions of A and T, and G and C, respectively.

The ssDNA extinction coefficients were determined by [103]:

$$\varepsilon_{260nm} = \sum_{i=1}^{N_b - 1} \varepsilon_{i,i+1} - \sum_{i=2}^{N_b - 1} \varepsilon_i \tag{2.8}$$

where N_b is the number of base pairs. $\varepsilon_{i,i+1}$ is the extinction coefficient at 260 nm for the nearest neighbor pairs base i and base $i+1$ when written 5' to 3', and ε_i is the extinction coefficient at 260 nm for the individual base. Values are given in tab 2.2.

Table 2.2: Extinction coefficients at 260 nm for nearest neighbor pairs and individual nucleotides.

	For nearest neighbors ε_{i+1}			
ε_i	A	C	G	T
A	27,400	21,200	25,000	22,800
C	21,200	14,600	18,000	15,200
G	25,200	17,600	21,600	20,000
T	23,400	16,200	19,000	16,800
From Warshaw & Tinoco (1966) [104]				
	For individual nucleotides			
	A	C	G	T
ε_i	15,400	7,400	11,500	8,700
From Warshaw & Cantor (1970) [105]				

CHAPTER 3: DIMERIZATION

3.1: Introduction

Bui *et al.* [89] modified the monomer from Douglas *et al.* [87] (see Section 2.3.1) by removing the dove-tail end structures to make the structure symmetric. The structural symmetry created by this modification was more amenable to nanoparticle attachment. Within this section, it was desired to determine if homodimers could be created by linker strands alone. In addition, it was desired to functionalize dimerized DNA origami nanostructures with quantum dots.

The purpose of the six-helix nanotubes created by Douglas *et al.* was to aid magnetic resonance imaging, replacing the Pf1 phage that is commonly used [87]. The Pf1 phage is a rod-like structure with dimensions of approximately 7 nm x 2000 nm. Given the length of the 7308-mer modified m13mp18 scaffold strand used by Douglas *et al.*, a six-helix DNA origami nanotube was only expected to have dimensions of approximately 6 nm x 400 nm. This was estimated to be too short to be a viable alternative to the Pf1 phage, so a heterodimer was designed to double the length while maintaining the same diameter. A front nanotube and a rear nanotube were created with dove-tailed ends designed to fit together like a lock and key and then be held in place by linker strands. The monomers were structurally the same, but the sequencing was changed by shifting the starting location of their scaffold strand creating two sequentially unique structures (see Section 2.3). In this experiment, the sequencing of the nanotube

monomers is the same, with modifications made only to the staple strands in columns 0 and 85. Dimers were, therefore, most similar to homodimers.

While calculating the yield of dimer formation, one of the nanotube monomers was functionalized with QDs (see Section 4.2). This was done to distinguish types of monomers, but appears to have created the first known instance of a QD functionalized DNA origami nanostructure dimer.

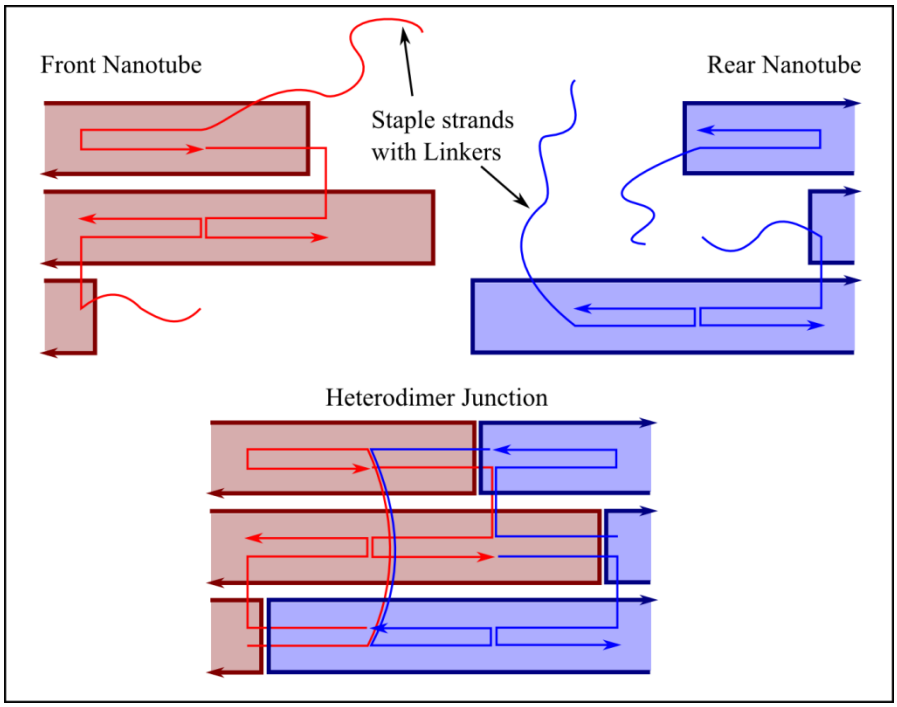

Figure 3.1: Dove-tailed ends of the Douglas *et al.* heterodimer [87]. Douglas *et al.* used two unique nanotubes, the front nanotube and the rear nanotube, with dove-tailed ends designed to fit together like a lock and key. Monomers where synthesized separately, then reacted at 37ºC. Liking strands were incorporated into the ends of the nanotubes that acted like staple strands while providing a bond between nanotubes to create the heterodimer. Adopted from ref. [87].

3.2: Symmetrical DNA Origami Nanotube Head and Tail Heterodimer

To maintain a parallel scaffold strand orientation, a head to tail configuration was used. Recall that there were two extra nucleotides after column 85 on helices 1-5 and

three extra nucleotides on helix 6. Henceforth, in this chapter, references to column 85 will include the extra nucleotides as well. The two staple strands from the standard nanotube design were omitted from column 85 to make room for linker strands. Nanotubes with the linkers added to the modified column 85 were designated as the 'head' nanotubes. As illustrated in Figure 3.2, helix 1 on the head nanotube was designed to hybridize with helix 1 on the tail, and so forth for the remaining helices. Three linker strands were incorporated into the space once occupied by staple strands. Sections of the linkers were complimentary to the inner 9 nucleotides of the scaffold strand sections of helix 2, helix 4, and helix 6. These linkers then crossed over to helices 1, 3, and 5, respectively, where they were complimentary to the full number of nucleotides for those helices. Seven nucleotides on each linker strand extended out of the nanotube in the 3' direction and were complimentary to the outermost seven nucleotides of the column 0 (the unbound unit cell from Section 2.3.2) sections of helices 1, 3, and 5, respectively. The naming convention of the linker strands included the type of nanotube followed by the helices through which the strand hybridized, 5' to 3'. Thus, the three linkers for the head nanotube were *head 2-1-1*, *head 4-3-3,* and *head 6-5-5*. The unbound nucleotides in column 0 of the head nanotube were capped with two staple strands to prevent the head nanotubes from hybridizing with each other.

Nanotubes with linkers incorporated into column 0 were designated tail nanotubes. The three linker strands for the tail nanotubes hybridized 5' to 3' on the innermost seven nucleotides on helices 1, 3, and 5. These then crossed over to helices 2, 4, and 6, respectively, and were complimentary to the full number of nucleotides on those helices. The 3' ends of the strands were then complementary to the outermost nine

nucleotides of the helices 2 and 4 and the outermost ten nucleotides of helix 6 of column 85. The naming convention for the linkers was similar as that of the head nanotube: *tail 1-2-2*, *tail 3-4-4*, and *tail 5-6-6*.

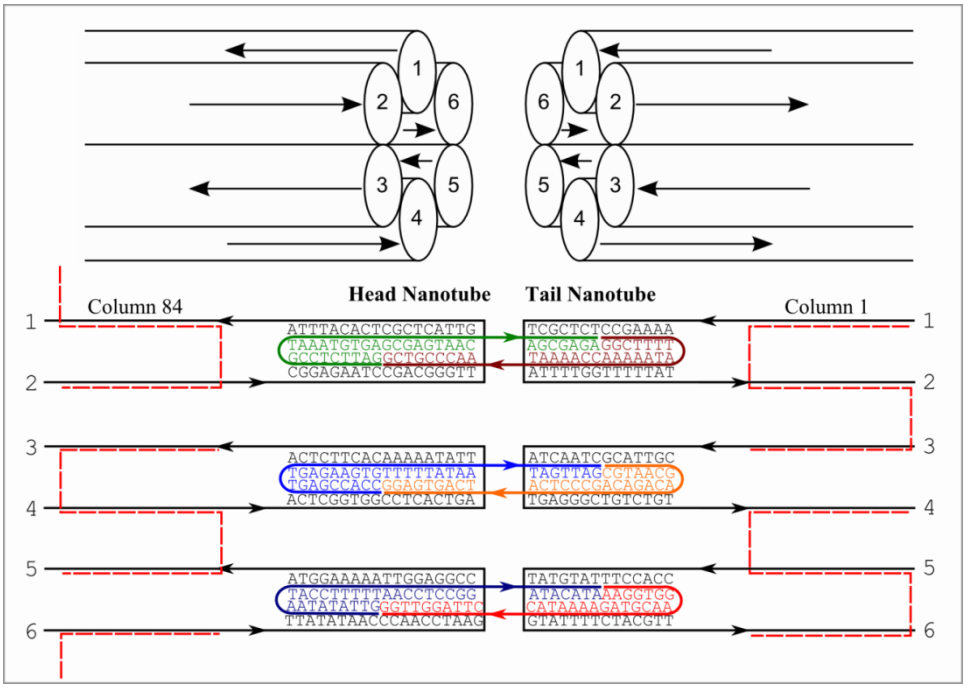

Figure 3.2: Head-to-tail dimerization utilized two unique monomers, a 'head' and a 'tail', designed to dimerize with both nanotubes oriented in the same direction laterally and axially as shown at top. The head nanotube was created by adding linkers to column 85, omitting the standard staple strands normally located there. The tail nanotubes were created by incorporating the linkers into column 0. Each monomer had three linker strands with the 5' ends complementary to approximately half of the interior of one helix before crossing over to an adjacent helix where each was complementary to the full length of the that helix. The 3' terminal end of each of the linkers was complementary to a 7 to 10 nucleotide section of target helix on the other monomer. Links were created between like numbered helices. For example, the orange strand above, named *tail 3-4-4*, begins hybridizing with the innermost 7 nucleotides of helix 3 on the tail nanotube. The linker then crosses over to helix 4 of the tail and hybridizes with all 14 nucleotides before exiting the tail nanotube and finding its target region of 9 nucleotides on helix 4 of the head nanotube.

Nanotubes were synthesized and filtered separately, then reacted in equal volumes of 20 nM solutions for two hours at 37ºC. AFM analysis indicated the presence of dimers

and unreacted monomers.

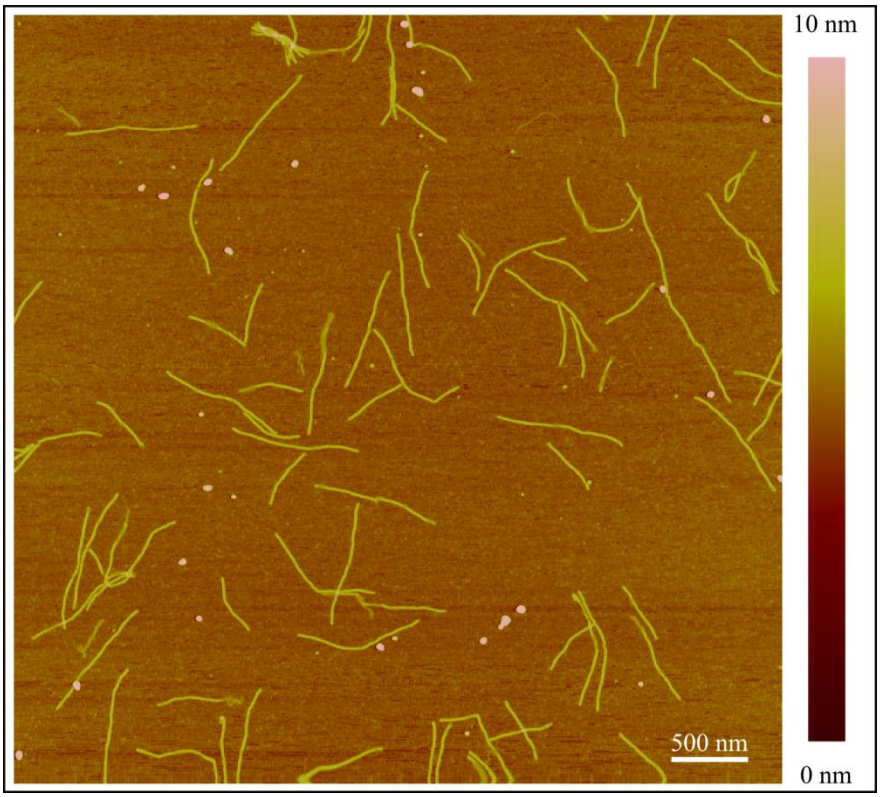

Figure 3.3: Atomic force microscopy (AFM) micrograph showing successful dimerization of uniquely structured head and tail nanotube monomers.

3.3: Yield for Head to Tail Dimers

The tail monomers were functionalized with biotin using a 71 nm periodicity (see Section 4.2). The biotin molecules allowed attachment of streptavidin conjugated QDs, thus enabling the distinction of tail monomers versus head monomers via atomic force microscopy (AFM) analysis. A 25 nM solution of the biotinylated nanotubes was reacted in a 1:4 ratio of nanotubes to biotin using 1μM QD solution. After reaction with QDs, the tail solution was reacted with an equal volume of 25 nM head nanotubes. This solution was reacted for 2 hours at 37ºC before a 5 μL aliquot was removed for AFM analysis. Four 10 μm x 10 μm AFM micrographs were obtained and the structures

binned into the following categories: dimer, head nanotube, tail nanotube, indeterminate. Indeterminate was defined as a monomer that had a QD in close enough proximity that it was not possible to determine if there was an attachment event or if the QD was deposited on the mica near the structure by random chance alone. To be counted, each structure was required to be clearly distinguished from any neighbors. Figure 3.4 shows example structures.

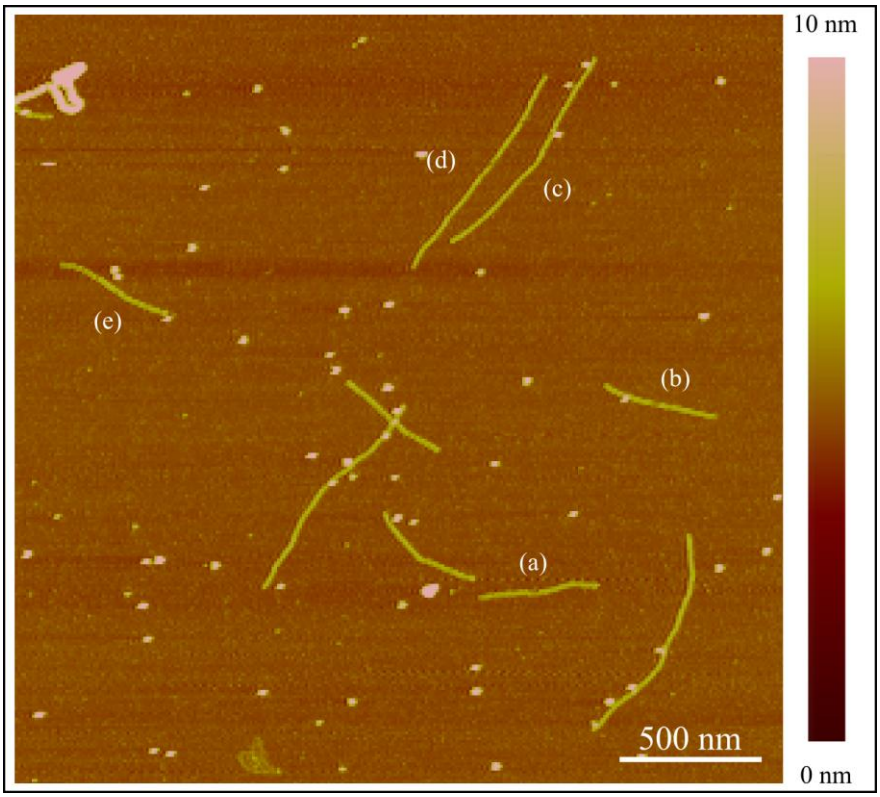

Figure 3.4: Dimerization of head nanotube monomers and tail nanotube monomers with five biotinylated sites. Results of the process include (a) unreacted head monomers, (b) unreacted tail monomers, (c) dimer structures, (d) anomalous structures, in this case a possible head-head structure or a head-tail structure with no attached QDs, (e) indeterminate.

Results of the analysis showed 157 dimers, 65 head monomers, 102 tail monomers, and 59 indeterminate monomers. Total number of items counted, *N*, was 383.

Calculating the yield as a straight percentage of *N* produces a yield of 41%. However, this under-represents the true yield since it takes two monomers to create a dimer. Effectively, there were 314 monomers required to create 157 dimers. Calculating yield taking this into account by counting a monomer as ½ a dimer produces a yield of 60%. The true yield likely was somewhere in between.

3.4: Conclusion

Heterodimers were successfully created from six-helix DNA origami nanotubes with a yield of 41% to 60%. These tests confirm that dimerization as conducted by Douglas *et al*. [87] is possible using linker strands alone with the simplified nanotubes developed by Bui *et al.* [89]. Jungmann *et al.* [106] used a similar linking method to arrange DNA origami tiles with attached streptavidin into ribbons, but this is the first known example of QD functionalized dimerized DNA origami nanostructures.

This method could likely be extended to connect three-dimensional DNA origami at different angles, and even stacked in a three-dimensional superstructure.

Extending the linking domains, thus increasing the melting temperature could increase yield. Forty-nine base pair bonds were involved in dimerizing the nanotubes compared to 64 for Douglas *et al.* [87]. The length of each linking domain ranged from 7 to 10 base pairs. Melting temperatures ranged from 44ºC to 16ºC with an average of 28ºC.

CHAPTER 4: FUNCTIONALIZATION

4.1: Introduction

To create DNA-based nanoscale devices, functional nanomaterials must be arranged with nanoscale precision. In this study, two types of nanoparticles were arranged using DNA origami nanotubes described in Chapter 2: semiconductor QDs and AuNPs.

Sharma *et al.* created the first periodic QD array by incorporating a biotin labeled DNA strand into a selection of tiles. The tiles were self-assembled into sheets forming an array of biotin molecules. When streptavidin conjugated QDs were added to the solution containing the biotin arrays, they selectively bound to the biotin sites creating the QD array [45]. Bui *et al.* [89] used a similar method but used a modified version of the DNA origami nanotubes developed by Douglas *et al.* [87] in lieu of tiles. The study by Bui *et al.* is presented here in brief.

4.2: Streptavidin Conjugated Quantum Dots

It was desired to create a linear array of biotin molecules as a binding site for streptavidin conjugated QDs down a single helix of the six-helix DNA origami nanotube described in Chapter 2. By choosing a staple strand from the first unit cell in the motif to contain the biotin binding site, a total of 29 binding sites on a single helix could be obtained due to the one extra unit cell. The 3' end of each of the H4 staples (H4-C1, H4-C4…H4-C85) was chosen as the location of the biotin, thus the 29 binding sites would be

located on helix 6. The modified staple strands were purchased from a commercial manufacturer (Integrated DNA Technologies) with a 5-mer polythymine tether added as a spacer between the biotin and the surface of the nanotube. These strands were incorporated into the structure during synthesis by omitting the unmodified staple strands in the locations where the biotin was desired.

The minimum distance between binding sites is one motif, or 14.3 nm. Four periodic structures were designed based on this dimension with 14.3 nm, 28.6 nm, 42.8 nm, and 71.4 nm periodicities, corresponding to 29, 15, 9, and 5 binding sites. For simplicity, these structures will be henceforth written shorthand as QDA*x*, for quantum dot array and *x* number of binding sites. The periodicities are written in truncated lengths. For example, the 15 site, 28.6 nm period nanostructures will be referred to as QDA15 with a 29 nm period design. A scale schematic of these designs is shown in Figure 4.1.

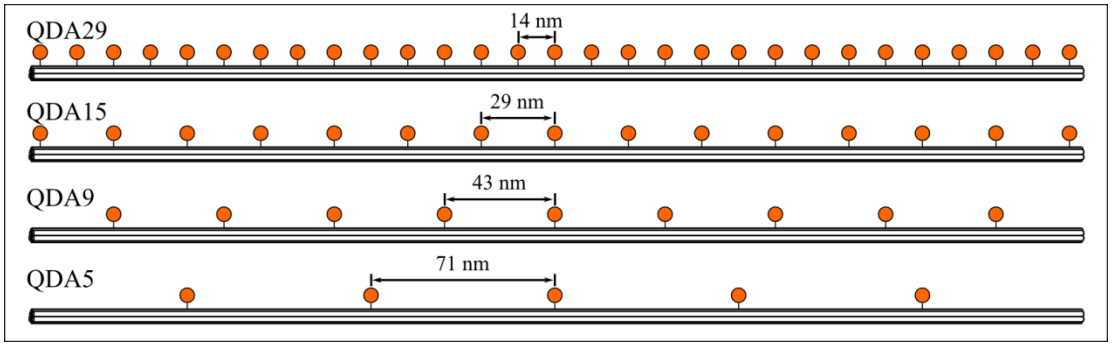

Figure 4.1: Quantum dot arrays were created on DNA origami nanotubes using biotinylated staple strands. Four periodicities were created: 14 nm, 29 nm, 43 nm, and 71 nm with possible numbers of attached streptavidin conjugated QDs of 29, 15, 9, and 5, respectively. The naming convention for each design is QDA*x* where *x* corresponds to the number of binding sites. The figure is drawn to scale, omitting the streptavidin coating on the 5 nm in diameter QDs (orange).

Streptavidin conjugated QDs (Invitrogen, QDot 585) were reacted with the biotinylated nanotubes for two hours at room temperature. QD solutions were diluted to 200 nM with 1x TAE Mg^{++} buffer. Nanotube solutions were diluted with 1x TAE Mg^{++} buffer to a concentration of 1 nM. Reactions were conducted in equal volumes, irrespective of the number of binding sites.

The number of attached particles was determined via atomic force microscopy. AFM samples were made by depositing 5 μL of quantum dot array nanotube solution on a freshly cleaved mica surface followed immediately with a 20 μL aliquot of 1x TAE Ni^{++} buffer. This was similar to the buffer used during synthesis but nickel acetate was used in lieu of magnesium acetate. The mixture was allowed to incubate for 5 minutes before being rinsed with three 100 μL aliquots of ultra-pure water. The excess liquid was dried using laboratory grade compressed nitrogen.

The numbers of attached nanoparticles were counted visually from the AFM micrographs. The mean attachment probability, *p*, was determined by:

$$p = \frac{\sum attached\_QD}{\sum available\_sites} \tag{4.1}$$

Probabilities of attachment were calculated to be 0.77, 0.76, 0.68, and 0.64 for QDA5, QDA9, QDA15, and QDA29, respectively. The two QD arrays with the largest periodicities had similar *p* values, as did the nanotubes with the two smallest periodicities. There was a step function between these two groups, though, indicating a blocking mechanism present at smaller periodicities but not the larger periodicities. To confirm this observation, it was postulated that if each attachment event had an equal

probability of occurring for each attachment site, then the distribution of attached particles should follow a binomial distribution where the probability that *m* QDs are attached to a nanotube with *n* available sites is *P(m)*:

$$P(m) = \frac{n!}{m!(n-m)!} \cdot p^m \cdot (1-p)^{(n-m)} \tag{4.2}$$

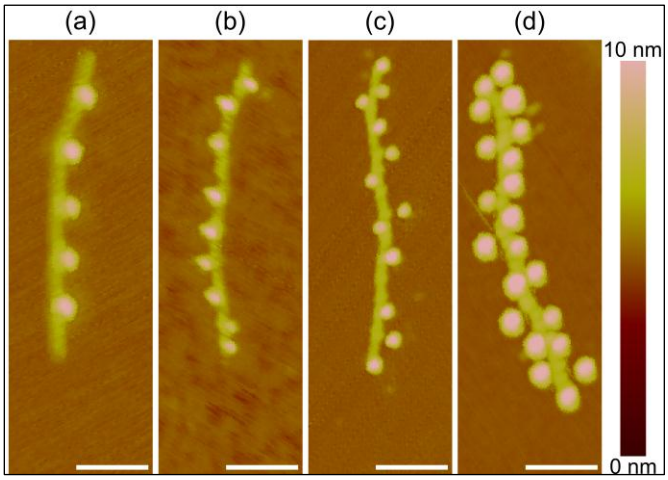

Figure 4.2: Representative AFM micrograph in height scale of the four QD array nanotube designs. The designs are (a) QDA5, (b) QDA9, (c) QDA15, and (d) QDA29 with periodicities of 71 nm, 43 nm, 29 nm, and 14 nm, respectively. Scale bars are 100 nm. Note that the actual number of attached QDs is less than the designed value for (c) and (d). Adopted from [89].

As shown in Figure 4.3, for QDA5 and QDA9, the actual extent of attachment, represented by the histograms, was very close to the binomial distribution, represented by the lines. However, for the QDA15 and QDA29 designs, the actual number of attached QDs was less than predicted by the binomial distribution. This supported the notion of a blocking mechanism that affected the attachment when the periodicity became smaller than 43 nm. It was postulated that the effects of steric hindrance, bridging of adjacent sites, or both steric hindrance and bridging were responsible for the shift in attachment probability. Steric hindrance is when a particle blocks access to a location by occupying

space nearby. Bridging occurs when a particle is large enough to span between two or more binding sites.

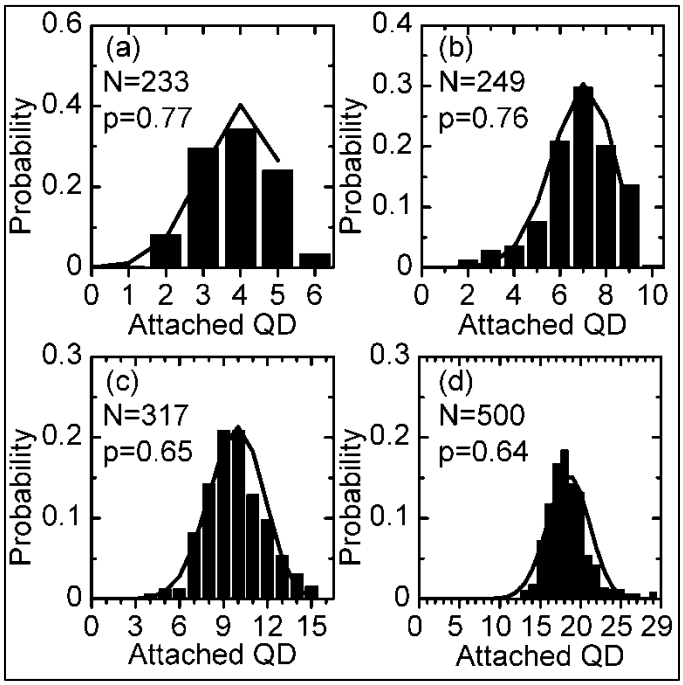

Figure 4.3: Calculated binomial distribution of attached QDs (line) vs. histogram data (bars) for (a) QDA5, (b) QDA9, (c) QDA15, and (d) QDA29 designs with periodicities of 71 nm, 43 nm, 30 nm, and 15 nm, respectively. The *p* value in each plot is the probability of attachment and *N* is the nanotube population size. The binomial distribution modeled the actual data well for (a) and (b), but (c) and (d) showed actual attachment that was lower than predicted. This indicated that the assumptions of the binomial distribution—equal probability of attachment for each binding site—was not supported by the data and thus a blocking mechanism was suspected to occur at periodicities less than 43 nm. Adopted from [89].

To determine the natural periodicity of each design (e.g., how did the nanoparticles distribute themselves since not all binding sites had equal probability of attachment), the center-to-center distance of nearest neighbor nanoparticle was measured for a population of nanostructures from each design. In Figure 4.4, the histograms indicated that, for the QDA5 and QDA9 designs, the preponderance of nearest neighbor distances was close to the design periodicities of 71 nm and 43 nm, respectively. For the

QDA15, the preponderance of the data was in the range of 40-50 nm, and for QDA29, the range was 35-40 nm. The larger center-to-center distance demonstrated by the QDA15 compared to QDA29 was likely due to the discrete nature of the binding site distances where actual binding events occurred predominately with one and two design periods between them, giving an average separation in the range of 43 nm. This data supports the earlier data shown in Figure 4.3 that steric hindrance becomes a problem around 43 nm for QDs, and that this may the predominant blocking mechanism for attaching streptavidin conjugated QDs with small periodicities. If bridging were more prevalent for the QDA29, it was expected that there would have been a higher number of nanoparticles in the range of 28-29 nm apart, but Figure 4.4 (d) indicates that these occurrences were rare.

Another important piece of information supporting steric hindrance obtained in the Figure 4.4 data was that no center-to-center distance was less than 20 nm. Twenty nanometers was the upper-size limit the quantum dot manufacturer provided for the aggregate diameter of the QD core and streptavidin coating. This suggests that, at a range of about twice the diameter of the QD, further attachment is encumbered due to the presence of the first attached QD, but attachment stops completely when the center-to-center distance is equal the particle diameter. The encumbrance can be explained by random motion of the QD and random motion of the nanotube itself in solution. Both are vibrating and translating through space and it can be imagined that a 20 nm particle on a flexible tether could act as a flail, impacting free nanoparticles as the approach the next binding site.

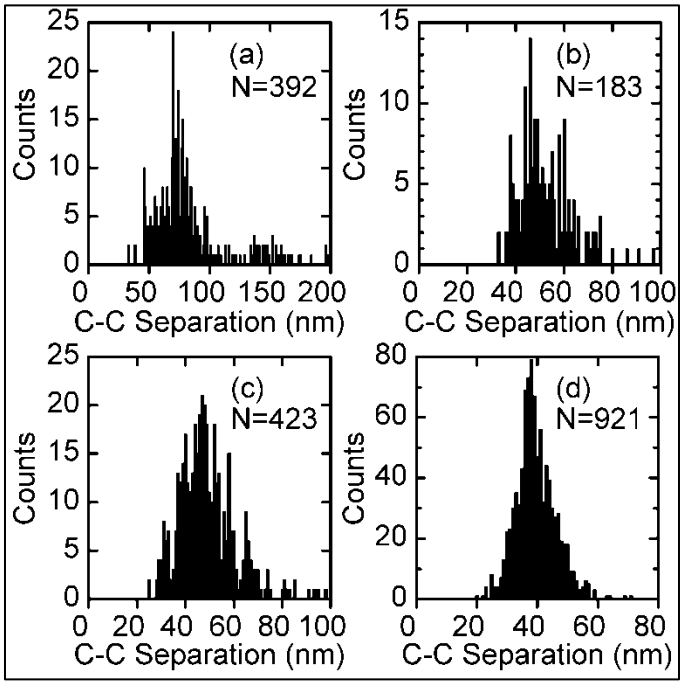

Figure 4.4: Center-to-center nearest neighbor distances of attached QDs for (a) QDA5, (b) QDA9, (c) QDA15, and (d) QDA29. Distances were close to the designed periodicity for (a) and (b). For (c), the majority of particles were separated by 40-50 nm, and for (d) the range was 35-40 nm. It is likely that steric hindrance began to have an effect around 40 nm. No center-to-center distance was less than 20 nm, the upper-size limit of the streptavidin conjugated QD. It is likely that the first QD to attach rotated about its tether like a flail, blocking other nanoparticles from adjacent sites. No nanoparticle could get closer than 20 nm to another due to physical contact between the streptavidin coatings. The QDA29 nanostructure is the only one with a periodicity small enough to bridge, but it was expected that if bridging occurred there would be a high degree of binding events 28-29 nm apart, but there were only a few. Thus, this data suggest steric hindrance is the predominant mechanism of blocking for the two smaller period nanostructures. Adopted from [89].

Other mechanisms that could have reduced the probability of attachment for all of the designs were site poisoning due to loose streptavidin, missing biotin, and intercalated biotin. However, these should have affected all of the periodicities equally. These mechanisms could have reduced the probability of attachment as a whole, hence the maximum probability of only 0.77 for five nanoparticles, but they could not explain the dichotomy. A visual guide to site blocking mechanisms is given in Figure 4.5.

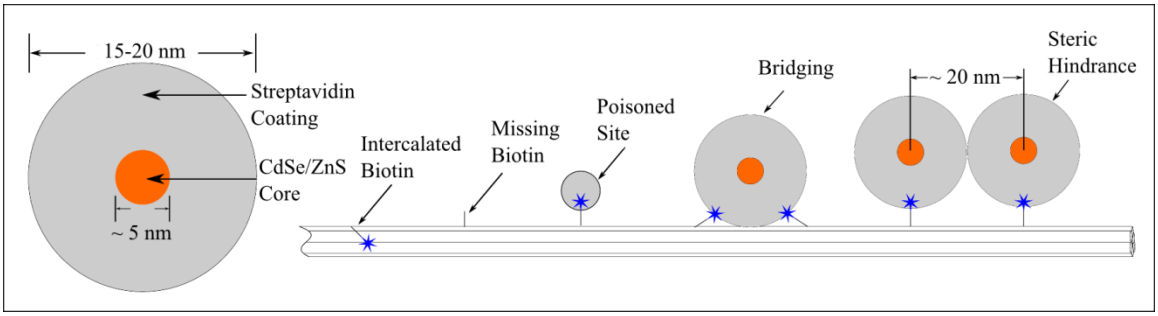

Figure 4.5: Mechanisms of site blocking. The QD consists of a CdSe/ZnS core with an average diameter of 5 nm surrounded by a streptavidin coating. The aggregate diameter with a streptavidin coating is 15-20 nm. Intercalated biotin is when the biotin is extended into the nanotube rather than extending outward from it. A staple strand with a missing biotin would not form a viable binding site. Site poisoning can occur if free streptavidin in solution finds a biotin before a QD does. Bridging can only occur when the period size is less than the diameter of the bonding material and two or more binding sites get occupied by a single nanoparticle. Steric hindrance—physical exclusion due to occupation by another body—could be an issue if the period is less that the diameter of the QD conjugate.

4.3: DNA Conjugated Gold Nanoparticles

The first use of DNA conjugated AuNPs was to create close-packed nanoparticle arrays [11, 12]. ssDNA sticky ends were attached to AuNPs via a thiol bridge. The complementary DNA oligonucleotides were added to the ssDNA conjugated AuNP solutions to bring the AuNPs together. This method has since been used to incorporate AuNPs into tiles [5, 33-37] and scaffolded DNA origami [76, 78]. Ding *et al.* [77] used a DNA origami triangle borrowed from Rothemund [55] to arrange AuNPs in precise locations and were even able to differentiate sites by sequencing. In this study, the QD array origami nanotubes used by Bui *et al.* were modified, exchanging biotin for DNA sticky ends to arrange DNA conjugated AuNPs.

4.3.1: Single ssDNA Sticky Ends

Utilizing the same six-helix DNA origami nanotube, used in the quantum dot array experiment (Section 4.2), the biotin binding sites were replaced with a 15 nucleotide sticky end. The sticky end sequence was named *SA* (*strand A*) and was designed to have a low self-affinity using an in-house program written by Bernard Yurke at Boise State University. The program uses an evolutionary algorithm that minimizes self-complementarity 2 to 3 bases at a time. The strands were ordered from a commercial vendor (Integrated DNA Technologies) and were integrated during synthesis in the same manner as the biotinylated strands. Design names were changed to AuNPA*x* for gold nanoparticle array, *x* binding sites, thus there were AuNPA5, AuNPA9, AuNPA15, and AuNPA29 nanostructures. The complementary strand to SA, *cSA*, was added to the 5' end of a 12-mer polythymine spacer and attached to 5 nm AuNPs via a thiol linker. The Department of Chemistry at Boise State University synthesized AuNPs with 5 nm nominal diameters and conjugated them with the cSA-polythymine complex using a thiol linker on the 5' end of the tether (see Appendix 2).

Reaction of the modified nanotubes and AuNP was controlled to maintain a 2:1 ratio of nanoparticles to binding sites. Initial results were obtained by reacting for two hours at room temperature in a 1x TAE Mg^{++} buffer solution. AuNPs were expected to diffuse to the surface of a nanotube where intimate contact between complementary sticky ends would allow hybridization and attachment as shown in Figure 4.6. Hybridization is believed to occur in two steps: an energetically unfavorable nucleation step (free energy estimated to be between 1.8-6.0 kcal/mol) followed by the energetically favorable helical 'zippering' [107]. Nucleation for DNA hybridization is defined to the

first complete base pair binding event and is the rate limiting step for duplex formation. Once the nucleation process begins, the particle is partially stabilized in the location of the complement strand allowing for hybridization to continue to completion. AFM was used for analysis. Representative atomic force micrographs of each design are shown in Figure 4.7. The results are summarized in Table 4.1.

The probability of attachment for all four designs using the ssDNA sticky end method was lower than for the streptavidin-biotin ligation QD attachment method. There is an anomaly were the 71 nm period structure showed a lower *p* value than the 43 nm nanostructure. There was a similar dichotomy between the two larger period nanostructures and the two smaller period structures, as was seen with QD attachment. However, an even greater difference in the probability of attachment was seen between the AuNPA15 and the AuNPA29 nanostructures. Although hindering effects are similar for AuNPA5, AuNPA9, and AuNPA15, a significant difference is seen when the periodicity drops to 14 nm in the AuNPA29 structures.

Table 4.1: Summary data of probability of AuNP attachment using DNA sticky ends for four periodic designs. QD attachment is via streptavidin-biotin ligation. The results of QD attachment are from the previous study and reported here for comparison [89]. Both binding mechanisms show a dichotomy between the two designs with large periodicity and the two with the smallest periodicities; indicating different blocking mechanisms as the periodicity decreased.

Design Name	Nominal Periodicity	no. of binding sites	n	AuNP p value	QD p value[a]
AuNPA5	71 nm	5	100	0.63	0.77
AuNPA9	43 nm	9	63	0.67	0.76
AuNPA15	29 nm	15	50	0.59	0.65
AuNPA29	14 nm	29	50	0.38	0.64

[a]Data from Bui *et al.* [89]

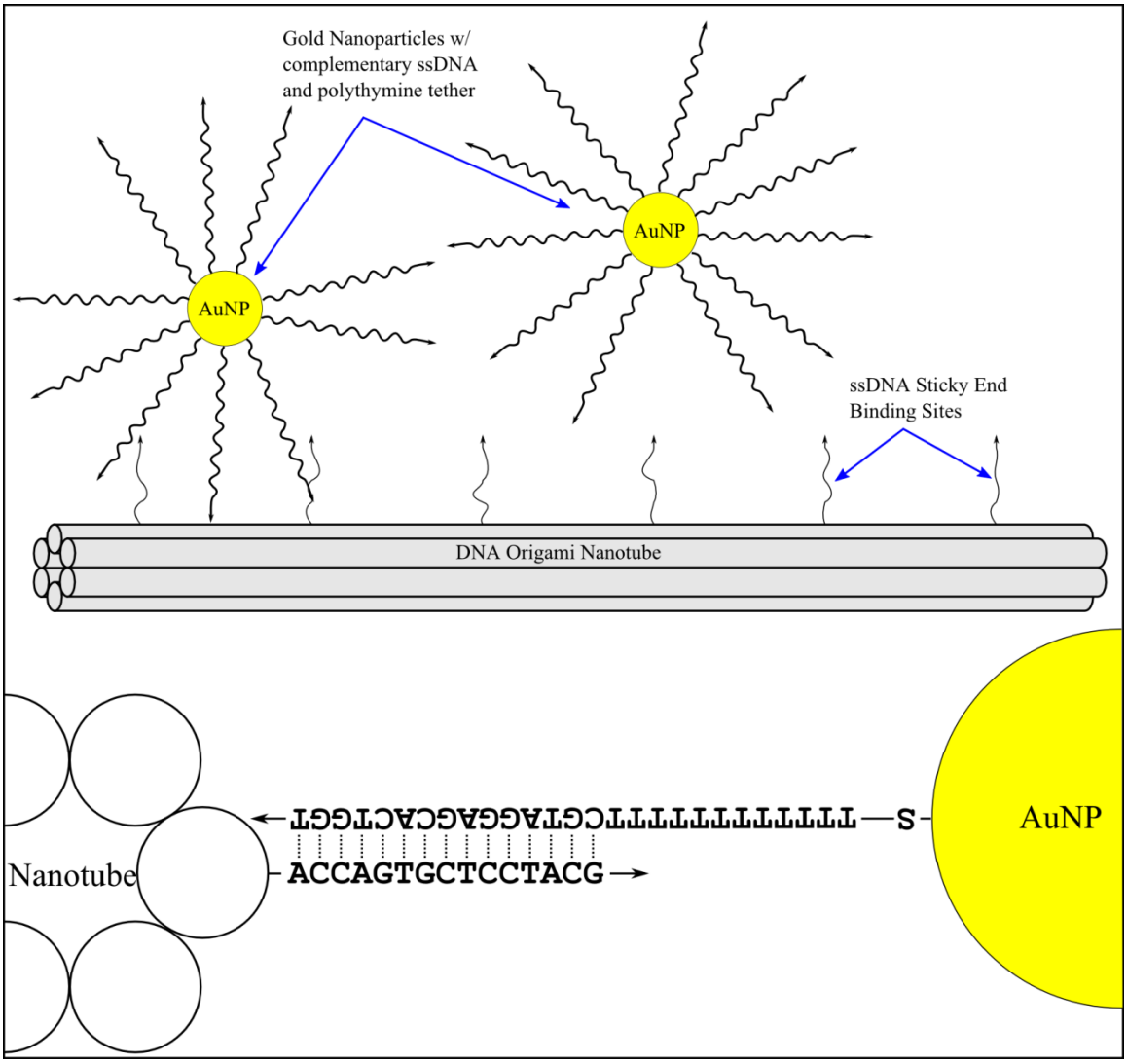

Figure 4.6: Attachement of AuNPs to DNA origami nanotubes was achieved using complementary sticky end oligonucleotides. Fifteen-nucleotide SA sticky ends were designed to extend outward from the surface of the nanotube at specific locations. Complement strands at the end of 12 nucleotide polythymine tethers were attached to AuNPs via a thiol bond. Oligomer sticky ends on the nanotubes had the same period and number as the previously reported biotinylated nanotubes. The number of oligomers attached to each AuNP is estimated to be in the range of 50-100. Enlarged view of nanotube and AuNP is drawn to scale.

It is likely that bridging is the predominant blocking mechanism in these structures with steric hindrance and electrostatic repulsion contributing to a lesser degree. Bridging is suspected of causing the large difference in *p* value between the AuNPA15

and AuNPA29. Each 5 nm diameter AuNP with 15 nucleotide sticky ends and 12 nucleotide polythymine spacers had an effective diameter of approximately 27 nm based on ssDNA. The 14 nm period of the AuNPA29 is well within this range whereas the next larger period device, AuNPA15, with a 29 nm period is just outside the bridging range.

The distance that QDs were suspected of causing steric hindrance was approximately twice their diameter. Applying the same rough calculation in this case would mean that the range at which an attached AuNP could block an incoming AuNP would be approximately 54 nm. Although this distance is greater than the period of the AuNPA9, there is no conclusive difference in attachment probability between it and AuNPA5. It is possible that the hydrated radius of the ssDNA is not as large as the fully extended strands would suggest. Parak *et al*. determined that the length and number of oligonucleotides attached to the surface of a AuNP determine their configuration [108]. When the surface of the AuNP is fully saturated with ssDNA via a thiol linker, oligonucleotides up to 30-mer extend to their full lengths. The oligonucleotide sticky ends attached to the AuNPs in this study fall into that range at 27-mer. Oligonucleotides with low surface concentrations were found to wrap around the AuNP due to non-specific interaction with the gold. Parak *et al.* found that saturation of 10 nm diameter AuNPs occurred when the ratio of ssDNA to AuNPs was ~750:1. The nominal diameter of the AuNPs used in this study was 5 nm, thus the surface area was 1/4 that of those used in the study by Parak *et al.* Thus, the required ratio to saturate the surface of the 5 nm AuNPs would be ~190:1. The ratio used to conjugate the AuNPs in this study was 50:1 (Appendix B), therefore it is likely the surface was not saturated and the ssDNA on the surface of the AuNPs was in some form of a random coil with a length shorter than its

fully stretched length. If the oligonucleotides were only extended half of their full length, the hydrated radius would be 13.5 nm, yielding an expected range of steric hindrance of 27 nm. This distance is much closer to the 29 nm periodicity of the AuNPA15 but far from the 43 nm periodicity of the AuNPA9. This could explain the small step function in attachment probability between these two structures.

Zhang *et al.* suggested that electrostatic repulsion between the ssDNA sticky ends on neighboring AuNPs was likely to blame for the lower than expected attachment efficiency they observed [5]. In that study, tiles arranged ssDNA sticky ends, one per site, with a lateral spacing of 35-39 nm and a diagonal spacing of 25-27 nm. The average center-to-center spacing of attached 5 nm AuNPs reported was 38 ± 1 nm. Electrostatic repulsion was suspected over steric hindrance since the voids in the tile lattice were large enough for a particle to easily fit. The difference between the smallest designed periodicity of ~26 nm and the actual average periodicity of ~38 nm is similar to the difference in periodicity of 29 nm and 43 nm periodicities for the AuNPA15 and AuNPA9 designs, respectively. Since Zhang *et al.* used 15-mer sticky ends on their AuNPs compared to the 27-mer oligonucleotides used in this report, the distance at which electrostatic repulsion caused attachment hindrance was likely even closer to the periodicity gap between the AuNPA15 and AuNPA9 nanostructures.

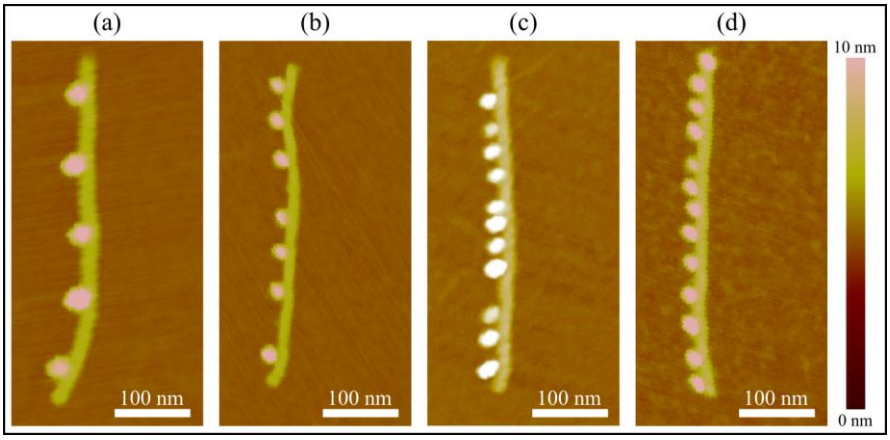

Figure 4.7: Representative AFM height images of the four gold nanoparticle array nanotube designs discussed in this report. The designs are (a) AuNPA5, (b) AuNPA9, (c) AuNPA15, and (d) AuNPA29 with periodicities of 71 nm, 43 nm, 29 nm, and 14 nm, respectively.

4.3.2: Multiple Sticky Ends per Binding Site Attachment

In the study by Zhang *et al.* [5] in which electrostatic repulsion was cited as the primary cause of reduced nanoparticle attachment efficiency, it was noted that tile-based studies by Le *et al.* [34] showed center-to-center distances between AuNPs in the 15-25 nm range were possible by attaching to multiple periodic sticky ends arrange 4 nm apart. This suggested that multiple sticky ends could overcome electrostatic repulsion. While the small center-to-center distances obtained by Le *et al.* were serendipitous, other studies [77, 78] have successfully utilized multiple sticky ends per binding site to attach AuNPs with small periodicities by design. The six-helix DNA origami nanotube design was not optimized for this attachment scheme. However, modifications to the design, which allowed multiple sticky ends in proximity to the desired binding location, were possible.

The 29 available binding sites previously described positioned the sticky end on the 3' terminal end of what would otherwise be a standard staple strand. Other terminal ends were identified that were close to the original binding sites and for which the offset

was exactly the same for all of the binding sites. Figure 4.8 shows a two-dimensional plan view of a staple motif plus one unit cell. The red strands, (a) and (e), represent two adjacent single sticky end binding sites, which will now be referred to as standard binding sites. These are the strands used in the single sticky end attachment scheme (Figure 4.1). The closest staple strand terminal end to (a) is (b), which is on the same helix but extending from the adjacent staple strand in the 5' direction. The next two closest terminal ends are located on helix 5 and shifted to the left as drawn. Site (c) is a 3' sticky end whereas (d) is a 5' sticky end. Combinations of these additional sites were used to augment the standard 3' binding site. The AuNPA9 design was chosen as the initial test vehicle for the multiple sticky end attachment scheme. In addition to the three new sticky ends per binding site, another new strand that replaces the standard site with a serial sticky end sequence was also designed. A serial sticky end was simply two SA sequences, one after another in series on the same ssDNA sticky end.

Note that the binding site is offset from the single sticky end design when sites (c) and (d) are used. Since all of the binding sites shift their centers, the target periodicity does not change. However, the minimum distance between sticky ends in adjacent binding sites does change. The new sticky ends augmenting standard sticky end (a) are 2 nm rotated away from the adjacent standard binding site, (e), on helix 5 but are 4.8 nm closer laterally. Therefore, the left-most sticky ends are 2.8 nm closer to the adjacent standard binding sites.

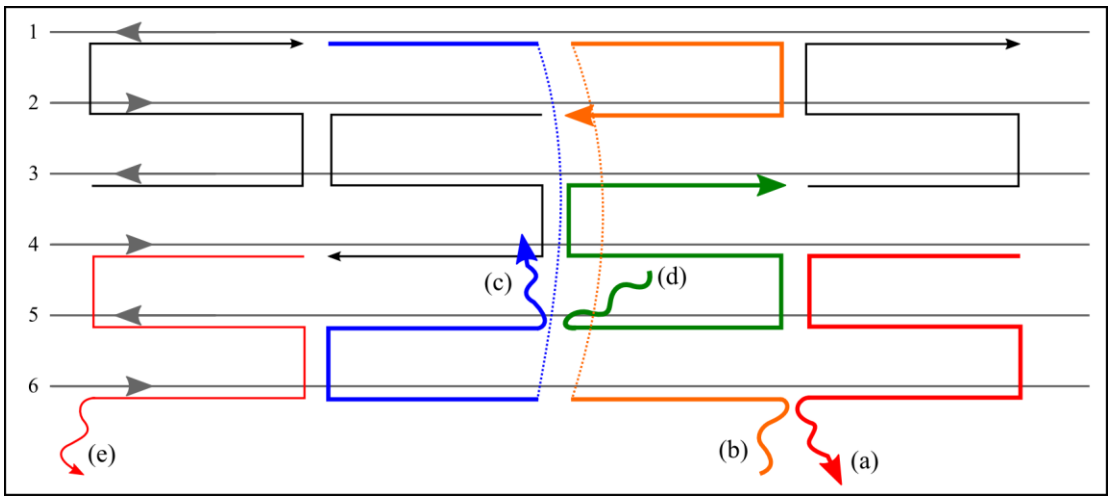

Figure 4.8: Terminal end multiple sticky end binding sites: (a) is the standard 3' sticky end previously used in Section 4.3.1, (b) is the next closest terminal end, (c) and (d) are the next two closest terminal ends located on an adjacent helix. (a) and (c) are 3' whereas (b) and (d) are 5' ends. (e) is the standard binding site for the next lower numbered binding site (e.g., if (a) is binding site 4, (e) would be binding site 3) based on the AuNPA29 periodicity. Other terminal binding sites are available but they are equivalent due to symmetry. Using either (c) or (d) in conjunction with the standard binding site delocalizes the binding site, shifting the expected location of the binding site. While this change does not affect the periodicity, (e) and (c) are now 2.8 nm closer—4.8 nm laterally closer but rotated 2 nm further away on helix 5—than in the case of the single sticky end.

Various configurations of multiple sticky end designs were synthesized and reacted with 5 nm AuNP in a 2:1 ratio of AuNP to binding sites. Solutions were allowed to react for two hours in 1x TAE Mg^{++} buffer at room temperature for two hours. The results are summarized in Table 4.2.

It was determined that the 5' sticky end strands had much lower probability of binding. Two 5' sticky ends had a *p* value of 0.63 compared to 0.67 for a single 3' sticky end. The serial 3' sticky ends increased attachment events, but not nearly as much as two 3' sticky ends located on separate helices. Maximum attachment was achieved with the full complement of four sticky ends per binding site, but the additional two 5' sticky ends did little to increase the *p* value over dual 3' sticky ends, 0.97 compared to 0.95.

Table 4.2: Summary of probability of attachment for several multiple sticky end binding site AuNP arrays. All arrays were based on the AuNPA9 design. Using all four available sticky ends per binding site resulted in the highest extent of attachment at 0.97, but only using the 3' strands was nearly as good with a value of 0.95. *n* is the number of nanotubes counted.

Sticky End Locations	No. of Sticky Ends	*n*	*p*	+/-
5'-5'	2	62	0.63	0.18
3'-5'-5'	3	119	0.89	0.09
Serial 3'	2	87	0.71	0.14
3'-3'	2	96	0.95	0.06
3'-3'-5'-5'	4	63	0.97	0.06

The observation that 5' sticky ends had a lower probability of attachment was expected. Since the AuNPs have the complementary strand oriented to hybridize with an extended 3' strand, the AuNP must be much closer to the nanotube surface in order for the complement strand to be able to contort to the correct orientation to hybridize with an extended 5' strand. It is postulated that a sticky-end-to-sticky-end contact event sufficient to cause a 3' sticky end to hybridize may not allow nucleation for a 5' sticky end. However, a nanoparticle close enough to the surface to allow a 5' binding event would still allow a 3' binding event. This is graphically illustrated in Figure 4.9 (a) and (b).

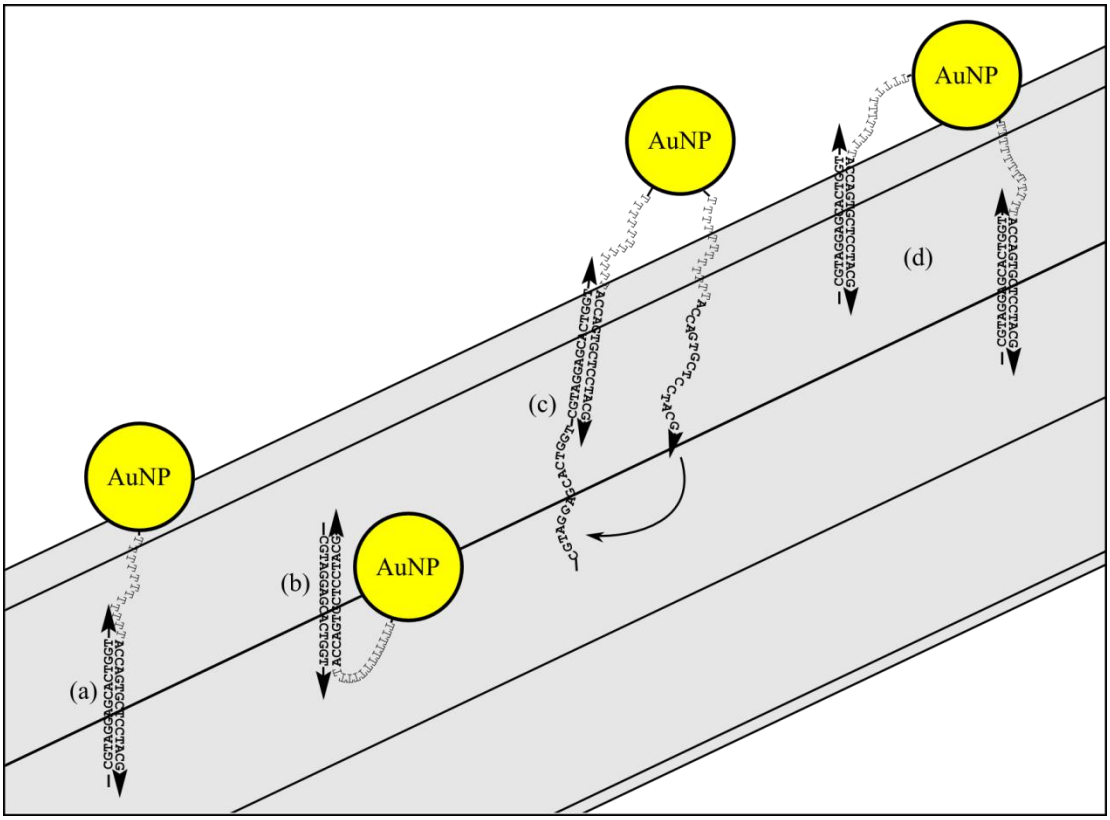

Figure 4.9: Elements of the multiple sticky ends per binding site attachment (not to scale). (a) The standard method of attachment used a single sticky end extending out from the nanotube in the 3' direction to hybridize with the complementary strand on AuNPs, also extending outward in the 3' direction. (b) A 5' sticky end extending from the nanotube required that the AuNP be much closer to the surface of the nanotube for nucleation to begin. This resulted in a lower probability of attachment than a 3' sticky end. (c) Serial 3' sticky ends were designed to capture AuNPs like a grappling hook due to their longer reach. After the nanoparticle was captured, it was expected that other complementary strands on the AuNP would then hybridize with the second sticky end bringing the AuNP as close to the surface as a single 3' sticky end. (d) Dual 3' sticky ends showed high levels of attachment and was chosen as the method of attachment for continued research. The sticky ends are on different helices and separated by one staple strand unit cell. It is possible the delocalization of the binding site on the surface of the nanotube contributed to the success of the dual 3' sticky ends.

It was assumed that the sticky ends extend outward from the surface of the nanotube due to negative charge interaction from the phosphate groups. Likewise, the complementary strands on the AuNPs were assumed to be mutually repulsive and thus

extended outward from the surface of the nanoparticle. If this where the case, there should have existed an effective radius where enough contact is made between the DNA strands to initiate nucleation. The longer the reach of the sticky ends, it was surmised, the larger the effective radius would be. The higher probability of attachment to a 3' end compared to a 5' end supports this assumption since the 5' sticky end lowers the effective radius. The serial 3' sticky ends were expected to have a higher effective radius than the single 3' sticky end and therefore higher probability of attachment. The probability of attachment did increase from 0.67 for a single 3' sticky end to 0.71 for serial 3' sticky ends, however, two separate 3' ends were much more effective than even the serial sticky ends as evident from the *p* value of 0.95.

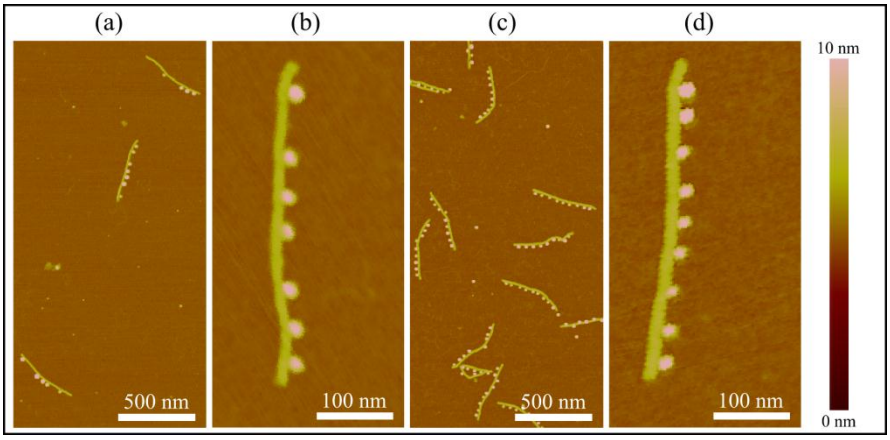

Figure 4.10: Comparison of single sticky end AuNP attachment and dual sticky end attachment. (a) Low and (b) high magnification AFM micrographs of single sticky end AuNPA9 nanostructures. Low extent of attachment is noted and missing nanoparticles can be clearly seen. (c) Low and (d) high magnification AFM micrographs of AuNPA9DT (AuNPA9 structure with dual 3' sticky ends). High extent of attachment can be seen in the sample population with AuNPs evenly spaced.

One possible explanation for the lower *p* value obtained from serial sticky ends compared to two 3' sticky ends separated by one helix is the effect of random coiling of

the binding site sticky ends. It has been shown that ssDNA can be modeled like a polymer and is expected to behave like a worm-like chain [109]. A fully extended chain is entropically unfavorable, thus the chain would be expected to be in a loosely coiled form. If the extent of coiling was very high, the expectation for the serial sticky end to extend outward from the nanotube like a grappling hook may have been incorrect. This could explain the similar probability of attachments for single sticky ends and serial sticky ends. It is possible that the intimate contact necessary for nucleation to begin was initiated by a collision—an actual impact of nanoparticle and nanotube, rather than sticky-end-to-sticky-end interaction in the fluid space. Hybridization initiated by nanoparticle-to-nanotube collisions may explain why the delocalized 3' sticky ends had a significantly higher extent of attachment by occupying more nanotube surface area, thus increasing their probability of encountering the AuNP sticky ends when a nanoparticle-nanotube collision occurs.

Another possibility for the lower than expected *p* value for the serial sticky end is the presence of secondary structure of the serial sticky ends. It was assumed that because the original SA ssDNA strand was designed to exhibit minimal secondary structure, the serial sticky ends would also show low self-affinity. However, analysis using the computer program Nupack [110] indicated that there was predicted secondary structure at room temperature (approximately 25ºC). As shown in Figure 4.11, Nupack predicted a compact structure with two loops connected by four base pairs (the ends of the oligonucleotide are not connected, therefore what appears to be a loop containing the free ends should be a random coil). The mean free energy (MFE) of the structure is -1.01 kcal/mol in solution containing 50 mM NaCl (Nupack does not allow a NaCl

concentration lower than this) and 12.5 mM Mg^{++}. The MFE for this structure is small, on the order of a single hydrogen bond or the energy barrier to nucleation. Still, the potential problem was not the increased energy required to denature the secondary structure during hybridization, but the decreasing of the volume the strand occupies, thus decreasing the probability of intimate contact between complementary strands.

At 37ºC (chosen because this is the temperature at which Douglas *et al.* annealed their nanotubes for dimerization [87]), the predicted structure is a small loop with a MFE of only -0.10 kcal/mol. In solution, this structure would likely not be significantly shorter than a random coil configuration. At 50ºC, the structure is not expected to have any secondary structure. This is the configuration expected from the single sticky end at room temperature; therefore, a reaction at this elevated temperature was expected to closely resemble the reaction as it was expected to occur had no secondary structure been present at during the room temperature reaction.

Two serial 3' sticky end nanotubes solutions were reacted with AuNPs, 1 each for 1 hour at 37ºC and 1 hour at 50ºC with a 1-hour ramp down to room temperature. Post reaction, the *p* values increased to 0.79 (n = 71) and 0.81 (n = 54), respectively. The 37ºC anneal data was skewed since it came from a separate experiment where the ratio of AuNPs to binding sites was increased to 5:1 from the previous 2:1. A 10-hour anneal at 37ºC using a 2:1 ratio resulted in a probability of attachment of 0.83 (n = 70). This data indicated that increasing the temperature to limit or remove secondary structures increased the probability of attachment, but with a rapidly decreasing effect. After 10 hours of reaction at a temperature at which the serial 3' sticky end was expected to behave as a worm-like chain with minimal secondary structure, the probability of

attachment was still 12% lower than what two separate 3' sticky ends were able to achieve in 2 hours at room temperature. Thus, it is likely that secondary structure contributed to the initial lower *p* value of 0.71, but the fact that the probability of attachment never reached that of the room temperature dual offset 3' sticky end design further supports that nucleation begins with a nanoparticle to nanotube interaction rather than sticky-end-to-sticky-end.

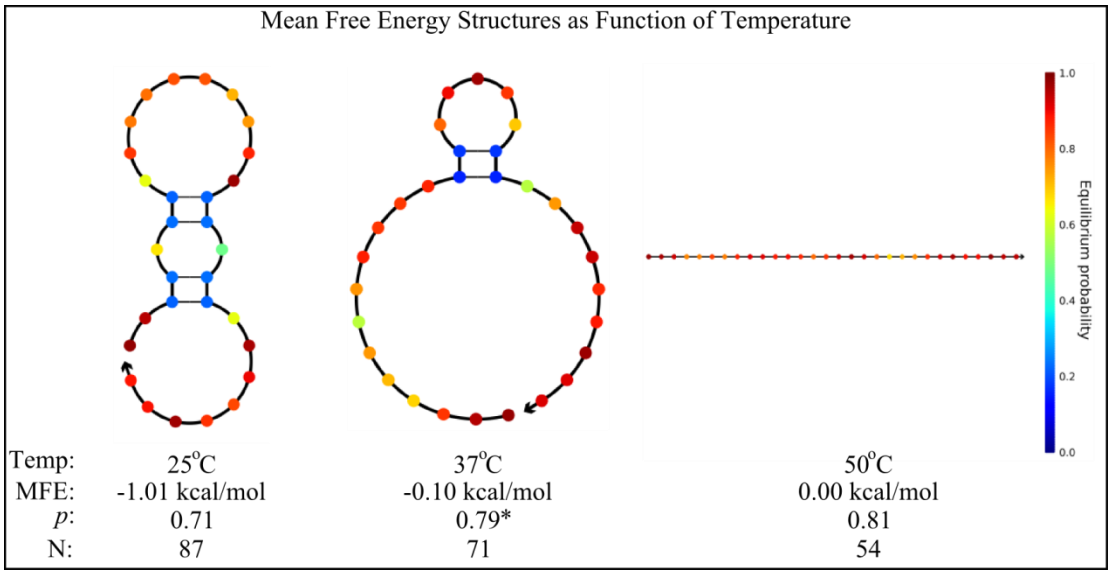

Figure 4.11: Predicted mean free energies (MFE) of the serial sticky end secondary structure at 25ºC, 37ºC, and 50ºC using the computer program Nupack (www.nupack.org) [110]. At 25ºC, approximately room temperature, a predicted secondary structure forms a compact form that may interfere with nucleation. The predicted MFE was in the energy range of the nucleation energy barrier. Note that the ends of the oligonucleotide are free to form a random coil. At 37ºC, the secondary structure is reduced to one small loop with a low MFE. By 50ºC, no secondary structure is predicted. AuNP attachment efficiencies at these temperatures were 0.71 (2 h), 0.79 (1 h), and 0.81 (1 h), respectively. Reactions at 37ºC differed by using a 5:1 nanoparticle to binding site ratio instead of the 2:1 ratio previously used. A 10 h reaction at 37ºC with 2:1 ratio yielded a *p* value of 0.83. Even after 10 h, the efficiency was less than that achieved in 2 h at room temperature by dual 3' sticky ends located on different helices and offset by a unit cell.

4.3.3: Dual 3’ Sticky End Designs

The dual 3’ sticky end method was the most efficient and cost-effective multiple sticky end arrangement in the AuNPA9 design providing 95% attachment with only two modified staple strands per binding site. It was decided to apply this method to the AuNPA15 and AuNPA29 designs to make AuNPA15DSE and AuNPA29DSE structures where the ‘DSE’ indicates dual sticky end. It should be noted that the first binding site on these two designs could not have multiple sticky ends due to its location at the extreme end of the nanotube. The nominal periodicities were again 29 nm and 14 nm, respectively, and the binding site patterns were the same as was used in the QDA9 and QDA29 structures shown in Figure 4.1. All modified staple strands were added prior to synthesis and nanotubes synthesized as normal. A 2-hour 37ºC reaction sequence with 15 minute ramp-down to 22ºC was adopted to eliminate room temperature variation. Reactions utilized the same 2:1 ratio of AuNP to binding site as the single sticky end design. The probabilities of attachment for the AuNPA15DSE and AuNPA29DSE designs were 0.79 (n = 87) and 0.54 (n = 67), respectively. These values were 34% and 42% higher than the single sticky end designs, compared to a 42% increase for the AuNPA9DT design over its single sticky end counterpart.

The AuNPA15DSE design showed many nanotubes with what appeared to be paired nanoparticles. After some observation, it was believed that the nanoparticles were drawn together as the solution dried, perhaps due to mutual hydrophilicity, thus giving the appearance of an aperiodic attachment pattern. As shown in Figure 4.12, paired nanoparticles are nearly touching and had center-to-center distances of (a) 11.4 nm and (b) 13.1 nm. The distance to the adjacent nanoparticles to the left and right were enlarged

as a result. The average center-to-center distance for this design was 27.5 nm (n = 11). Only linear sections of attached nanoparticles (e.g., choosing nanotubes with high attachment and excluding large gaps or areas where the nanoparticles fall to the opposite side of the nanotube) were measured to avoid skewing the data upwards due to the large number of missing nanoparticles. It was estimated that the periodicity was close to the designed value.

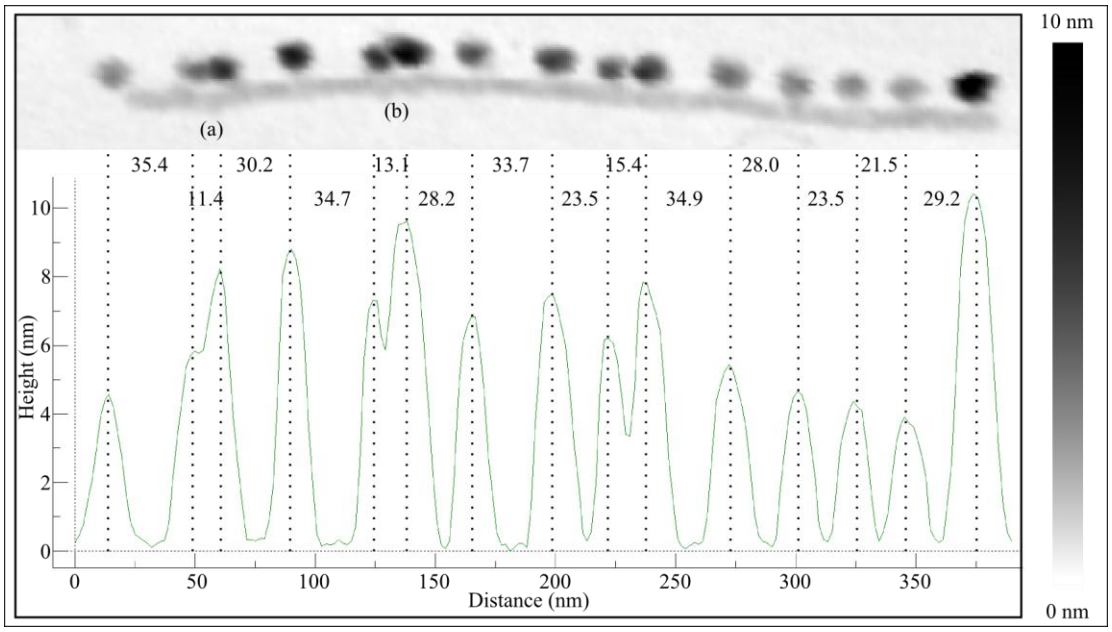

Figure 4.12: AFM micrograph of a representative AuNPA15DSE nanostructure with full attachment of AuNPs. Regions of aperiodicity may be caused by nanoparticles clustering during drying of the sample solution on mica. Center-to-center distances are shown in profile, with units of nanometers. AuNPs can rotate 13 nm even when properly tethered to a binding site, thus two nanoparticles can appear to touch one another as is shown at (a) and (b) where the center-to-center distances are 11.4 nm and 13.1 nm, respectively. This closeness caused the spacing between adjacent nanoparticles to increase to compensate.

The AuNPA29DSE nanotubes looked very similar to the AuNPA15DSE in AFM micrographs. The maximum numbers of attached nanoparticles were 18 and 15, respectively. The mean center-to-center period between nanoparticles on the

AuNPA29DSE nanostructure was 27.9 nm (n = 11), nearly identical to the 27.5 nm periodicity of the AuNPA15DSE design. A representative AFM micrograph of an AuNPA29DSE nanotube is shown in Figure 4.13.

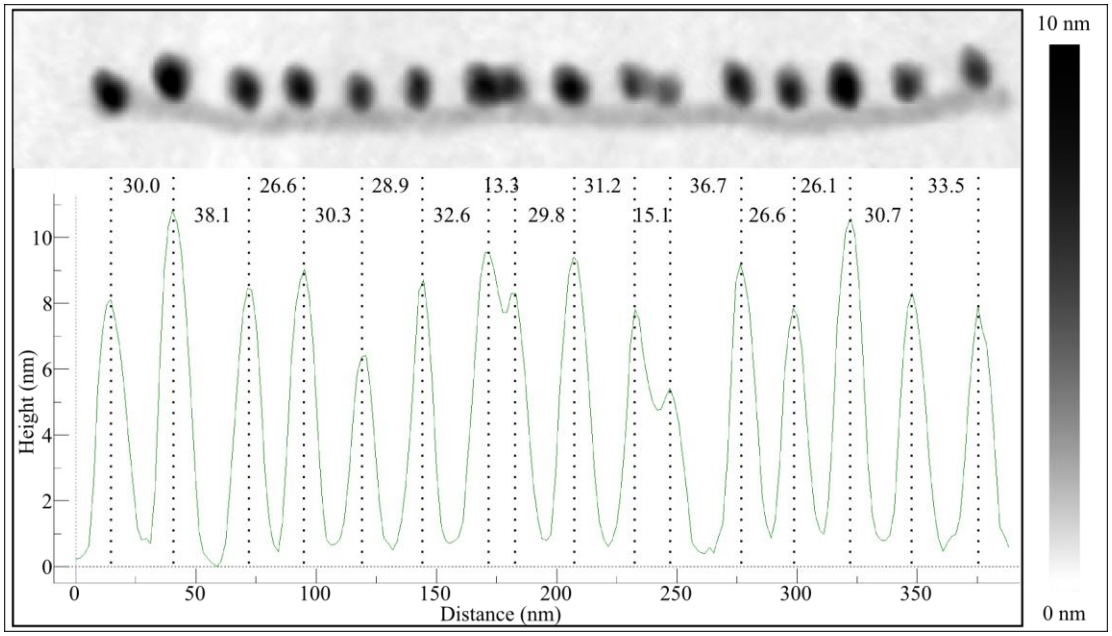

Figure 4.13: AFM micrograph of a representative AuNPA29DSE nanostructure with 16 attached AuNP. The mean periodicity for this structure was 27.9 nm, nearly the same as for the AuNPA15DSE and close to the design value of 28.6 nm.

The periodicities did not change from the single sticky end designs, so steric hindrance and electrostatic repulsion should have had the same level of effect. The minimum distance between sticky ends on adjacent binding sites was reduced by 2.8 nm (see Figure 4.8) compared to the single sticky end design meaning that the AuNPA15DSE design had a minimum distance between sticky ends of 25.8 nm and was therefore within the 27 nm reach of the sticky ends on a 5 nm diameter nanoparticle. It was likely that the increased sticky ends helped increase the probability of attachment per nanoparticle-nanotube contact event, but at the same time the design became more

susceptible to bridging, lowering the number of attachment events from what they could have been if bridging was not occurring.

The 0.54 probability of attachment was expected for the AuNPA29DSE design because the periodicity was so small as to make bridging almost a certainty. The proximity of identical sticky ends on the nanotube made it similar to a four sticky end, 15 site nanostructure with ~29 nm periodicity. The high binding efficiency actually appears to have worked against this structure, locking in nanoparticles with high probability but at the same time occupying the adjacent spot with the same high probability. It is likely that no amount of increased affinity would help achieve higher numbers of attached nanoparticles for this design.

4.3.4: Alternating Binding Site Sequence—AuNPA29ABC

The AuNPA29DSE design was impaired by excessive bridging due to the small gap between sticky ends on adjacent binding sites. In that design, all of the binding site sticky ends had the same sequence. It was postulated that if adjacent binding sites were not complementary with a particular nanoparticle, bridging could be eliminated provided the distance between similar sequence binding sites was greater than the reach of the sticky ends on the nanoparticle. In order to accomplish this, more than one unique DNA sticky end sequence was necessary. This was achieved using an alternating ABC binding site design, where A, B, and C are unique sequences creating uniquely addressable binding sites. Ding *et al.* was able to attach AuNPs to triangular origami with 10 nm center-to-center periodicity by using a similar method [77].

The AuNPA29DSE design was modified to use three alternating 15 nucleotide

sticky ends, designated A, B, and C, that were designed to be minimally complementary to each other. The ABC pattern was repeated until all 29 sites were created. Each binding site consisted of two 3' sticky ends of the same sequence bounded by two binding sites in each direction of differing sequence. The nearest neighbor binding site was 14.3 nm away, however, the next closest same sequence binding site was 3 periods, or 42.8 nm away, the same distance as in the AuNPA9 design. The design is shown drawn to scale in Figure 4.14.

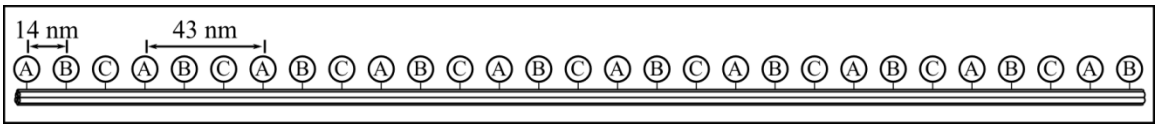

Figure 4.14: AuNPA29ABC nanostructure design. 5 nm diameter AuNPs can hybridize with binding sites 27 nm away. The 14 nm period was likely bridging to a very high degree. Utilizing the extraordinary specificity of DNA, three uniquely sequenced sticky ends were used as binding sites in a repeating pattern. 'A' strands, 'B' strands, and 'C' strands were designed to have minimal interaction and were spaced 14 nm apart to form 29 dual sticky end binding sites. Each like sequence binding site was separated by 3 periods, or 43 nm, the same period as the AuNPA9DT design and well outside the bridging distance. Three solutions of AuNPs were required, each with the complementary strand to only one of the sequences.

Three separate AuNP solutions were required, each with strands complementary to one of the binding sites. Modified staple strands were added prior to synthesis of the nanotubes. The AuNP solutions were added to AuNPA29ABC nanostructures in 2:1 ratios of AuNP to individual binding sites. The solution was reacted using the 37ºC protocol.

The AuNPA29ABC nanostructure was first reacted with B AuNPs only. This was to determine if the extent of attachment would be similar to the AuNPA9DSE design since the periodicity was the same but the sequence was different (all previous designs

used A AuNPs). With the B AuNP only, the ideal number of attached nanoparticles was 10. Experimentally, the probability of attachment was determined to be 0.97 (n = 44) with uniformly distributed nanoparticles. Figure 4.15 shows a representative AuNPA29ABC nanotube with B AuNPs only.

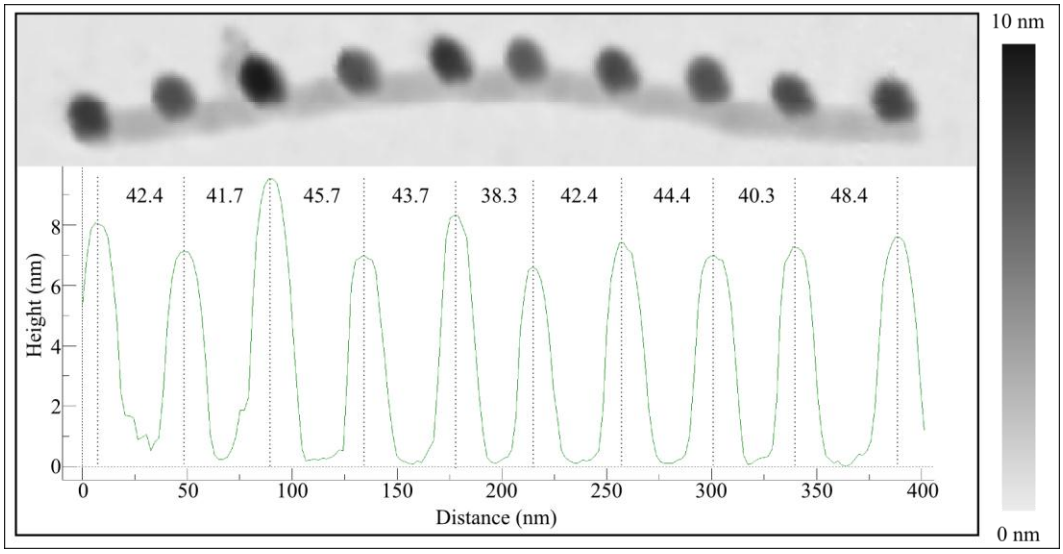

Figure 4.15: AFM micrograph of AuNPA29ABC with B AuNP only. The probability of attachment of 0.97 using a different ssDNA sticky end sequence was similar to the AuNPA9DT design, confirming that the dual 3' sticky end design could successfully be replicated with different sequenced sticky ends. Expected periodicity was 43 nm.

When all three AuNP types were reacted with nanotubes, AFManalysis required quality imaging to resolve individual nanoparticles. Only four AuNPA29ABC structures were imaged with enough detail to count the extent of attachment. On average, 20 nanoparticles were attached for a *p* value of 0.69. Nanoparticles were observed to arrange themselves into groups of two and three. In Figure 4.16, a nanotube with very pronounced pairing of nanoparticles is shown (along with examples of two others). The nearest neighbor distance periodicity alternated between approximately 14 nm (one period) and 29 nm (two periods), indicating that every third nanoparticle was missing. It

was postulated that one or more of the AuNPs had a lower than expected probability of attachment. Individual testing of nanoparticle attachment efficiency indicated that the A AuNP sample (using the cSA sticky end used in the single and multiple sticky end experiments) and C AuNP (using a new sequence) had lower probabilities of attachment than the B AuNP. The *p* values were not calculated. Since the A AuNP design was previously shown to have 95% attachment efficiency, it is likely that the lower than expected extent of attachment was due to batch-to-batch variation rather than a sequence design issue.

It was not possible to obtain new AuNP samples to repeat testing on this structure, however the occasional grouping of three nanoparticles with proper nearest neighbor distance and the increase of the p value to 0.69 from 0.54 indicate that the design is capable of greater nanoparticle extent of attachment.

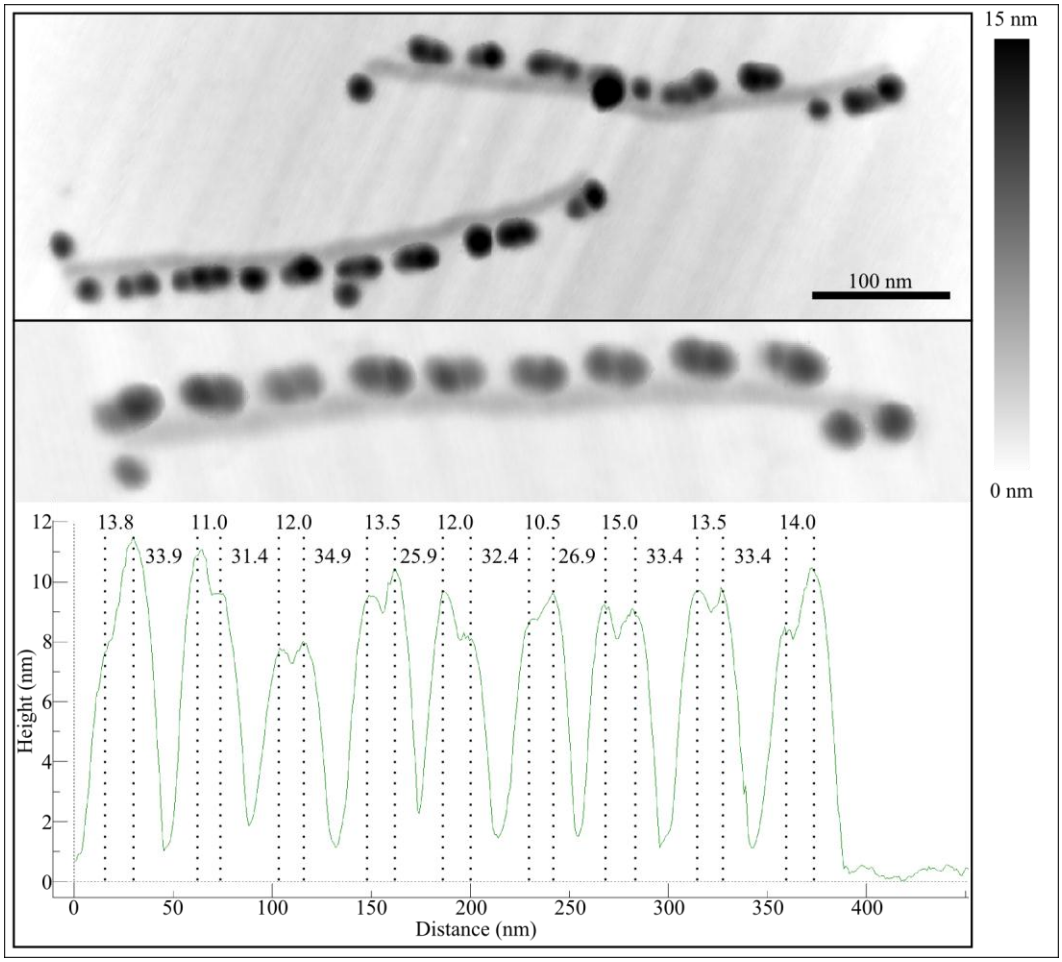

Figure 4.16: AFM micrograph of AuNPA29ABC structure with A, B, and C AuNPs attached. Nanoparticles appear to be clumping in groups of two and three. The periodicity one nanotube with pronounced pairing clearly shows the pattern of missing every third nanoparticle, indicated by the nearest neighbor distances alternating from approximately 14 nm and approximately 30 nm. Attachment efficiency was approximately 0.69, though only four nanotubes could be imaged clearly enough for imaging. This combined with the periodically missing particles indicates that one of the AuNP types was not attaching with the same probability as the others.

4.3.4: Stitched Staple Strand Sticky Ends

One drawback with the terminal sticky end design is that only two sections of each staple strand are available for use: the beginning or the end. A proposal was put forth to use an internal loop containing sticky end sequences that could be placed

anywhere along the staple except the terminal ends. There were several possibilities for sticky end sequencing, but the one that was expected to provide the most bonding potential per loop was a serial 3' sticky end. Similar to the terminal end design, a SA sticky end would be attached to another SA sticky end. Unlike the terminal end scenario, though, in a loop, the effect would be a 3' sticky end and a 5' sticky end due to the strand reversing directions to go back into the nanotube (Figure 4.17 (a) and (b)).

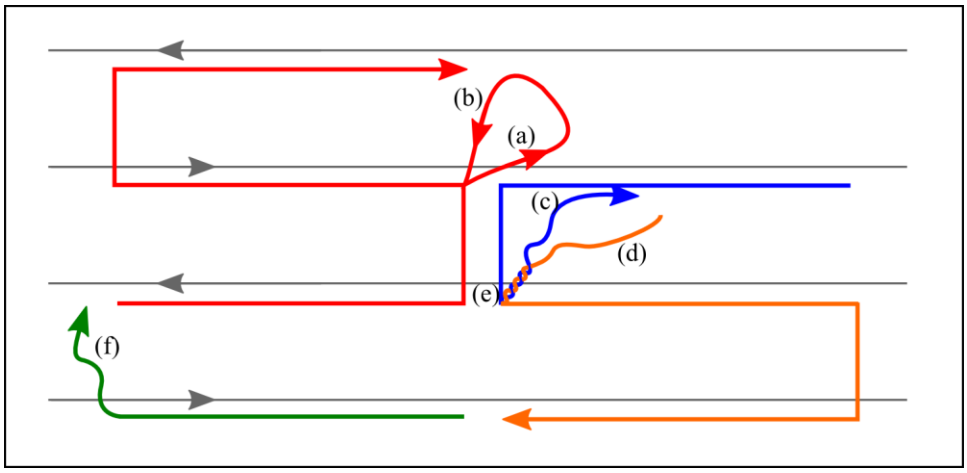

Figure 4.17: Loop and stitched staple strand sticky ends. A loop in the interior section of a staple strand was proposed to locate sticky end binding sites in locations other than terminal ends. The original idea would place two serial sticky ends in the loop creating a 3' sticky end (a) and a 5' sticky end (b) as the loop returns to the scaffold. Each staple strand is 42 base pairs in length, so adding two 15 nucleotide sticky ends would make the staple strand 72 base pairs long. This was expensive and would have low guaranteed yield from the manufacturer. Cutting the strand in the loop would create a 3' sticky end (c) and a 5' sticky end (d) on shorter staple strands. A 5 nucleotide section of complementary sequences on the two short staple strands stiches them together to strengthen the structure and better anchor the shorter of the two strands. If the stitched region was not present, Section (c) would look like Section (f) where only 14 nucleotides and no crossover holds the sticky end in place, weakening the structure.

A challenge with this design was the added length to the staple strand. The final strand length would have been 72 base pairs, dramatically increasing the cost of the strand while lowering the guaranteed yield from the manufacturer. To mitigate these

issues, it was decided to break the staple strands in what would have been the loop, between the serial sticky ends. The result would be two terminal sticky ends, one 3' and one 5' (Figure 4.17 (c) and (d)). While the two sticky ends were desirable, there was the undesirable effect of significantly shortening the staple strands and possibly affecting the stability of the structure by eliminating a crossover. The solution to this problem was to utilize 5 complementary base pairs on each staple at the base of the sticky ends. Since the sticky ends are adjacent, the complementary base pairs were expected to hybridize, thus stitching the staple strands together. The result was terminal 3' and 5' binding sites using staple strands no more than 49 nucleotides in length capable of being placed in internal sites.

Only one structure was designed using this attachment method: the left-hand spiral array. The expected attachment was comparable to dual 3' sticky ends. This design will be discussed in detail in Chapter 5.

4.4: Conclusion

Both streptavidin-biotin ligation and complementary ssDNA sticky ends can be used to attach semiconductor QDs and AuNPs to DNA origami.

The streptavidin-biotin ligation is non-selective and was not able to attach particles closer than 20 nm from its nearest neighbor. It was postulated that steric hindrance from the large streptavidin hydrated sphere surrounding the QD was a limiting factor, with bridging between adjacent binding sites a factor for periodicity lower than 20 nm.

ssDNA sticky ends are extremely site specific but had a lower probability of

attachment when using single sticky ends compared to streptavidin-biotin ligation. It was possible that the ssDNA sticky ends randomly coil, making the surface area available for intimate contact with a ssDNA conjugated nanoparticle much smaller than the expansive hydrated streptavidin molecules.

When dual 3' sticky ends were used, the probability of attachment exceeded that of biotin-streptavidin ligation except for on the AuNPA29DSE nanostructure with its 14 nm period. It was likely that bridging was the limiting factor once the periodicity dropped below the maximum span of the ssDNA sticky ends on the AuNPs.

The problem of specificity and close packing may have been solved by using three different DNA sticky end sequences in an alternating ABC binding sequence pattern. This pattern reduced the incidents of bridging, thus future attachment schemes likely will be designed around this technique.

Even smaller spacing may be possible with the successful use of stitched staple sticky ends, which can be incorporated in the middle of a staple strand.

CHAPTER 5: PURPOSE BUILT DNA ORIGAMI NANOSTRUCTURES

5.1: Four-Helix Bundle Chiral Nanoparticle Array

5.1.1: Background

Linearly polarized light can be modeled as the sum of right-hand circular polarized light and left-hand circular polarized light. The difference in magnitude between these two components due to differential absorption when initially linearly polarized light propagates through a medium is referred to as circular dichroism (CD) [111]. Many biological molecules are chiral and thus produce a circular dichroic effect. CD is an important method used to study conformal changes in biomolecules; the chirality of the molecule itself produces the CD signal. Artificially arranging non-chiral, optically active molecules in a chiral pattern was predicted to illicit a CD response [112]. It was desired to measure the circular dichroic effect introduced by arranging AuNPs in a chiral pattern. To be effective, the nanoparticles would need a precisely controlled pitch and axial rise and have a maximized persistence length. Shen *et al.* performed a similar experiment using a 24-helix, 90 nm x 60 nm DNA origami rectangular sheet [113] borrowed from Rothemund [55]. The sheet was used to align two diagonal lines of AuNPs. Helper strands were added that rolled the sheet up into a 23 nm diameter nanotube with 7 nanoparticles per right-hand helical pitch, 14 nanoparticles total with a center-to-center distance of 16 nm. Kuzyk *et al.* [114] performed a similar experiment using a 16 nm diameter, 24 helix semi-solid DNA origami nanostructure with hexagonal

cross-section of the type developed by Douglas *et al.* [72]. This structure arranged nine AuNPs in either a right-hand helix or a left-hand helix with an axial rise of 57 nm.

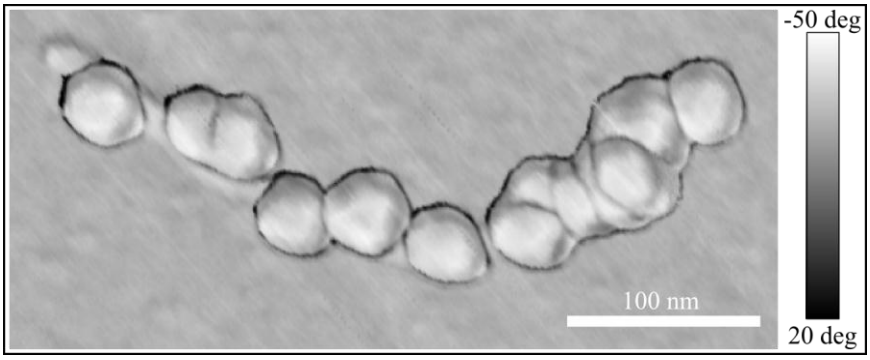

Figure 5.1: Proof of concept spiral array nanostructures. AFM phase micrograph of a six-helix nanotube with single tether binding sites in a right-hand chiral array. Attached AuNPs are approximately 15 nm in diameter.

A spiral pattern was created on the six-helix DNA origami nanotube developed by Bui *et al.* [89] as a proof of concept (Figure 5.1). To maximize the optical response, a purpose built nanostructure designed expressly for the intended experiments was created. The optimized structure was designed to be longer than the six-helix nanotube and arrange as many AuNPs as possible in a 4 particle per pitch spiral with a periodicity of 20 nm between binding sites, center-to-center. The structure chosen to meet these criteria was a four-helix bundle DNA origami nanostructure (4HB). This structure would be 50% longer by reducing the number of helices from six to four and would have the proper number of particles per pitch if each helix held a nanoparticle. A four-helix nanostructure required a square cross-section, and thus a 90º dihedral angle (Figure 5.2 (a)). An axial rise of 16 nm would provide the required 20 nm center-to-center periodicity (Figure 5.2 (b)). Since DNA has a natural right-hand chirality, both right-hand and left-hand nanoparticle chirality were required to ensure any optical shift was

due to the nanoparticles and not the DNA itself.

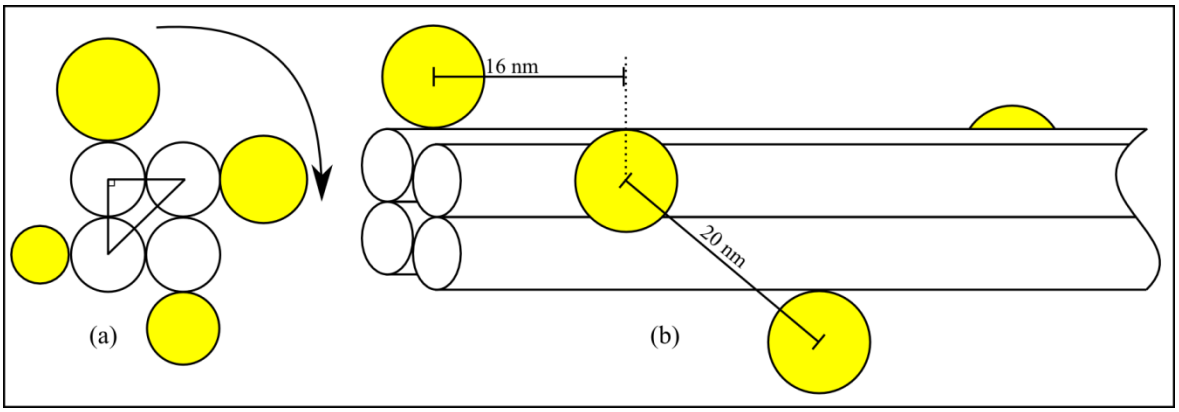

Figure 5.2: Criteria for four-helix spiral array nanostructure. (a) A square cross-section was necessary, thus the dihedral angle required was 90º. The right-hand chirality is shown with AuNPs moving away from the reader. (b) To obtain the desired 20 nm center-to-center periodicity, an axial rise of 16 nm was required.

5.1.2: The Four-Helix Bundle Nanostructure

Before binding site locations could be assigned, the structural design was investigated to determine if the nanostructure was feasible. The 90º dihedral angle could be obtained by twist angles of 90º*n*, where *n* is an integer. As was shown in Figure 2.8, eight base pairs produced a twist angle of 274.3º. This twist angle is close to *n* = 3 = 270º, or 3/4 of a full rotation. Of the available angles, 274.3º showed the least amount of deviation from ideal. The 4.3º excess is considered under-twisted and results in compressive stress [74]. Nevertheless, the angle was deemed close enough to produce origami structures and the ideal angle of 270º was used for design purposes.

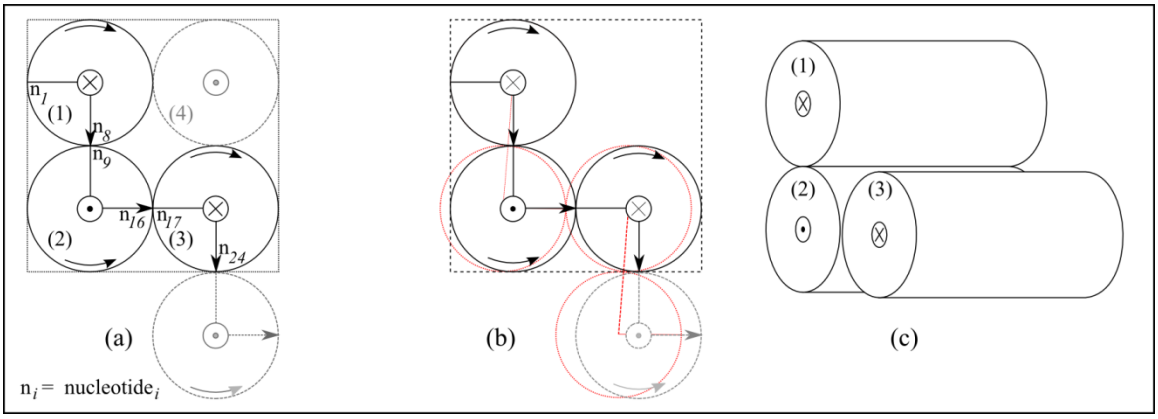

Figure 5.3: Four-helix bundle (a) ideal square cross-section, (b) actual cross section, (c) half unit cell. (a) The ideal cross-sectional shape of the four-helix bundle is a square, requiring a 90° dihedral angle. Recall that the '×' symbol represents the 5' end of a helix and thus a helix drawn axially will be translating 5' to 3' into the page in a right-hand helix. The symbol '·' indicates the 3' end and is coming out of the page. Using the approximation that 8 base pairs creates a twist angle of 270°, starting at n_1 (nucleotide 1) on the left of helix (1) in the plane of the page, translating 8 nucleotides into the page results in a crossover position to helix (2) shown by the downward facing arrow at n_8. Translating another 8 nucleotides toward the reader results in the horizontal crossover to helix (3) at n_{16}. Eight more nucleotides into the page places n_{24} at the edge of the square. If the pattern was repeated once more, the resulting helix would be outside the box and eventually a pleated sheet. Note that the fourth helix needed to form a square has not yet been created. (b) The twist angle created by 8 base pairs is not a perfect 270° but is over twisted by 4.3°. Thus, in reality, the crossovers are shifted as shown by the red helices superimposed over the ideal structure. (c) In three dimensions, this creates three cylinders with equal lengths.

The 4HB emulated a square cross-section, extended to form a rectangular prism by utilizing an 8 base pair spacing between staple strand crossover patterns. Recall from Section 2.3.2 that the symbol '×' indicates the 5' end of a staple strand, thus the strand is translating in a right-hand helix into the page, and the symbol '·' represents the 3' end. A staple strand with this symbol is coming out of the page towards the reader. Referring to Figure 5.3 (a), there are three helices in the square. Starting with n_1 (nucleotide 1) on helix 1 at the far left and translating 8 base pairs into the page results in a crossover between n_8 and n_9 at the vertical line shown between helix 1 and 2. Translating another 8

base pairs on helix 2 out of the page results in a crossover to helix 3 at the horizontal line between n_{16} and n_{17}. Continuing the raster 8 more base pairs into the page on helix 3 places n_{24} at the end of the arrow pointing downward at the edge of the box. If this raster pattern was continued, the result would be a pleated sheet—similar to what was seen with the six-helix nanotube, as illustrated by the helix on the outside of the box. The 4.3^{o} extra rotation in the actual nanostructure causes distortion as shown in Figure 5.3 (b) where the red helices represent the true crossover angles.

Note that helix 4 in Figure 5.3 (a) has not yet been created since no staple strands have been assigned to it. The raster pattern just described would only create the three equal length helices shown in Figure 5.3 (c). If helix 3 from Figure 5.3 (c) were extended 8 more base pairs to create a 16 base pair helix, one half of a pseudo unit cell would be formed as shown in Figure 5.4 (a). A pseudo rotoinversion operation utilizing a 1/4 axial rotation followed by a mirror image creates a structure, 5.4 (b), that could slide into the first half to form a unit cell consisting of 4 helices each 16 base pairs long, 5.4 (c). The unit cell would contain two 24 nucleotide staple strands. A 180^{o} pseudo screw operation with translation of one unit cell would form the staple motif shown in Figure 5.4 (d).

This design was compact, simple and repetitive, but did not yet allow terminal binding sites in a spiral pattern due to the locations of the terminal ends. In order to obtain the desired binding site locations, the terminal end locations would need to be manipulated.

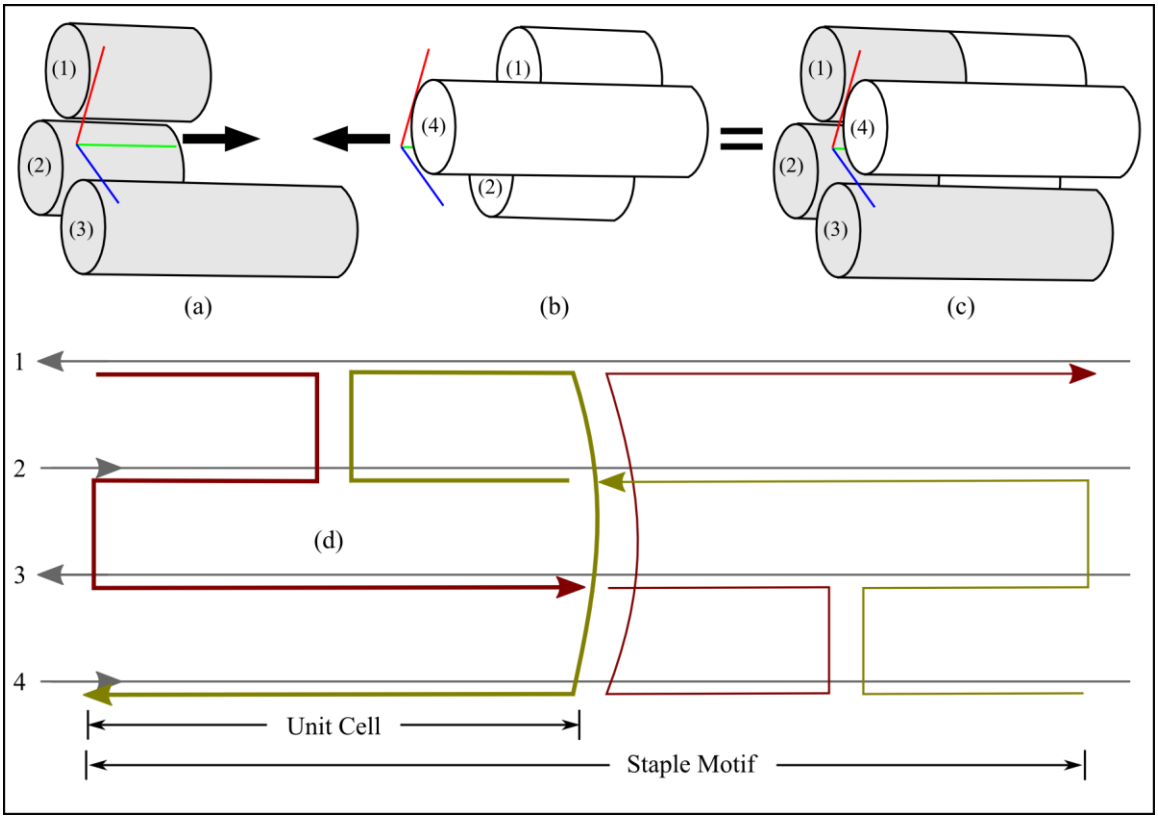

Figure 5.4: The missing helix 4 from Figure 5.3 (c) can be created by a pseudo rotoinversion operation, similar to the six-helix nanotube (Section 2.3.2). By extending helix 3 in (a) another 8 base pairs a structure is created that when a mirror image is created and rotated ¼ turn counterclockwise creates a structure that can nest into the original, as shown (b). The combined structure creates four cylinders of equal length, (c) and creates a pseudo unit cell. A 180º pseudo screw operation, rotation of the unit cell by 180° and translation by one unit cell, creates a staple motif (d).

5.1.3: The Asymmetric Four-Helix Bundle Binding Site Centric Design

The symmetrical structure (Section 5.1.2) indicated that a four-helix bundle was feasible using scaffolded DNA origami techniques. This basic staple motif was modified to make the nanostructure conform to the predetermined nanoparticle arrangement. This was a departure from previously published nanoparticle arrays where the structure dictated the possible periodicity of the nanoparticles. It was shown that 8*n* base pairs between crossover basis, where *n* is an integer, was required. The terminal ends and the

locations of the crossovers could be altered, for each staple strand until the proper binding sites were created, provided that this basis was satisfied. The difficulty lay in navigating the myriad combinations of staple strand patterns. This task was greatly simplified by using the DNA origami computer aided design program caDNAno [71]. caDNAno was developed by Douglas *et al.* at Harvard University and released to the public in 2009. This program allows the user to create structures based on a honeycomb cross-section, such as the six-helix nanotube, or on a square cross section, such as the 4HB. Appendix A contains details on setting up the design in caDNAno. Only the final design is presented here.

Figure 5.5 is the caDNAno screen display showing one staple strand motif. This two-dimensional image simulates a three-dimensional image similar to Figure 5.4 (c). Helices 0 and 1 (by default caDNAno numbers helices starting with 0) are on top and helices 3 and 4 fold clockwise into the page to form the bottom. The motif as shown in Figure 5.5 is broken into two sections to allow easier viewing. Each staple motif was 192 base pairs long with no repeating patterns. The shortest distance between crossovers occurred with $n = 1$ and the longest distance was with $n = 4$. The blue strands represent staple strands that had terminal 3' Strand A (SA) sticky ends, noted by the arrow points in blue circles. The orange strands represent staple strands that had terminal 5' Strand B (designed to bind the B AuNPs from Chapter 4), indicated by the squares in orange circles. The blue strands formed the right-hand spiral whereas the orange strands formed the left-hand spiral. Four single tether nanoparticle binding sites were present per motif per chiral design. The sticky end oligos for both spiral patterns were present at all times. The direction of the spiral array was determined by which AuNPs were reacted with the

finished nanostructures. The binding sites were separated by 48 base pairs and 1 helix for a 16.3 nm axial rise and a 20.3 nm center-to-center spacing for the attached nanoparticles. The gray staple strands were for structural support.

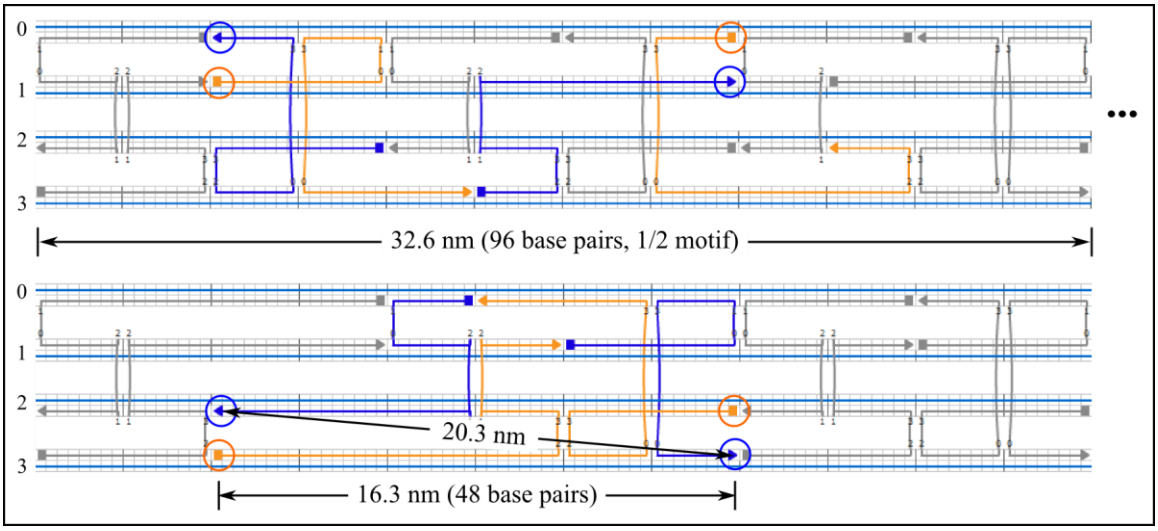

Figure 5.5: Binding site centric staple motif design. Four right-hand 3'A AuNP binding sites are contained in the motif, shown by the blue strands with the circled arrows indicating the sticky end location. Simultaneously, there are four left-hand 5' B AuNP binding sites represented by the orange strands. Circled square ends indicate 5' stick end locations. Sticky ends for both chiralities are always present, but differ in sequence to enable site selectivity. The binding site motif contains no repeating staple patterns and is 192 base pairs long. Forty-eight base pairs and one helix separate binding sites of the same type to create an axial rise of 16.3 nm and a center-to-center distance of 20.3 nm between binding sites. The motif is repeated 9 times, plus one additional binding site for a total of 37 binding sites.

The 4HB design contained 9 full motifs and one extra binding site for a total of 37 binding sites. Figure 5.6 shows the extreme ends of the structure. Instead of columns such as in the six-helix nanotube design, the output from caDNAno numbers nucleotides from left to right as shown above the two vertical markers. The green staple strands represent capping strands to bind the nucleotides at the ends. Each of the pairs of helices were 1802 base pairs long, using 7208 bases out of the 7249 bases contained in the

m13mp18 strand. The extra nucleotides form a loop at base pair 928 on helix 3. A scaffold strand crossover was located between nucleotides 887 and 888 between helices 1 and 2. The nominal length was 612.7 nm and the final design had 199 staple strands.

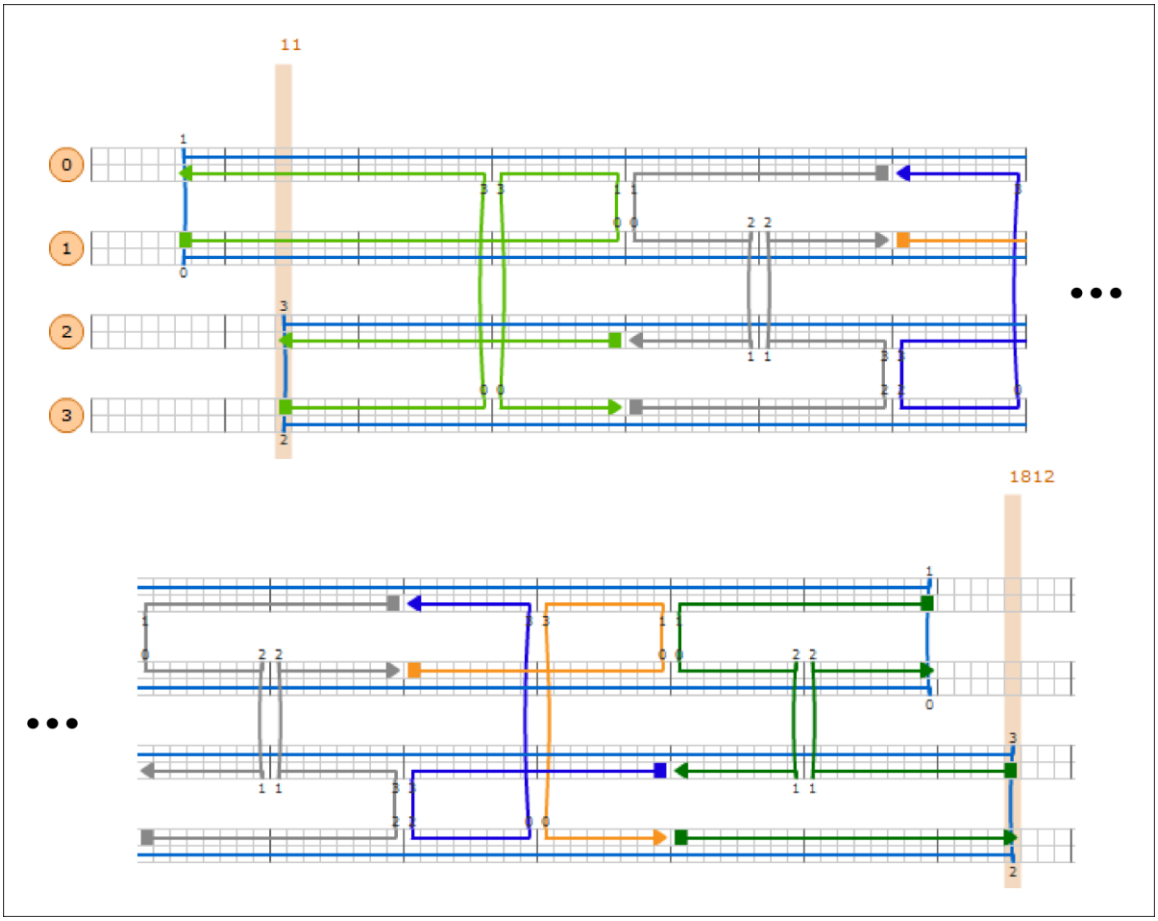

Figure 5.6: Extreme left-hand side (upper image) and right-hand side (lower image) of the nanostructure. The binding site motif was designed independently, then the maximum number of sites possible from the m13mp18 scaffold was calculated: 9 motifs plus on extra binding site. The binding site in the upper image is the first binding site of the series (binding site 1) while the binding site in the lower image is the extra binding site, binding site 37. The capping strands (green) were designed to allow dimerization while maintaining nanoparticle spacing.

Synthesis using m13mp18 was the same as was used for the six-helix nanotube. Reaction with 5 nm AuNPs was conducted using a 2:1 ratio between nanoparticles to binding sites. Solutions were reacted 2 hours at 37ºC and imaged via atomic force

microscopy. Recovery of functionalized 4HB structures was very low so the *p* value for the right-hand 4HB (Figure 5.7 (b)) of 0.54 was calculated using only five nanostructures. No *p* value was calculated for the left-hand structure, although the number of attached nanoparticles (19) in Figure 5.7 (c) is similar to the mean value of 19.8 for the right-hand 4HB.

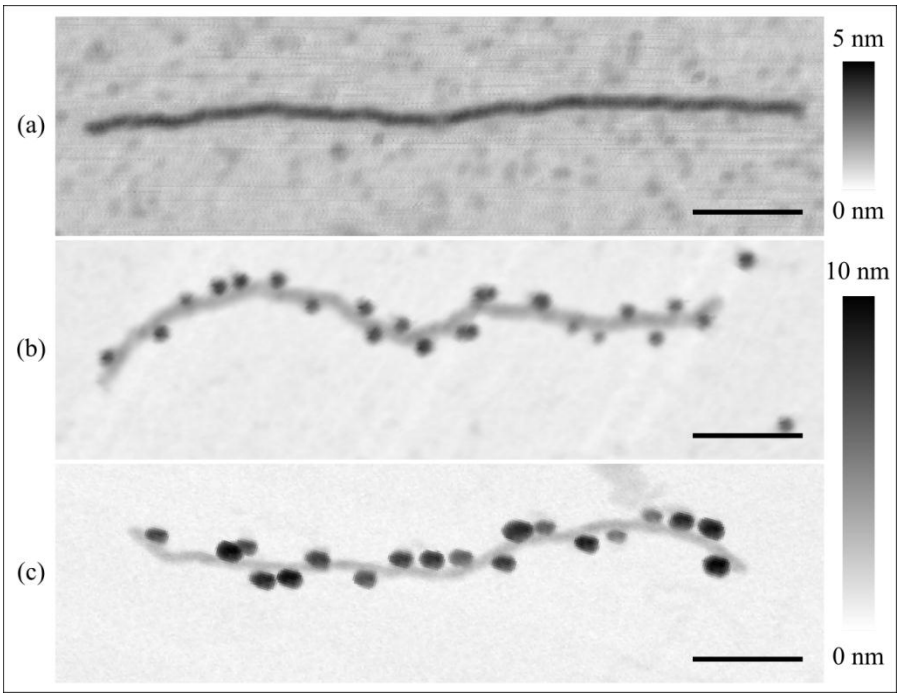

Figure 5.7: AFM micrographs of (a) bare four-helix spiral nanoparticle array, (b) 4HB with 20 right-hand AuNPs attached, and (c) 4HB with 19 left-hand AuNPs attached. The probability of attachment for right-hand chiral nanoparticles was 0.54. The *p* value for the left-hand array was not calculated but the 19 attached nanoparticles in (c) indicate attachment efficiency similar to the right-hand array. Scale bars are 100 nm.

Optical tests of four-helix bundle structures with attached AuNPs showed no CD response. It was suspected that the nanoparticles were missing in a periodic manner. Zhang *et al.* experienced periodic missing AuNPs when attempting to use single sticky ends to attach the AuNPs to a tiled grid [5]. In that experiment, the attachment pattern

indicated that, on average, every other nanoparticle was missing and electrostatic repulsion between ssDNA was suspected when nanoparticles were closer than 38 nm. In Section 4.3.1, electrostatic repulsion and steric hindrance were suspected of beginning to decrease AuNP attachment when the periodicity fell below 43 nm and approached 29 nm. Bridging became problematic when periodicity dropped below 27 nm. The 20 nm center-to-center periodicity of the 4HB meant that any of these blocking mechanisms could be in effect. With only four nanoparticles per helical pitch on the 4HB, an every-other missing nanoparticle pattern would create an alternating linear pattern with no chiral optical response. A *p* value of 0.54 and the relatively evenly distributed nanoparticles in Figure 5.7 (b) and (c), combined with the lack of CD response indicate that every other nanoparticle was likely missing. In order for this structure to be a success, a higher binding efficiency would be necessary.

5.1.4: Four-Helix DNA Origami Nanostructure Site Selectivity

As previously mentioned, a unique feature of the 4HB was the inclusion of two independently addressed binding site arrays simultaneously. It was expected that the selectivity of DNA was sufficient to control the chirality of the nanostructure solely by which complementary ssDNA strands the nanoparticles were conjugated with. Ding *et al.* used site specific sticky end sequencing to arrange AuNPs of differing sizes in precise order [77]. Since chirality could not be determined using AFM, the two types of AuNPs were reacted simultaneously to determine if the site selectivity could be determined in a manner similar to the experiment by Ding *et al.* Fifteen nanometer A AuNPs with the right-hand spiral complement, cSA, and 5 nm B AuNPs with the left-hand complement, cSB, were reacted with 4HB nanostructures for two hours at 37^{o} C in a 2:1 ratio between

each type of nanoparticle and their respective binding sites.

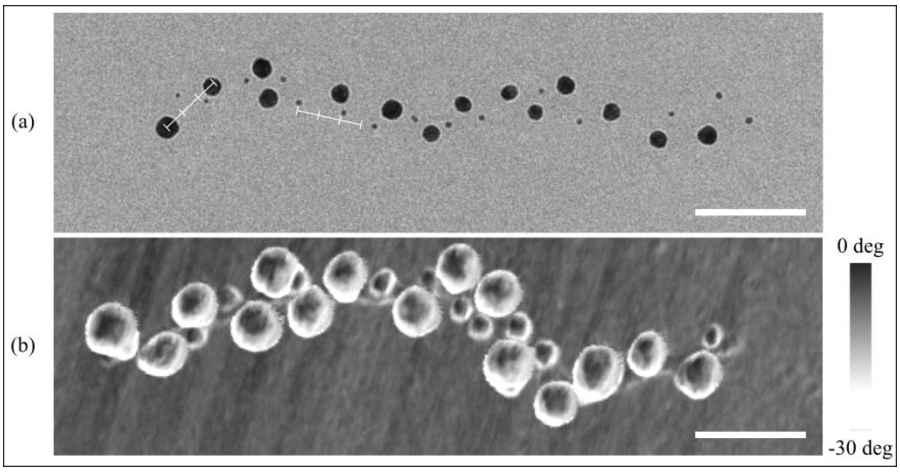

Figure 5.8: TEM micrograph of 4HB (a) and AFM phase micrograph of 4HBs with both right-hand and left-hand AuNPs reacted simultaneously (b). Right-hand AuNPs were 15 nm in diameter and the left-hand AuNPs were 5 nm in diameter. It appears that the nanoparticles are segregating by size/sequence. Small scale bars in (a) have tick marks 20 nm apart, indicating that none of the nanoparticles have the designed 20 nm center-to-center spacing. Large-scale bars are 100 nm.

Transmission electron microscopy (TEM) and AFM micrographs indicated that nanoparticles were binding to uniquely addressable sites, discriminating against non-complementary sticky ends. Figure 5.8 shows a TEM micrograph (a) and an AFM phase micrograph (b) of different 4HBs. Nanoparticles appear to arrange themselves in relatively periodic structures by size, and thus sequence, without interfering with each other. Missing particles create periodicities much larger than 20 nm. The number of attached particles appears to have increased over single particle types, but not nearly to the point of doubling. For example, the total number of particles in the two four-helix bundle structures shown in Figure 5.8 are 29 and 25 compared to single-particle attachment in the 18-20 particle range.

5.2: Six-Helix Nanotube Right-Hand Chiral Gold Nanoparticle Array

5.2.1: Six-Helix Nanotube Right-Hand Chiral Gold Nanoparticle Array

Proof of concept already showed a single tether right-hand spiral could be created on a six-helix DNA origami nanotube. Further inspection of the staple pattern of the six-helix nanotube revealed that dual 3' sticky end attachment was possible. The nanotube was tasked to arrange as many AuNP as would fit with a 20 nm center-to-center spacing between nanoparticles but now with 6 particles per spiral pitch. Separating binding sites by an axial rise of 19 nm (4 columns, 56 base pairs) plus a rotation of 2 nm (one helix) produced a total distance of approximately 21 nm center-to-center. By choosing the first binding site to start between helix 2 and 3, column 0, a total of 22 dual 3' sticky end binding sites was possible. The first six AuNP binding sites are shown in Figure 5.9 where the blue staple strands mark the locations of the 3' sticky ends at the tips of the arrows. The tether pattern alternated between having both modified staple strands attaching the AuNP in a single column, such as in columns 0, 8, and 16, or having sticky ends on the left and right of a column such as in columns 4, 12, and 20.

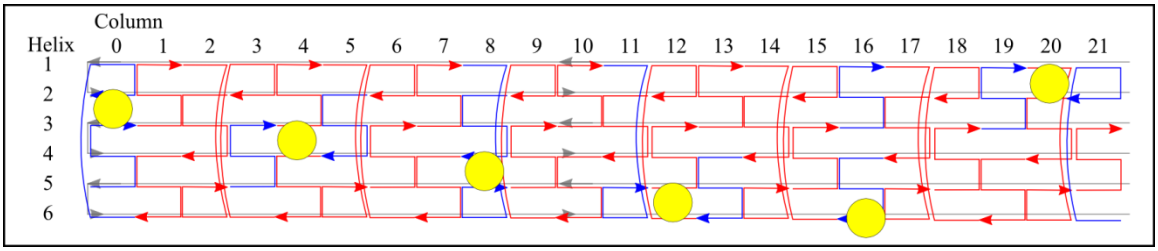

Figure 5.9: Locations of the first six binding sites for the six-helix nanotube right-hand chiral AuNP array. Sticky ends were located at the blue arrows. The first nanoparticle binding site located in column 0, created by modified staple strands within that column. The second site is in column 4 created by staple strands in the adjacent columns. This pattern was repeated for the remaining sites. A total of 22 binding sites were created in this design.

Scaffolded DNA origami synthesis and nanoparticle functionalization were the same as conducted for linear arrays. The probability of attachment was calculated to be 0.71 (n = 84). In Figure 5.10, the low magnification AFM height micrograph shows nanoparticles falling to either side of the nanotubes in groups of 2-3, which was expected with six particles per pitch (sets of 2 likely due to missing nanoparticles). A high magnification AFM micrograph of a randomly chosen nanostructure is shown with three sets of 3 nanoparticles, (a)-(c). The nearest neighbor center-to-center distances are shown for nanoparticles on the same side of the nanotube (units are in nanometers). The left most set of 3, (a), had periodicity in the range of 35 nm and a spread of 70.3 nm. The target axial rise was 19 nm with a center-to-center distance of approximately 21 nm, thus this section is likely missing one or two particles. The next two sets of 3 to the right, (b) and (c) had spreads in the range of 45 nm, close to the expected range of 38-42 nm. Considering that these AuNPs can rotate 13 nm from their anchor sites, this is well within the possible range of separation, thus (b) and (c) are likely what the proper distance should be.

The *p* value for this design fell between that of the AuNPA29DT and AuNPA15DT. Given the center-to-center distance of 20 nm, it appears that the *p* value scaled proportionally as if the structure were a linear array. It was expected that a slightly higher *p* value could be achieved due to the possible reduced steric hindrance and electrostatic repulsion enabled by the curvature. The chiral nanostructures created by Shen *et al.* showed evidence of increased attachment of AuNPs on their nanotube compared to the unrolled planar origami [113].

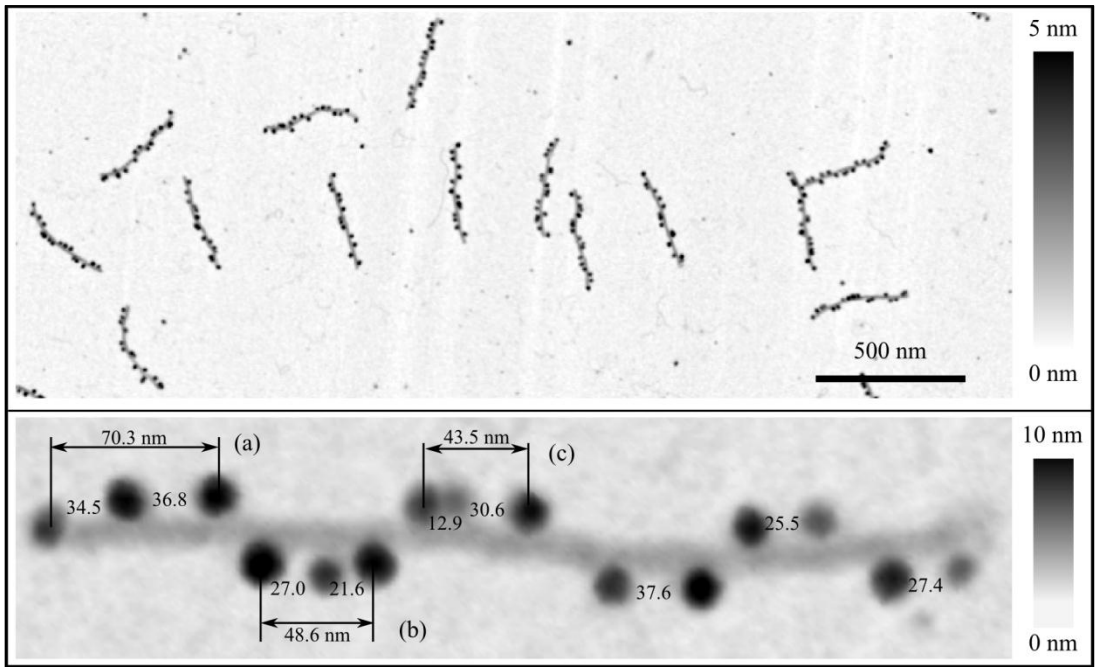

Figure 5.10: Low (top) and high (bottom) magnification AFM height micrographs of six-helix nanotube, right-hand chiral nanoparticle arrays with attached AuNPs. Low magnification: Nanotubes appear uniform and are in high number. The spiral pattern cannot be seen definitively, but the alternating pattern of nanotube clusters gives the appearance of a spiral. Six equally spaced nanoparticles in a helix would be expected to lay 3 per side per pitch on flat mica. Groups of 3 and pairs (likely due to missing a nanoparticle in the center) of nanoparticles can be seen alternating side to side as expected. High magnification of randomly selected nanotube shows details of alternating nanoparticles. There are three groups of 3 nanoparticles (a) – (c), and several pairs. The distance span of the nanoparticles for (a), (b), and (c) were 70.3 nm, 48.6 nm, and 43.5 nm, respectively. The design lateral distance between nanoparticles was 19 nm, thus (b) and (c) are relatively close to the proper periodicity. (a) is likely missing a nanoparticle. Nearest-neighbor center-to-center distances are shown in nanometers (units omitted due to space constraints). Center-to-center distances vary widely likely due to missing 7 nanoparticles and rotation of nanoparticles from their long tethers.

5.2.2: Six-Helix Nanotube Left-Hand Chiral Gold Nanoparticle Array

The staple motif of the six-helix bundle could not support the left-handed spiral using terminal sticky ends. Only two of the six binding site locations in the left-hand spiral pitch motif had two available terminal 3' ends. The solution to this problem had already been conceptualized with the stitched staple strand. This method was explained

in Section 4.3.4. The stitched staple strand sticky ends could not be implemented in all of the binding sites, so the left-hand spiral binding site motif was a hybrid with both stitched staple strand sticky ends and 3' terminal sticky ends in a 2:1 ratio. All of the binding sites were centered over unmodified columns, bound by sticky ends separated by one helix as illustrated in Figure 5.11. Blue staple strands with blue arrows represent 3' binding sites and blue staple strands with x's mark stitched staple strand sticky end locations. Recall that in addition to the 3' binding site, a 5' binding site is located where the staple strand is stitched. Synthesis and reaction was same as for the linear array nanostructures. The probability of attachment was calculated to be 0.72 (n = 31), roughly the same as for the right-hand spiral structure. Figure 5.12 shows an AFM height micrograph of a representative six-helix left-hand chiral array. Chirality cannot be discerned from the two-dimensional micrograph and there is no noticeable difference in appearance from the right-hand chiral structure.

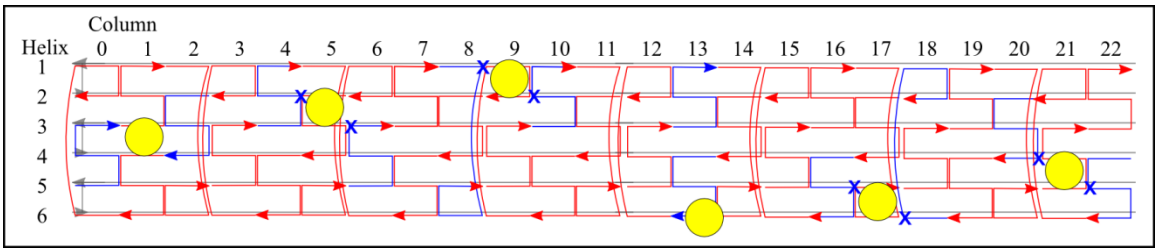

Figure 5.11: First six binding sites for the six-helix nanotube left-hand chiral nanoparticle array. A new method using stitched staple strand sticky ends was applied to this structure. The method breaks a staple strand and places sticky ends on the two terminal ends created at the break location. To retain the structural integrity of the unbroken staple strand, 5 complementary nucleotides were added at the base of the sticky ends to stitch the staple strand back together. The stitched sticky ends were combined with the dual 3' sticky ends in a 2:1 ratio. Here the 3' sticky ends are represented by blue arrows while the stitched sticky ends are represented by blue x's. The location of the x's show where on the staple the break and subsequent stitching occurred. The stitched staple strands contained both a 3' and a 5' sticky end.

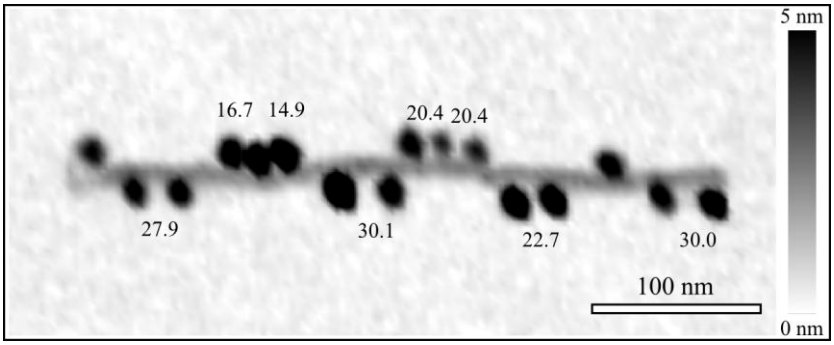

Figure 5.12: AFM micrograph of representative six-helix nanotube, left hand chiral nanoparticle array using dual 3' and stitched sticky end binding sites. Nearest neighbor center-to-center distances are shown in nanometers. The same alternating pattern of nanoparticles laying on opposite sides of the nanotube that was seen in the right-hand structure is also seen here. Extent of attachment was 0.72, nearly identical to that of the right-hand structure.

Both the right-hand and left-hand chiral six-helix DNA origami nanoparticle arrays formed well, however, the circular dichroism measurements were inconclusive. It was suspected that the recovered concentrations of nanostructures were too low. The 5 nm AuNPs used in this experiment were also smaller than the experiments of Shen *et al.* [113] and Kuzyk *et al.* [114], which were in the 10-13 nm range. The CD effect is greatly affected by nanoparticle size and concentration [112, 113], therefore an increase in one or both of these values likely would lead to a successful experiment.

5.3: Heterogeneous Nanoparticle Arrays

Combining metallic and semiconducting materials into a heterogeneous nanoparticle array is a logical step towards nanoelectronic device fabrication, as many current generation silicon-based microelectronics combine semiconductor materials with metal interconnects. The methods for attaching AuNPs and CdSe/ZnS semiconducting QDs discussed in Chapter 4 were combined to create a design for a prototypical nanoelectronic device.

The AuNPA29ABC nanostructure served as the base structure for the new heterogeneous nanoparticle array, called HNPA29. The first DNA sticky end A AuNP site was replaced with a dual biotin binding site intended for a QD. This pattern was repeated every fourth site, skipping three AuNP binding sites between QD binding sites. A total of three A and B sites and two C sites were replaced. As illustrated in Figure 5.13, the center-to-center distance between adjacent binding sites remained 14 nm while the distance between QD binding sites was 57 nm. AuNP binding sites clustered in sets of three with a span of 43 nm.

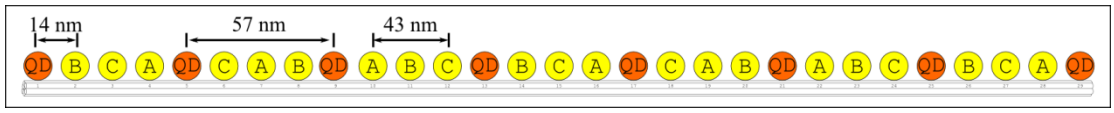

Figure 5.13: Heterogeneous nanoparticle array. The AuNPA29ABC served as the basis for the HNPA29 structure. The first AuNP dual sticky end binding was replaced by a dual biotin QD binding site, followed by every fourth AuNP thereafter. A total of 8 QDs and 21 AuNP binding sites were arrayed in this alternating pattern.

All binding site staple strands were added before synthesis. Nanostructures were synthesized and filtered per the procedure described in Section 2.3.3. All three AuNP types and QDs were combined simultaneously with the HNPA29 nanostructures in a 2:1 ratio of nanoparticle to their respective binding sites. The mixture was reacted for 2 h at 37ºC. From atomic force micrographs, it was difficult to discern between possible AuNPs and QDs bound to the surface of the structure so control experiments were run, attaching only B AuNP, QD, and B AuNP with QD.

As can be seen in Figure 5.14, the images of HNPA29 structures with QDs only (Figure 5.14 (a)) and AuNPs only (Figure 5.14 (b)) were clear and distinct. Nominal core

diameters for AuNPs and QDs were both 5 nm, which is reflected in the micrographs by their similar appearance. In Figure 5.14 (c), the pattern of attached nanoparticles appeared to be close to what was designed, however there were marked size differences between what were expected to be QDs compared to what were expected to be AuNPs. It was suspected that the nanoparticles in Figure 5.10 (c) and those in Figure 5.14 (d) that were expected to be QDs were actually streptavidin molecules.

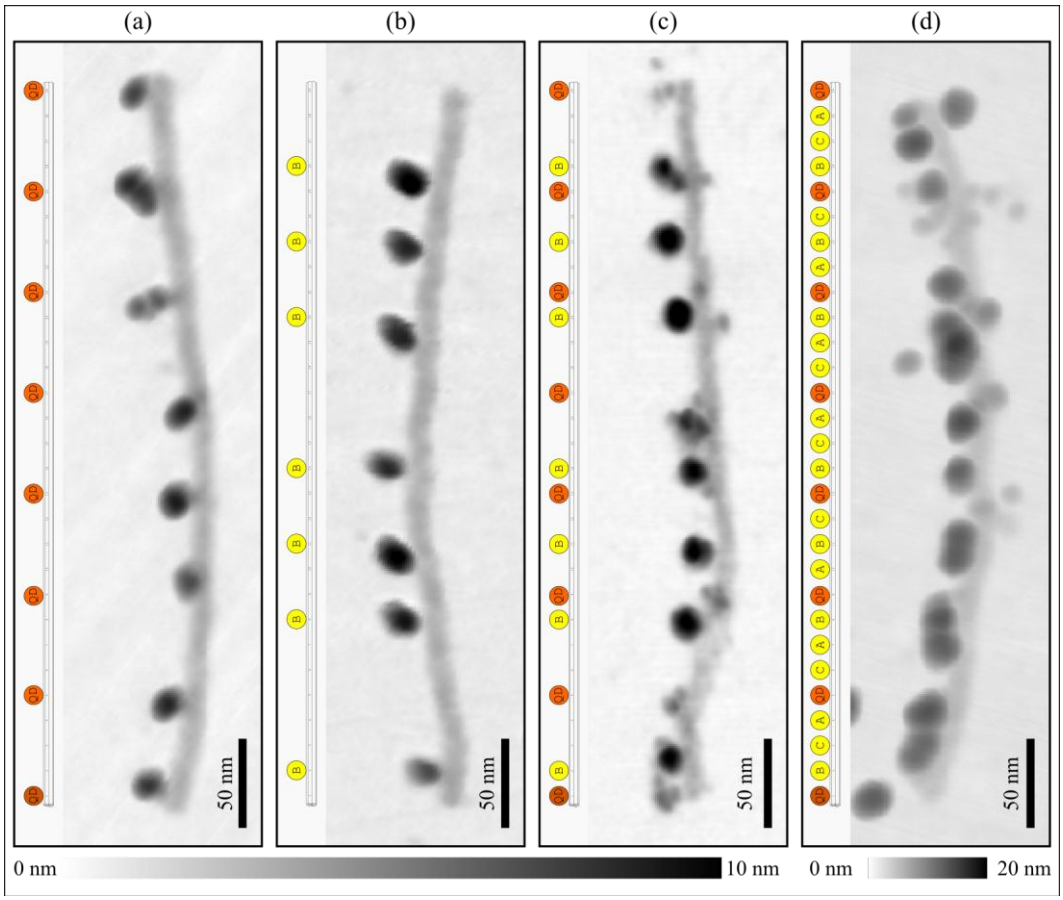

Figure 5.14: AFM micrographs of the HNPA29 nanostructure with (a) QD only, (b) B AuNP only, (c) QD and B AuNP, (d) A, B, and C AuNP and QD. The expected attachment pattern of each is shown at the left of each micrograph. Attached QD and AuNP show good agreement with expected attachment locations and nanoparticles are clear and distinct. When B AuNP and QD are added together (c), areas where QDs are expected show small molecules that resemble streptavidin. This was exacerbated when all three AuNP types (A, B, and C) are attached along with QDs as well (d).

AFM imaging analysis was performed to determine the appearance of AuNPs, QDs and streptavidin separately without any obfuscating foreign objects. Samples of each type of nanoparticle were deposited on mica and imaged under the same conditions as was used for the HNPA29 nanostructures. The images are shown in Figure 5.15. The analysis showed that AuNPs, Figure 5.15 (a), were distinct and largely spherical with a mean height of 8.8 nm. The QDs, Figure 5.15 (b) were more asymmetrical with a mean height of 8.2 nm. What appeared to be the streptavidin coating could be seen on the edges of many of the QDs. Moreover, it appeared that loose streptavidin with a mean height of 2.9 nm was also present. The image of pure streptavidin with a mean height of 2.9 nm, Figure 5.15 (c), indicated that the small items in Figure 5.15 (b) were indeed streptavidin molecules from their height and appearance.

Comparing the visual and height data from figs. 5.15 (a)-(c) with the nanostructure in Figure 5.15 (d), it appears likely that the small light gray nanoparticles are indeed streptavidin, but the identity of the remaining nanoparticles could not be determined for certain from AFM height data alone. It should be noted that the AuNPs are from the same samples as were used in the AuNPA29ABC experiment, so gaps with missing AuNPs were likely.

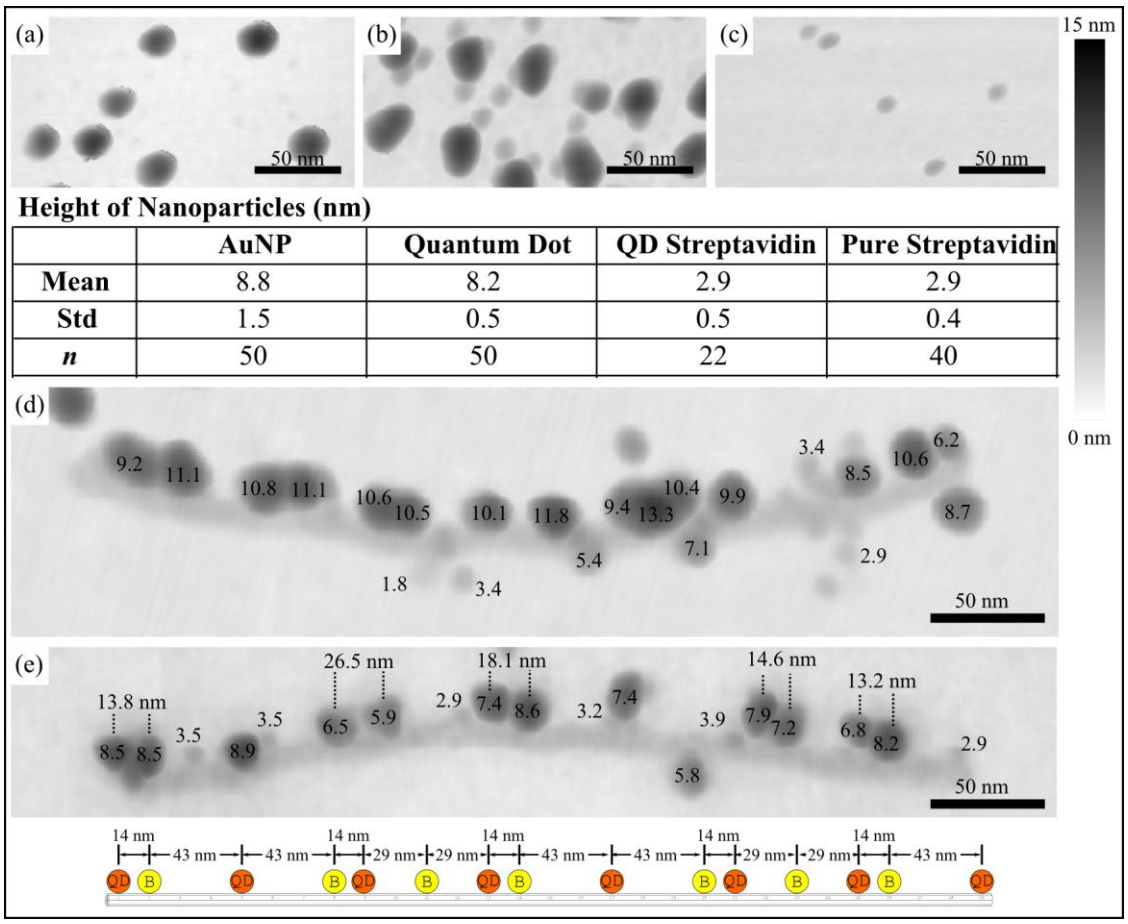

	AuNP	Quantum Dot	QD Streptavidin	Pure Streptavidin
Mean	8.8	8.2	2.9	2.9
Std	1.5	0.5	0.5	0.4
n	50	50	22	40

Figure 5.15: AFM micrographs of: (a) B AuNP, (b) streptavidin conjugated QD, (c) pure streptavidin, (d) HNPA29 nanostructure with all nanoparticles attached, heights of nanoparticles superimposed on nanoparticle in nanometers, (e) HNPA29 with B AuNP and QD processed without vortex mixing. The heights of pure nanoparticle solutions were measured to with values listed in the table above. AuNPs (a) appear spherical and distinct. (b) QDs are less distinct and show what appears to be attached and free streptavidin. Suspected streptavidin height averages 2.9 nm. (c) Pure streptavidin appears similar to the suspected molecules in (b) and average height was also 2.9 nm. This indicated it was likely that the small molecules in (b) were indeed streptavidin. (d) Height data of individual nanoparticles of HNPA29 with A, B, and C AuNP and QD attached shows likely streptavidin molecules attached. The AuNPs and QDs cannot be distinguished from height alone. (e) B AuNPs and QDs attached to HNPA29 without vortex mixing show good agreement with expected nanoparticle pattern. Likely QDs are large and distinct, though they cannot be distinguished from AuNP. Center-to-center distances of suspected neighboring nanoparticles show good agreement with design (distances shown above nearest-neighbor pairs with units of nanometers shown).

It is not certain why the QDs could be attached to the nanostructure by themselves, but when AuNPs were added mostly streptavidin remained. It was suspected that vortex mixing—a combination of rotary and linear up and down mixing to form a vortex in the fluid—of the samples could be pulling the QD cores away from the streptavidin coating. An HNPA29 structure with only B AuNP and QDs was created but was mixed with a pipet instead of vortex mixing before incubation at 37ºC. Figure 5.15 (e) is an AFM height micrograph of a nanotube from this sample. As can be seen, the pattern corresponds well with the expected pattern. Height data (superimposed on nanoparticles, units in nanometers) and center-to-center distances (marked above paired nanoparticles in figure with units of nanometers) are in the expected range for the design. Thus, it is possible that the QDs are missing from the HNPA29 structure due to lab procedures rather than design issues.

5.4: Conclusions

The method of scaffolded DNA origami was successfully applied to a four-helix bundle. Unlike past DNA origami structures, which identified available binding site patterns on a structure, this design fit a structure to a predetermined nanoparticle array pattern. This procedure likely will be applied to future purpose built DNA origami nanostructures. The methods to increase nanoparticle attachment from Chapter 4 would also likely be incorporated in to any future structure during the design phase.

Chiral AuNP arrays on six-helix DNA origami nanotubes were successfully synthesized and obtained over 70% nanoparticle attachment using dual terminal 3’ sticky ends. An ABC spiral pattern would likely increase the extent of attachment. With the current probability of attachment, an increase in concentration, nanoparticle diameter or

both likely would yield a CD response due to the presence of complete nanoparticle helical rotations.

A prototypical nanoelectronic device was designed and synthesized. Attachment efficiency of AuNPs may have been affected by batch-to-batch AuNP variation and QDs may have been separated from their streptavidin coatings by vortex mixing, leaving only the streptavidin attached to the nanostructure. However, HNPA29 nanostructures with known viable B AuNP and QDs that were not vortex mixed indicated that the design is viable.

CHAPTER 6: CONCLUSION

Two DNA origami supermolecular nanostructures were functionalized with semiconductor quantum dots (QDs), gold nanoparticles (AuNPs), or both QD and AuNPs. The first was a six-helix DNA origami nanotube from a previously published source and the second was a four-helix DNA origami nanostructure that was purposely designed and synthesized from the conceptual stage forward. In addition, the six-helix nanostructure was modified to form homodimers.

The six-helix DNA origami nanotube was a mostly symmetrical nanostructure that used a repeating staple strand motif arranging six staple strands in three columns. The crossover pattern was based on 7*n* base pairs between crossovers, creating a hexagonal cross-section with a 120º dihedral angle. These nanostructures formed pseudo homodimers using ssDNA linker strands, which targeted complementary domains on the scaffold strand of another monomer nanotube. Modifications were only required in the first (tail monomer) or last (head monomer) columns. It is likely that this method could be expanded to link nanotubes in locations other than end-to-end to form extended networks.

The symmetry of the six-helix DNA origami nanotube provided an adaptable platform on which many functionalization experiments were performed. In linear arrays, up to 29 nanoparticle binding sites were possible. These were used to successfully attach QDs using biotin-streptavidin ligation, and AuNPs using ssDNA sticky ends. Once

below a threshold periodicity, extent of attachment was encumbered by steric hindrance for QDs and by steric hindrance and electrostatic repulsion for the AuNPs. Bridging became the limiting factor for AuNP attachment once the periodicity of the nanotube binding sites dropped below the diameter of the ssDNA sticky ends of the AuNPs.

The attachment efficiency of AuNPs was increased dramatically by adding multiple sticky ends per binding site. The increased efficiency was likely due to overcoming the effects of steric hindrance and electrostatic repulsion. Bridging could not be abated in this manner provided the reach of the AuNP sticky ends was greater than the periodicity. To combat bridging, an alternating binding sequence was required, which maintained binding site periodicity but increased the distance between like sequenced binding sites. This method was hindered by possible batch-to-batch variation in the AuNP solutions, but data indicated that significantly higher attachment efficiency was possible.

A right-hand chiral AuNP array was created using 22 dual 3' sticky end binding sites. Attachment efficiency was in line with similar linear nanostructures. A left-hand chiral AuNP array was also possible after a new method of providing sticky ends was developed. This method was called 'stitched staple strand sticky ends' and enabled placement of a sticky end binding site at locations other than the terminal ends of a staple strand. The method required that a staple strand be broken prior to nanotube synthesis and sticky ends attached to the staple strand sections on each side of the break. To maintain the structural integrity of the nanotube, a 5-mer complementary sequence was added to each half of the staple strand between the break and the sticky ends. This provided the 'stitched' part of the name, stitching the staple strand back together during

synthesis.

The four-helix DNA origami nanostructure was a *de novo* design developed expressly to arrange AuNPs into right-hand and left-hand chiral nanoparticle arrays. The structure was based on a staple strand crossover pattern of 8*n* base pairs between crossovers, creating a square cross-section with a dihedral angle of 90º. Unlike the six-helix nanotube, this design created 4.3º*n* of over twist. Staple crossovers and terminal end locations were adjusted using a computer-aided design program to form the nanostructure around the desired nanoparticle attachment pattern in a binding site centric design. The capability to form both right-hand and left-hand chirality was incorporated simultaneously into each nanostructure, utilizing ssDNA sticky ends of differing sequence. The actual chirality was determined by the sequencing on the ssDNA used to link the nanoparticles to the nanostructure.

REFERENCES

1. Houlton, A. and S.M.D. Watson, *DNA-based nanowires. Towards bottom-up nanoscale electronics.* Annual Reports Section "A" (Inorganic Chemistry), 2011. **107**.
2. Alberts, B., *Essential cell biology*. 2009, New York: Garland Science.
3. Haddon, R.C. and A.A. Lamola, *The Molecular Electronic Device and the Biochip Computer-Present Status.* Proceedings of the National Academy of Sciences of the United States of America, 1985. **82**(7): p. 1874-1878.
4. Robinson, B.H. and N.C. Seeman, *The Design of a Biochip - A Self-Assembling Molecular-Scale Memory Device.* Protein Engineering, 1987. **1**(4): p. 295-300.
5. Zhang, J., et al., *Periodic Square-Like Gold Nanoparticle Arrays Templated by Self-Assembled 2D DNA Nanogrids on a Surface.* Nano Letters, 2006. **6**(2): p. 248-251.
6. Nadrian C, S., *Nucleic acid junctions and lattices.* Journal of Theoretical Biology, 1982. **99**(2): p. 237-247.
7. Kallenbach, N.R., R.-I. Ma, and N.C. Seeman, *An immobile nucleic acid junction constructed from oligonucleotides.* Nature, 1983. **305**(5937): p. 829-831.
8. Fu, T.J. and N.C. Seeman, *DNA double-crossover molecules.* Biochemistry, 1993. **32**(13): p. 3211-3220.
9. Zheng, J., et al., *From molecular to macroscopic via the rational design of a self-assembled 3D DNA crystal.* Nature, 2009. **461**(7260): p. 74-77.
10. Seeman, N.C. and P.S. Lukeman, *Nucleic acid nanostructures: bottom-up control of geometry on the nanoscale.* Reports on Progress in Physics, 2005. **68**(1): p. 237-270.
11. Mirkin, C.A., et al., *A DNA-based method for rationally assembling nanoparticles into macroscopic materials.* Nature, 1996. **382**(6592): p. 607-609.
12. Alivisatos, A.P., et al., *Organization of 'nanocrystal molecules' using DNA.* Nature, 1996. **382**(6592): p. 609-611.
13. Nykypanchuk, D., et al., *DNA-guided crystallization of colloidal nanoparticles.* Nature, 2008. **451**(7178): p. 549-552.
14. Aldaye, F.A. and H.F. Sleiman, *Sequential Self-Assembly of a DNA Hexagon as a Template for the Organization of Gold Nanoparticles.* Angewandte Chemie International Edition, 2006. **45**(14): p. 2204-2209.
15. Tikhomirov, G., et al., *DNA-based programming of quantum dot valency, self-assembly and luminescence.* Nat Nano, 2011. **6**(8): p. 485-490.
16. Zhang, Y. and N.C. Seeman, *Construction of a DNA-Truncated Octahedron.* Journal of the American Chemical Society, 1994. **116**(5): p. 1661-1669.
17. Goodman, R.P., et al., *Rapid Chiral Assembly of Rigid DNA Building Blocks for Molecular Nanofabrication.* Science, 2005. **310**(5754): p. 1661-1665.

18. Goodman, R.P., R.M. Berry, and A.J. Turberfield, *The single-step synthesis of a DNA tetrahedron.* Chemical Communications, 2004(12).
19. Smith, D.M., et al., *A Structurally Variable Hinged Tetrahedron Framework from DNA Origami.* Journal of Nucleic Acids, 2011. **2011**.
20. Erben, C.M., R.P. Goodman, and A.J. Turberfield, *A Self-Assembled DNA Bipyramid.* Journal of the American Chemical Society, 2007. **129**(22): p. 6992-6993.
21. Aldaye, F.A. and H.F. Sleiman, *Modular Access to Structurally Switchable 3D Discrete DNA Assemblies.* Journal of the American Chemical Society, 2007. **129**(44): p. 13376-13377.
22. Yang, H., et al., *Metal–nucleic acid cages.* Nat Chem, 2009. **1**(5): p. 390-396.
23. Mathieu, F., et al., *Six-Helix Bundles Designed from DNA.* Nano Letters, 2005. **5**(4): p. 661-665.
24. Winfree, E., et al., *Design and self-assembly of two-dimensional DNA crystals.* Nature, 1998. **394**(6693): p. 539-544.
25. Schulman, R. and E. Winfree, *Synthesis of Crystals with a Programmable Kinetic Barrier to Nucleation.* Proceedings of the National Academy of Sciences of the United States of America, 2007. **104**(39): p. 15236-15241.
26. LaBean, T.H., et al., *Construction, Analysis, Ligation, and Self-Assembly of DNA Triple Crossover Complexes.* Journal of the American Chemical Society, 2000. **122**(9): p. 1848-1860.
27. He, Y., et al., *Self-Assembly of Hexagonal DNA Two-Dimensional (2D) Arrays.* Journal of the American Chemical Society, 2005. **127**(35): p. 12202-12203.
28. He, Y., et al., *Highly Connected Two-Dimensional Crystals of DNA Six-Point-Stars.* Journal of the American Chemical Society, 2006. **128**(50): p. 15978-15979.
29. Sun, X., et al., *Surface-Mediated DNA Self-Assembly.* Journal of the American Chemical Society, 2009. **131**(37): p. 13248-13249.
30. Malo, J., J.C. Mitchell, and A.J. Turberfield, *A Two-Dimensional DNA Array: The Three-Layer Logpile.* Journal of the American Chemical Society, 2009. **131**(38): p. 13574-13575.
31. Liu, Y., Y. Ke, and H. Yan, *Self-Assembly of Symmetric Finite-Size DNA Nanoarrays.* Journal of the American Chemical Society, 2005. **127**(49): p. 17140-17141.
32. Rothemund, P.W.K., N. Papadakis, and E. Winfree, *Algorithmic Self-Assembly of DNA Sierpinski Triangles.* PLoS Biol, 2004. **2**(12): p. e424.
33. Pinto, Y.Y., et al., *Sequence-Encoded Self-Assembly of Multiple-Nanocomponent Arrays by 2D DNA Scaffolding.* Nano Letters, 2005. **5**(12): p. 2399-2402.
34. Le, J.D., et al., *DNA-Templated Self-Assembly of Metallic Nanocomponent Arrays on a Surface.* Nano Letters, 2004. **4**(12): p. 2343-2347.
35. Sharma, J., et al., *DNA-Templated Self-Assembly of Two-Dimensional and Periodical Gold Nanoparticle Arrays.* Angewandte Chemie International Edition, 2006. **45**(5): p. 730-735.
36. Zheng, J., et al., *Two-Dimensional Nanoparticle Arrays Show the Organizational Power of Robust DNA Motifs.* Nano Letters, 2006. **6**(7): p. 1502-1504.
37. Sharma, J., et al., *Control of Self-Assembly of DNA Tubules Through Integration of Gold Nanoparticles.* Science, 2009. **323**(5910): p. 112-116.

38. Park, S.H., et al., *Finite-Size, Fully Addressable DNA Tile Lattices Formed by Hierarchical Assembly Procedures.* Angewandte Chemie, 2006. **118**(5): p. 749-753.
39. Yan, H., et al., *DNA-Templated Self-Assembly of Protein Arrays and Highly Conductive Nanowires.* Science, 2003. **301**(5641): p. 1882-1884.
40. Park, S.H., et al., *Programmable DNA Self-Assemblies for Nanoscale Organization of Ligands and Proteins.* Nano Letters, 2005. **5**(4): p. 729-733.
41. Lund, K., et al., *Self-Assembling a Molecular Pegboard.* Journal of the American Chemical Society, 2005. **127**(50): p. 17606-17607.
42. Liu, Y., et al., *Aptamer-Directed Self-Assembly of Protein Arrays on a DNA Nanostructure.* Angewandte Chemie, 2005. **117**(28): p. 4407-4412.
43. Chhabra, R., et al., *Spatially Addressable Multiprotein Nanoarrays Templated by Aptamer-Tagged DNA Nanoarchitectures.* Journal of the American Chemical Society, 2007. **129**(34): p. 10304-10305.
44. Williams, B.A.R., et al., *Self-Assembled Peptide Nanoarrays: An Approach to Studying Protein–Protein Interactions.* Angewandte Chemie, 2007. **119**(17): p. 3111-3114.
45. Sharma, J., et al., *DNA-Tile-Directed Self-Assembly of Quantum Dots into Two-Dimensional Nanopatterns.* Angewandte Chemie International Edition, 2008. **47**(28): p. 5157-5159.
46. Liu, D., et al., *DNA Nanotubes Self-Assembled from Triple-Crossover Tiles as Templates for Conductive Nanowires.* Proceedings of the National Academy of Sciences of the United States of America, 2004. **101**(3): p. 717-722.
47. Rothemund, P.W.K., et al., *Design and Characterization of Programmable DNA Nanotubes.* Journal of the American Chemical Society, 2004. **126**(50): p. 16344-16352.
48. Mitchell, J.C., et al., *Self-Assembly of Chiral DNA Nanotubes.* Journal of the American Chemical Society, 2004. **126**(50): p. 16342-16343.
49. Ke, Y., et al., *A Study of DNA Tube Formation Mechanisms Using 4-, 8-, and 12-Helix DNA Nanostructures.* Journal of the American Chemical Society, 2006. **128**(13): p. 4414-4421.
50. Liu, H., et al., *Approaching The Limit: Can One DNA Oligonucleotide Assemble into Large Nanostructures?* Angewandte Chemie International Edition, 2006. **45**(12): p. 1942-1945.
51. Yin, P., et al., *Programming DNA Tube Circumferences.* Science, 2008. **321**(5890): p. 824-826.
52. Aldaye, F.A., et al., *Modular construction of DNA nanotubes of tunable geometry and single- or double-stranded character.* Nat Nano, 2009. **4**(6): p. 349-352.
53. Yan, H., et al., *Directed Nucleation Assembly of DNA Tile Complexes for Barcode-Patterned Lattices.* Proceedings of the National Academy of Sciences of the United States of America, 2003. **100**(14): p. 8103-8108.
54. Shih, W.M., J.D. Quispe, and G.F. Joyce, *A 1.7-kilobase single-stranded DNA that folds into a nanoscale octahedron.* Nature, 2004. **427**(6975): p. 618-621.
55. Rothemund, P.W.K., *Folding DNA to create nanoscale shapes and patterns.* Nature, 2006. **440**(7082): p. 297-302.

56. Andersen, E.S., et al., *DNA Origami Design of Dolphin-Shaped Structures with Flexible Tails.* ACS Nano, 2008. **2**(6): p. 1213-1218.
57. Qian, L., et al., *Analogic China map constructed by DNA.* Chinese Science Bulletin, 2006. **51**(24): p. 2973-2976.
58. Fujibayashi, K., et al., *Toward Reliable Algorithmic Self-Assembly of DNA Tiles: A Fixed-Width Cellular Automaton Pattern.* Nano Letters, 2007. **8**(7): p. 1791-1797.
59. Barish, R.D., et al., *An Information-Bearing Seed for Nucleating Algorithmic Self-Assembly.* Proceedings of the National Academy of Sciences of the United States of America, 2009. **106**(15): p. 6054-6059.
60. Zhao, Z., H. Yan, and Y. Liu, *A Route to Scale Up DNA Origami Using DNA Tiles as Folding Staples.* Angewandte Chemie International Edition, 2010. **49**(8): p. 1414-1417.
61. Liu, W., et al., *Crystalline Two-Dimensional DNA-Origami Arrays.* Angewandte Chemie International Edition, 2011. **50**(1): p. 264-267.
62. Li, Z., et al., *Molecular Behavior of DNA Origami in Higher-Order Self-Assembly.* Journal of the American Chemical Society, 2010. **132**(38): p. 13545-13552.
63. Zhao, Z., Y. Liu, and H. Yan, *Organizing DNA Origami Tiles into Larger Structures Using Preformed Scaffold Frames.* Nano Letters, 2011. **11**(7): p. 2997-3002.
64. Rajendran, A., et al., *Programmed Two-Dimensional Self-Assembly of Multiple DNA Origami Jigsaw Pieces.* ACS Nano, 2010. **5**(1): p. 665-671.
65. Endo, M., et al., *Two-dimensional DNA origami assemblies using a four-way connector.* Chemical Communications, 2011. **47**(11).
66. Woo, S. and P.W.K. Rothemund, *Programmable molecular recognition based on the geometry of DNA nanostructures.* Nat Chem, 2011. **3**(8): p. 620-627.
67. Ke, Y., et al., *Scaffolded DNA Origami of a DNA Tetrahedron Molecular Container.* Nano Letters, 2009. **9**(6): p. 2445-2447.
68. Endo, M., et al., *DNA Prism Structures Constructed by Folding of Multiple Rectangular Arms.* Journal of the American Chemical Society, 2009. **131**(43): p. 15570-15571.
69. Andersen, E.S., et al., *Self-assembly of a nanoscale DNA box with a controllable lid.* Nature, 2009. **459**(7243): p. 73-76.
70. Kuzuya, A. and M. Komiyama, *Design and construction of a box-shaped 3D-DNA origami.* Chemical Communications, 2009(28).
71. Douglas, S.M., et al., *Rapid prototyping of 3D DNA-origami shapes with caDNAno.* Nucleic Acids Research, 2009. **37**(15): p. 5001-5006.
72. Douglas, S.M., et al., *Self-assembly of DNA into nanoscale three-dimensional shapes.* Nature, 2009. **459**(7245): p. 414-418.
73. Ke, Y., et al., *Multilayer DNA Origami Packed on a Square Lattice.* Journal of the American Chemical Society, 2009. **131**(43): p. 15903-15908.
74. Dietz, H., S.M. Douglas, and W.M. Shih, *Folding DNA into Twisted and Curved Nanoscale Shapes.* Science, 2009. **325**(5941): p. 725-730.
75. Han, D., et al., *DNA Origami with Complex Curvatures in Three-Dimensional Space.* Science, 2011. **332**(6027): p. 342-346.

76. Sharma, J., et al., *Toward Reliable Gold Nanoparticle Patterning On Self-Assembled DNA Nanoscaffold.* Journal of the American Chemical Society, 2008. **130**(25): p. 7820-7821.
77. Ding, B., et al., *Gold Nanoparticle Self-Similar Chain Structure Organized by DNA Origami.* Journal of the American Chemical Society, 2010. **132**(10): p. 3248-3249.
78. Zhao, Z., et al., *Encapsulation of Gold Nanoparticles in a DNA Origami Cage.* Angewandte Chemie International Edition, 2011. **50**(9): p. 2041-2044.
79. Saccà, B., et al., *Orthogonal Protein Decoration of DNA Origami.* Angewandte Chemie International Edition, 2010. **49**(49): p. 9378-9383.
80. Kuzyk, A., K.T. Laitinen, and P. Torma, *DNA origami as a nanoscale template for protein assembly.* Nanotechnology, 2009. **20**(23).
81. Kuzuya, A., et al., *Precisely Programmed and Robust 2D Streptavidin Nanoarrays by Using Periodical Nanometer-Scale Wells Embedded in DNA Origami Assembly.* ChemBioChem, 2009. **10**(11): p. 1811-1815.
82. Numajiri, K., et al., *Stepwise and reversible nanopatterning of proteins on a DNA origami scaffold.* Chemical Communications, 2010. **46**(28).
83. Shen, W., et al., *NTA Directed Protein Nanopatterning on DNA Origami Nanoconstructs.* Journal of the American Chemical Society, 2009. **131**(19): p. 6660-6661.
84. Stephanopoulos, N., et al., *Immobilization and One-Dimensional Arrangement of Virus Capsids with Nanoscale Precision Using DNA Origami.* Nano Letters, 2010. **10**(7): p. 2714-2720.
85. Maune, H.T., et al., *Self-assembly of carbon nanotubes into two-dimensional geometries using DNA origami templates.* Nat Nano, 2010. **5**(1): p. 61-66.
86. Pal, S., et al., *DNA-Origami-Directed Self-Assembly of Discrete Silver-Nanoparticle Architectures.* Angewandte Chemie, 2010. **122**(15): p. 2760-2764.
87. Douglas, S.M., J.J. Chou, and W.M. Shih, *DNA-Nanotube-Induced Alignment of Membrane Proteins for NMR Structure Determination.* Proceedings of the National Academy of Sciences of the United States of America, 2007. **104**(16): p. 6644-6648.
88. Stearns, L.A., et al., *Template-Directed Nucleation and Growth of Inorganic Nanoparticles on DNA Scaffolds.* Angewandte Chemie, 2009. **121**(45): p. 8646-8648.
89. Bui, H., et al., *Programmable Periodicity of Quantum Dot Arrays with DNA Origami Nanotubes.* Nano Letters, 2010. **10**(9): p. 3367-3372.
90. Sinden, R.R., *DNA structure and function*. 1994, San Diego: Academic Press.
91. Bates, A.D. and A. Maxwell, *DNA topology*. 1993, Oxford; New York: IRL Press at Oxford University Press.
92. Kool, E.T., *Hydrogen Bonding, Base Stacking, and Steric Effects in DNA Replication.* Annual Review of Biophysics & Biomolecular Structure, 2001. **30**(1): p. 1-22.
93. Roesky, H.W. and M. Andruh, *The interplay of coordinative, hydrogen bonding and π–π stacking interactions in sustaining supramolecular solid-state architectures.: A study case of bis(4-pyridyl)- and bis(4-pyridyl-N-oxide) tectons.* Coordination Chemistry Reviews, 2003. **236**(1–2): p. 91-119.

94. Kabsch, W., C. Sander, and E.N. Trifonov, *The 10 Helical Twist Angles of B-DNA.* Nucleic Acids Research, 1982. **10**(3): p. 1097-1104.
95. Ornstein, R.L., et al., *Optimized Potential Function for Calculation of Nucleic-Acid Interaction Energies. 1. Base Stacking.* Biopolymers, 1978. **17**(10): p. 2341-2360.
96. Holliday, R., *A mechanism for gene conversion in fungi (Reprinted).* Genetics Research, 2007. **89**(5-6): p. 285-307.
97. Thompson, B.J., M.N. Camien, and R.C. Warner, *Kinetics of Branch Migration in Double-Stranded DNA.* Proceedings of the National Academy of Sciences of the United States of America, 1976. **73**(7): p. 2299-2303.
98. Rothemund, P.W.K. *Design of DNA origami*. in *Computer-Aided Design, 2005. ICCAD-2005. IEEE/ACM International Conference on*. 2005.
99. Yurke, B., et al., *A DNA-fuelled molecular machine made of DNA.* Nature, 2000. **406**(6796): p. 605-608.
100. Wallace, R.B., et al., *Hybridization of Synthetic Oligondeoxyribonucleotides to ϕ–χ-174 DNA-Effect of Single Base Pair Mismatch.* Nucleic Acids Research, 1979. **6**(11): p. 3543-3557.
101. SantaLucia, J., H.T. Allawi, and P.A. Seneviratne, *Improved Nearest-Neighbor Parameters for Predicting DNA Duplex Stability†.* Biochemistry, 1996. **35**(11): p. 3555-3562.
102. Owczarzy, R., et al., *Effects of Sodium Ions on DNA Duplex Oligomers: Improved Predictions of Melting Temperatures.* Biochemistry, 2004. **43**(12): p. 3537-3554.
103. Tataurov, A.V., Y. You, and R. Owczarzy, *Predicting ultraviolet spectrum of single stranded and double stranded deoxyribonucleic acids.* Biophysical Chemistry, 2008. **133**(1–3): p. 66-70.
104. Warshaw, M.M. and I. Tinoco, *Optical Properties of 16 Dinucleoside Phosphates.* Journal of Molecular Biology, 1966. **20**(1): p. 29-&.
105. Warshaw, M.M. and C.R. Cantor, *Oligonucleotide Interactions .4. Conformational Differences Between Deoxynucleoside and Ribodinucleoside Phosphates.* Biopolymers, 1970. **9**(9): p. 1079-&.
106. Jungmann, R., et al., *DNA origami-based nanoribbons: assembly, length distribution, and twist.* Nanotechnology, 2011. **22**(27).
107. Manyanga, F., et al., *Origins of the "Nucleation" Free Energy in the Hybridization Thermodynamics of Short Duplex DNA.* Journal of Physical Chemistry B, 2009. **113**(9): p. 2556-2563.
108. Parak, W.J., et al., *Conformation of Oligonucleotides Attached to Gold Nanocrystals Probed by Gel Electrophoresis.* Nano Letters, 2002. **3**(1): p. 33-36.
109. Bustamante, C., Z. Bryant, and S.B. Smith, *Ten years of tension: Single-molecule DNA mechanics.* Nature, 2003. **421**(6921): p. 423-7.
110. Zadeh, J.N., et al., *NUPACK: Analysis and Design of Nucleic Acid Systems.* Journal of Computational Chemistry, 2011. **32**(1): p. 170-173.
111. Kelly, S.M., T.J. Jess, and N.C. Price, *How to study proteins by circular dichroism.* Biochimica Et Biophysica Acta-Proteins and Proteomics, 2005. **1751**(2): p. 119-139.

112. Fan, Z.Y. and A.O. Govorov, *Plasmonic Circular Dichroism of Chiral Metal Nanoparticle Assemblies.* Nano Letters, 2010. **10**(7): p. 2580-2587.
113. Shen, X., et al., *Rolling Up Gold Nanoparticle-Dressed DNA Origami into Three-Dimensional Plasmonic Chiral Nanostructures.* Journal of the American Chemical Society, 2011. **134**(1): p. 146-149.
114. Kuzyk, A., et al., *DNA-based self-assembly of chiral plasmonic nanostructures with tailored optical response.* Nature, 2012. **483**(7389): p. 311-314.

APPENDIX A

Design of Four-Helix Bundle Chiral Nanoparticle Array DNA Origami Nanostructure Using caDNAno

caDNAno is open source software provided by Harvard University and can be downloaded at www.cadnano.org [71]. The program was recently updated and the version used in the work presented here is no longer available. Nevertheless, the methodology should transfer to the new version. Two legacy tutorials are available from the website and new users are encouraged to view them before attempting to replicate these results. It is assumed the user is familiar with DNA origami theory and with the four-helix bundle spiral nanoparticle array DNA origami nanostructure (4HB) described in Chapter 5.

Part 1 of the design consisted of the overall structure such as the shape, number of helices, and the maximum number of nucleotides per helix. In caDNAno, this manifests itself in the arrangement of the scaffold strand, similar to the scaffold raster step in Rothemund's method [55]. The desired shape was a square cross-section extended into a rectangular prism. Given 7249 base pairs in the m13mp18 sequence, the maximum number of base pairs per helix was 1812 with one remainder. Figs. A.1 to A.4 illustrate how these criteria were incorporated into the software to create the scaffold strand superstructure.

Part 2 of the design determined the binding site spacing and pattern. The end result was the staple strand motif. In caDNAno this step involves arrangement of the staple strands. Binding sites were terminal sticky ends in a spiral pattern with four particles per pitch. To obtain a center-to-center spacing between bound AuNPs on adjacent helices of 20 nm, an axial rise of approximately 16 nm per nanoparticle was required. The minimum number of base pairs between crossovers was determined to be 8. Forty-eight base pairs spans a distance of approximately 16.3 nm, thus there would be

48 base pairs between binding sites. Figures. A.5 to A.10 illustrate how the binding site motif was created using caDNAno.

After Part 1 and Part 2 were completed, the staple strand motif from Part 2 was manually inserted into the scaffold layout from Part 1 until the maximum number of binding sites was obtained.

Part 1: Arranging the Scaffold Strand into the Desired Shape Using caDNAno

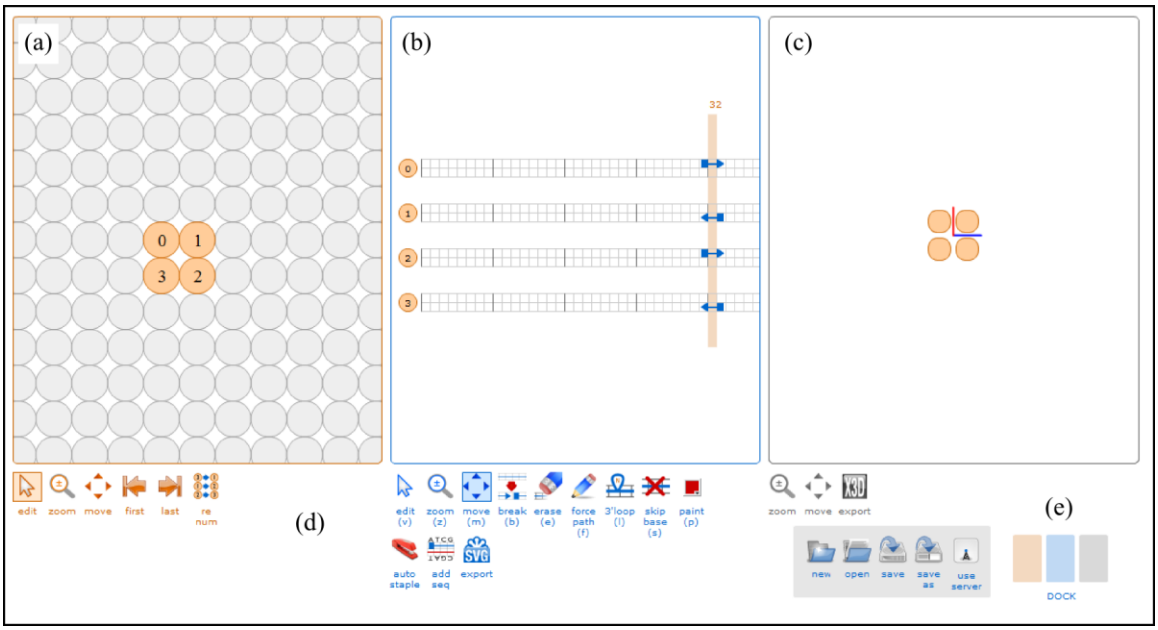

Figure A.1: Setting up the cross-sectional pattern. caDNAno SQ (square) was used to create the 4HB. Upon opening the software, three panels are visible: the slice panel (a), the path panel (b), and the 3D panel (c). Only the slice panel and the path panel are used during design. Each panel has toolbars (d), and a dock allows the user to hide/unhide panels (e). The desired cross-section is selected in the slice panel by left-mouse clicking. This populates the path panel with a two-dimensional, unrolled, side view of the structure. The blue arrows in (b) represent scaffold strands. Most design work in caDNAno occurs in the path panel. Clicking on the other two panels in the dock will hide them, providing more room in the path panel. The pattern used for this design is shown in (a).

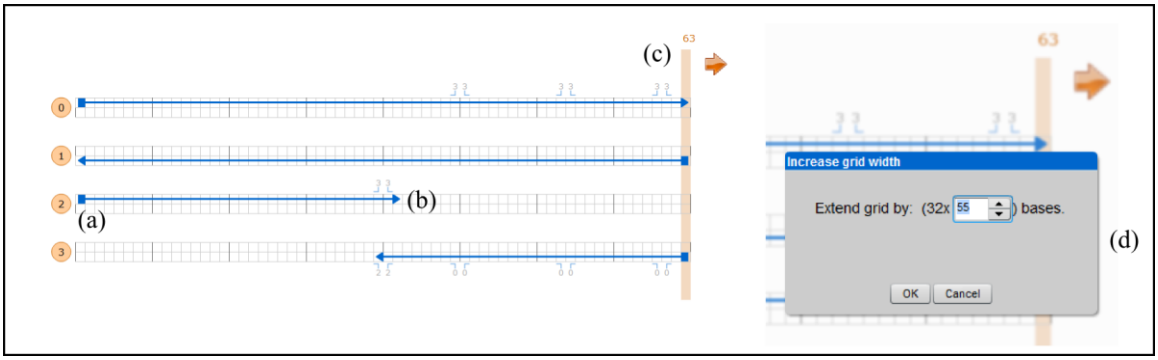

Figure A.2: Extending the scaffold into rough dimensions of the design space. On the scaffold strands, squares indicate 5'ends (a) while arrow points indicate 3' ends (b). The scaffold strands can be extended to fill all of the design space by using ALT+Click on the terminal ends. The vertical bar is called the slice bar. This relates the slice panel to the path panel and indicates the nucleotide number over which it is currently residing by the number above it (c). Numbering begins at far left with 0. If the slice bar is moved to either extreme end, an arrow appears. Clicking on the arrow brings up a dialog box to add more bases in groups of 32 (d). In this design, 55 extra sets of bases was needed to exceed the maximum length of the number of base pairs per helix of 1812.

64 bases + (32 bases)·55 = 1824 bases

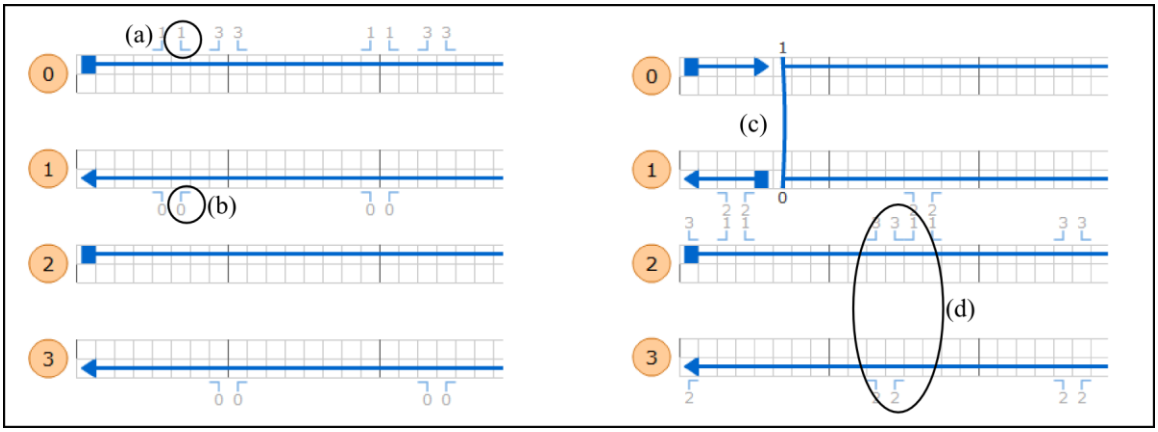

Figure A.3: Using allowed scaffold crossover points to close the left side of the structure. The 4HB was designed using a circular scaffold strand raster pattern, thus the individual scaffold strands needed to be connected into a circle in the software. By clicking on the scaffold strand in helix 0, numbers with tick marks appear. The numbers indicate which helices can be connected, and the direction of the horizontal section of the tick marks point to the side where an end loop will be formed if the crossover is made. For example, there are two number 1's located at (a). The number 1 means a crossover can be made from helix 0 to helix 1. The circled number at (a) indicates that a loop will form on the right side by crossing over to helix 1 at point (b). Left-mouse clicking on either the 1 at (a) or the 0 at (b) connects the two helices and forms the loop shown at (c) in the image on the right. caDNAno keeps track of the scaffold twist and indicates optimal locations where a crossover can occur based on twist angle. Helices 0 and 1 are linked, causing the crossover between helices 2 and 3 to be set back by 5 bases (d). It is possible to override this feature, but for this design it was decided to use the default program settings.

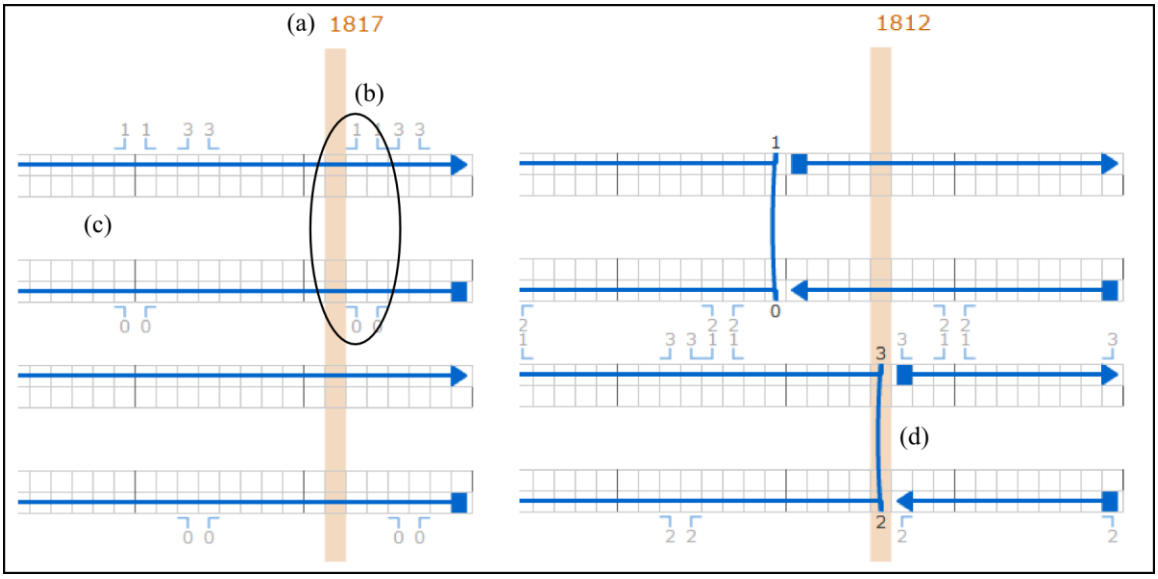

Figure A.4: Closing the right-hand side of the structure. The length of the structure was determined to contain a maximum of 1812 nucleotides per helix. As noted earlier, the slice bar shows the nucleotide over which it is currently laying starting at left with zero. After connecting the scaffold strands on the left side, helices 0 and 1 began at nucleotide 5 and helices 2 and 3 began at nucleotide 11. Using the provided scale of the slice bar, the maximum crossover point for helix 0 and helix 1would occur at nucleotide (1812 + 5) = 1817 (a). However, the closest allowed crossover point is one nucleotide too far to the right (b). Given the finite number of nucleotides in the m13mp18 scaffold strand, the previous allowed scaffold crossover located at 1807 (c) had to be used to avoid running out of nucleotides. To keep helices 2 and 3 close to the same length, the closest allowed crossover to the right of (c) was used at nucleotide 1812 (d). The result was helices 0 and 1 being 1802 nucleotides in length and helices 2 and 3 being 1801 nucleotides long and offset by 5 to 6 nucleotides to the right. Only 7206 nucleotides of the scaffold strand were used leaving 43 unhybridized nucleotides.

Part 2: Staple Strand Arrangement to Create the Binding Site Motif Using caDNAno

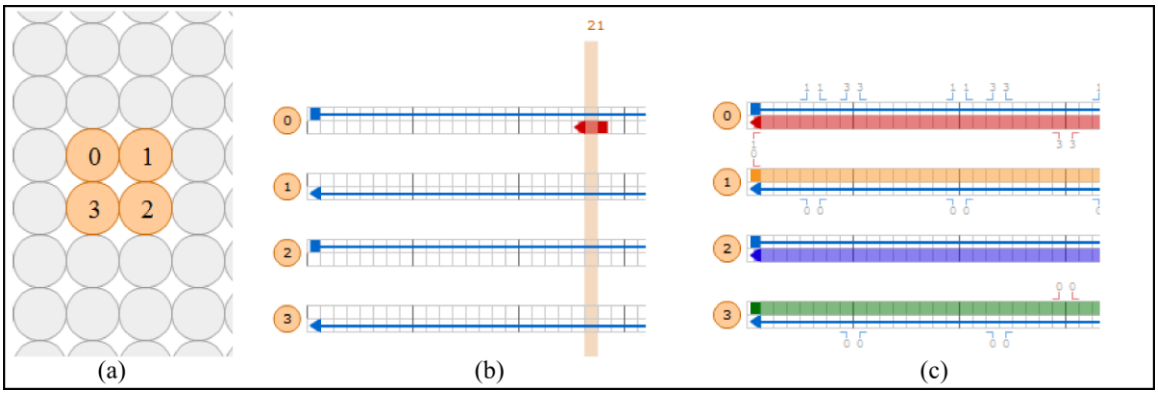

Figure A.5: Creating design space and adding staple strands. There are two ways to add staple strands to the scaffold: manual and automatic. Since the staple strand pattern must be strictly controlled to achieve the desired binding site motif, the manual technique is preferred. Select the cross-sectional pattern and extend the scaffold strands to provide ample work space—in this case, it would need to be greater than 192 nucleotides. Next, Shift+Click on each of the highlighted helices in the slice panel (a). This will create a 3 nucleotide staple strand centered on the current location of the slice bar (b). Using Alt+Click extends the staple strands the same way the scaffold strands were extended. The staple strands run antiparallel to the scaffold strands and can be different colors (c). caDNAno automatically assigns colors to staple strands, but this can be changed by the user using the *Paint* feature on the tool bar.

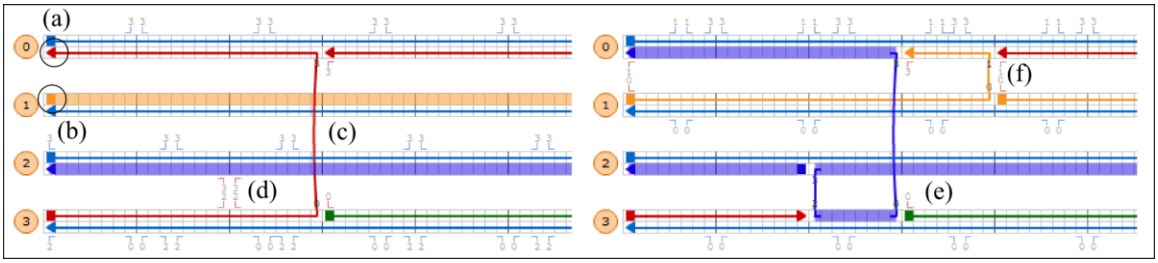

Figure A.6: Identify the biding site locations and adjust staple size to fit the pattern.

Right-hand spiral binding sites were to be 3' sticky ends while the left-hand spiral binding sites were to be 5'. The first 3' site (a) and 5' site (b) were chosen arbitrarily, allowing possible staple strand patterns to be designed around them. Choosing site (a) first, the goal was to create a staple strand with two crossovers (this involves three helices and is therefore referred to as a triple crossover) and a length of between 40-48 nucleotides. Clicking on a staple strand brings up a numbering system to identify allowed crossover locations similar to what was seen when the scaffold strand for a particular helix was selected. The numbers indicate to which helix the staple strand is allowed to cross over at a particular location. In Figure A.5 (c), the red staple on helix 0 shown has a '3' with a tick mark to the left and the green staple has a '0' with a tick mark to the left. Clicking on either of these numbers creates the crossover from helix 0 to helix 3 as shown above (c). This creates a staple strand that is of the target length (48 nucleotides), but it only has one crossover. A second crossover is possible at (d), which creates the long purple strand shown at right. A single crossover for the 5' binding site staple strand was created by the allowed crossover shown at (f). A second crossover could be created by crossing to helix 3 at (e). This is shown in Figure A7.

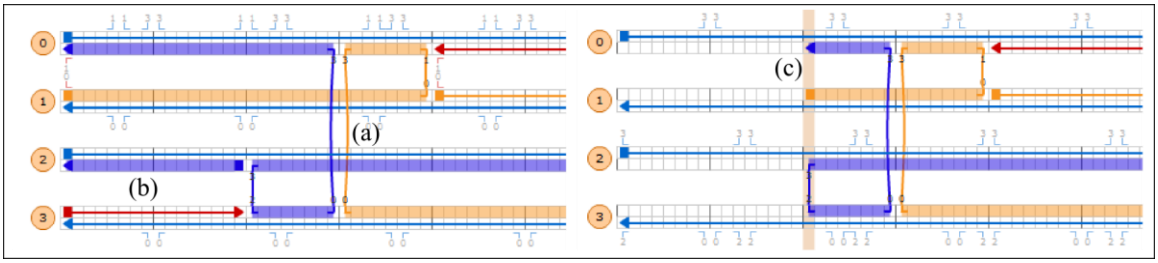

Figure A.7: Continue shaping the binding site staples. After the crossover from Figure A.6 (e) was made (a), the two binding site staple strands had two crossovers each. The two very short oligos on helices 2 and 3 are at a dead end since there is no scaffold further to the left (b). Deleting these and moving the binding sites 16 base pairs to the right created a blunt end that was more stable than if the two short oligos were joined with only one crossover (c). (Note: there appears to be some symmetry in these crossovers. Indeed, the raster pattern would be that of the symmetrical design if the purple strand and the orange strands were blunted on the right as well.)

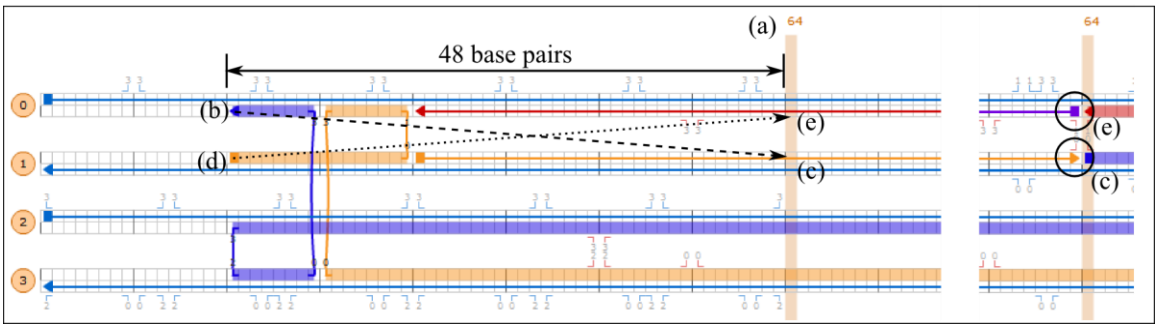

Figure A.8: Identify the next binding site and continue to shape the staples. It was determined during the conceptual design that the binding sites would be separated by 48 base pairs and one helix. The slice bar is used to locate the next binding site. The first two sites were 16 base pairs to the right of the end of the scaffold, thus the next binding sites would be at nucleotide 63 (a). The right-hand spiral requires the binding site to move from (b) to (c) whereas the left-hand helix moves in the opposite direction from (d) to (e). The *Break* tool from the tool bar is used to break the staples at these two locations providing the terminal end binding sites (circled at right).

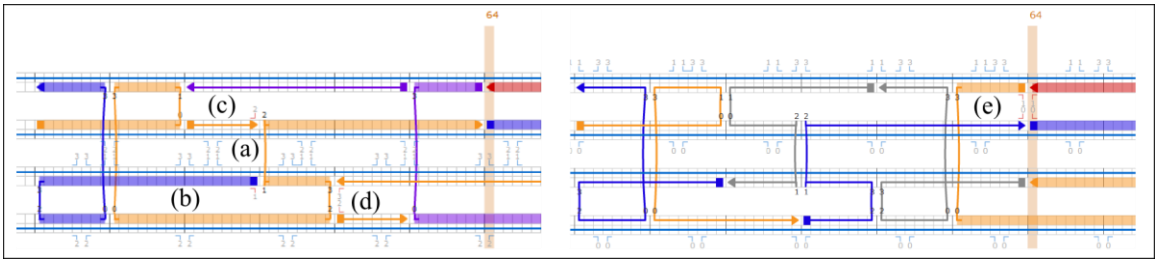

Figure A.9: Fine tuning the staple strand lengths. At this point, two binding sites for each chirality are known and the goal was to find the optimal staple strand pattern between the two locations. The long staples were not cut to size prior to this step to make it easier to see the interactions between the strands. Compare this figure with Figure A.8; when the crossover was made at (a), the blue binding site staple was cut close to proper size simultaneously (b). This also created undesirable short strands at (c) and (d). Single crossovers could be created at these locations to simply hold the structure together, but careful manipulation was able to give all of the staple strands two crossovers and lengths between 40 and 48 nucleotides (right). The 5' binding site staple strand (e) was not finalized in this step since its second crossover would be located in the next section of staples for binding site 3.

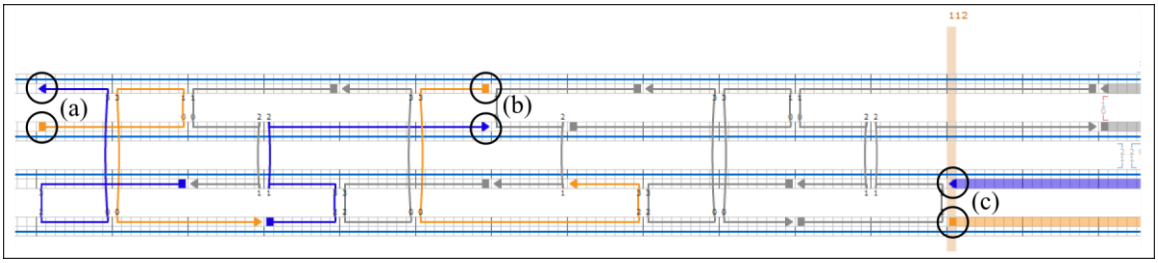

Figure A.10: Binding sites 1, 2 and 3. The process was repeated for binding site 3 and binding site 4. Shown here are binding sites 1 (a), 2 (b), and 3 (c) to illustrate their relationship to each other. Once all four binding sites were created the binding site motif was complete. This pattern was repeated until the scaffold strand structure created in Part 1 was filled. The final binding site motif was shown in Figure 5.5. End cap filler staples were added to the termini of the structure for rigidity as was shown in Figure 5.6.

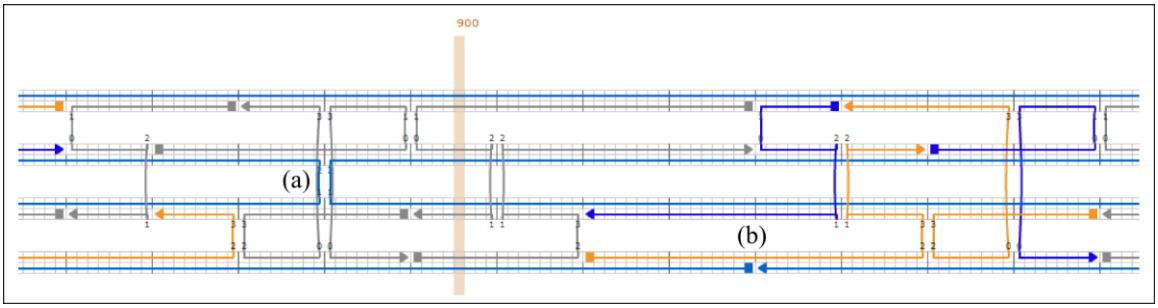

Figure A.11: Adding the internal scaffold crossover scaffold 'break.' The scaffold pattern set up in Part 1 was actually two continuous loops, one creating helices 0 and 1, and the other creating helices 2 and 3. Up until this point this did not affect the structure. Before the final step of adding the sequence of the m13mp18 strand and determining the sequences of the staple strands the scaffold must be linked together as it would be in reality using internal scaffold crossovers. For a four-helix bundle, only one internal scaffold crossover was used. It was desired to locate it near the center of the structure, but in a location where staple strands were available to bridge the seam. The final location chosen as nucleotide 888 (a), which was situated between the longest available staple strand lengths on helices 1 and 2. The scaffold 'break' is not a physical break but rather a way of indicating where the sequencing would start and end. caDNAno uses this point to begin laying out the sequence of the scaffold. In the real structure, all of the excess nucleotides not consumed in the design will end up at the break location. Thus, it was desired to locate it in a stable location towards the center of the structure with a long staple strand to stabilize the region. The break was located at nucleotide 928 (b).

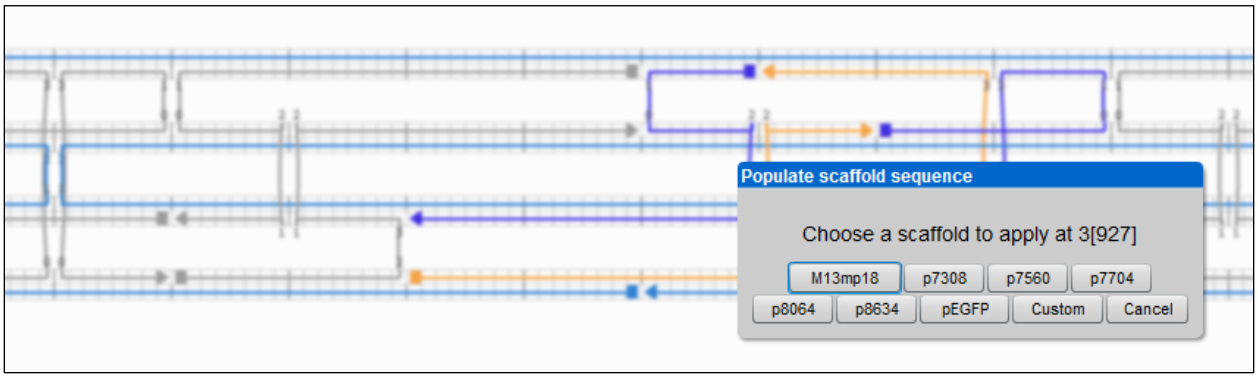

Figure A.12: Adding the sequence. The final step in the process adds the sequence to the scaffold to determine the staple strand sequences. On the tool bar the *add seq* tool is selected and the user clicks on the 5' end of the scaffold break. A dialogue box appears with several sequences. In this design, m13mp18 was chosen, however there are several preset sequences in caDNAno. There is also a *Custom* choice, which allows the user to add a sequence manually. Once a sequence is selected, a dialogue box appears with the option to copy to clip board. The output is then pasted into a spreadsheet program. The output from this design is shown below in Table A.1. Sticky ends were added to the proper staple strands manually in the spread sheet program. Sticky end sequences are listed below along with their complements:

SA: ACCAGTGCTCCTACG

cSA: CGTAGGAGCACTGGT

SB: TCTCTACCGCCTACG

cSB: CGTAGGCGGTAGAGA

SC: CCCTTCATGCTTCCC

cSC: GGGAAGCATGAAGGG

Table A.1: Output from caDNAno after sequence is added to a design. The 199 oligos for the four-helix bundle spiral nanoparticle array are shown. *Start* indicates the 5' end with helix number followed by the nucleotide number in brackets. *End* indicates the location of the 3' termini. Strands were color coded manually to allow easy sorting by type. In this design, orange was used for left-hand binding site staples and blue was used for right-hand binding site staples, gray indicated 'common' staple strands not used for anything but structure, and green was used for the end caps.

Note: Some sequences are shown with wrapped text due to length. These are not sections of dsDNA.

Start	End	Sequence	Length	Color
0[47]	2[32]	CTTTGACCCCCAGCGATTGTGTCGTTCCTGTA	32	#888888
0[79]	2[64]	AAAGAGGCAAAAGAATCTTAGCCGGGAACGCC	32	#888888
0[95]	2[104]	GCACCAACGTGTAGATGGGCGCATCGTAACCGCATTAAAT	40	#f7931e
0[111]	2[96]	TAATGCCACTACGAAGTAAGGGAATTTTGTTA	32	#888888
0[159]	2[128]	ACTAAAGACTTTTTCATGAGGAAGTTTCCATTGACAGATGACGTTAAT	48	#888888
0[167]	2[144]	CTTTGAGGGGCTGGCTGAAGATTGTATAAGCAAATATTTA	40	#1700de
0[207]	2[192]	AAAGACAGCATCGGAACAAGAACCCCGGTTGA	32	#888888
0[239]	2[224]	CCGCTTTTGCGGGATCTAACAAAGATCGTAAA	32	#888888
0[271]	2[256]	TTCGGTCGCTGAGGCTGCCCTGACTCTGGAGC	32	#888888
0[287]	2[296]	ACGCATAACGCCAGCTGGCGAAAGGGGGATGTTTGAGAGA	40	#f7931e
0[303]	2[288]	ACAACAACCATCGCCCATTGGGCTTCTACAAA	32	#888888
0[351]	2[320]	GAGGTGAATTTCTTAAACAGCTTGATACCGATATCATTGTTAATGCCG	48	#888888
0[359]	2[336]	TTGCTTTCACTGGCTCAATATGATATTCAACCGTTCTAGC	40	#1700de
0[399]	2[384]	AGGCTCCAAAAGGAGCAGAAAAATTGAGAAAG	32	#888888
0[431]	2[416]	TAATTTTTTCACGTTGGAACAACACTGAGTAA	32	#888888
0[463]	2[448]	TAGAAAGGAACAACTAAGTTGAGATTTAGAAC	32	#888888
0[479]	2[488]	TTCAGCGGTCCGCTCACAATTCCACACAACATTTGCGGGA	40	#f7931e
0[495]	2[480]	AACAACTTTCAACAGTTGCAGATAGAAGCCTT	32	#888888
0[543]	2[512]	CGTCTTTCCAGACGTTAGTAAATGAATTTTCTGCATAGTAAAACATTA	48	#888888

0[551]	2[528]	AGTTTTGTTTTACCAGCTCAGAGCATAAAGCTAAATCGGT	40	#1700de
0[591]	2[576]	CATTCCACAGACAGCCAGAGGCTTGGCAAAGA	32	#888888
0[623]	2[608]	TTCGTCACCAGTACAAGGGTAATATAGCATTA	32	#888888
0[655]	2[640]	CCAATAGGAACCCATGTCCAATACTGAAAAGG	32	#888888
0[671]	2[680]	TTCAGGGAGGGTGGTTTTTCTTTTCACCAGTGCAATAACC	40	#f7931e
0[687]	2[672]	AGCCACCACCCTCATTTGAATCCCTGTTTAGC	32	#888888
0[735]	2[704]	TAGTACCGCCACCCTCAGAACCGCCACCCTCAAAAACGAGCATTAGAT	48	#888888
0[743]	2[720]	AGGAGGTTTCTTTACCCCAATTCTGCGAACGAGTAGATTT	40	#1700de
0[783]	2[768]	TGATATAAGTATAGCCGCGGATTGCTGGAAGT	32	#888888
0[815]	2[800]	AGTACCAGGCGGATAACGAAAGACCATGTTTT	32	#888888
0[847]	2[832]	AGAGAAGGATTAGGATGCTTCAAAGCTTAATT	32	#888888
0[863]	2[872]	AGGCTGAGTCCAGTTTGGAACAAGAGTCCACTGCTCCTTT	40	#f7931e
0[879]	2[864]	ACATGAAAGTATTAAGCAACAGGTTGATAAGA	32	#888888
0[927]	2[896]	TATAAACAGTTAATGCCCCCTGCCTATTTCGGTGTGATAATTTAATGG	48	#888888
0[935]	2[912]	AGTGCCCGACCGGAATATATTTTAGTTAATTTCATCTTCT	40	#1700de
0[975]	2[960]	ACTGGTAATAAGTTTTTAGTATCAAAGACAAA	32	#888888
0[1007]	2[992]	GTCATACATGGCTTTTGTATAAAGCTATATGT	32	#888888
0[1039]	2[1024]	GCGCAGTCTCTGAATTTTGAGAATTTTTAACC	32	#888888
0[1055]	2[1064]	AAAGCCAGAGCGGGCGCTAGGGCGCTGGCAAGATAGTGAA	40	#f7931e
0[1071]	2[1056]	CAAATAAATCCTCATTGTAATTTATTTATCAA	32	#888888
0[1119]	2[1088]	TGACAGGAGGTTGAGGCAGGTCAGACGATTGGATAAGAGAAGATTAAG	48	#888888
0[1127]	2[1104]	GCCAGCATAGTAATTCCCTTAGAATCCTTGAAAACATAGC	40	#1700de
0[1167]	2[1152]	CACCCTCAGAGCCGCCCATGTTCACTTCTGTA	32	#888888
0[1199]	2[1184]	GCCACCCTCAGAACCGTCAACAATCATAAATC	32	#888888
0[1231]	2[1216]	GAGCCACCACCGGAACAATATCCCCATTTGAA	32	#888888
0[1247]	2[1256]	AAAATCACCGCCAGAATCCTGAGAAGTGTTTTCAAACATC	40	#f7931e
0[1263]	2[1248]	CCATCTTTTCATAATCACCAATCAAAGAAAAC	32	#888888
0[1311]	2[1280]	GCGCGTTTTCATCGGCATTTTCGGTCATAGCCTTCCAAGACCTGAGCA	48	#888888
0[1319]	2[1296]	AGACTGTACTCATCGAATCGCGCAGAGGCGAATTATTCAT	40	#1700de
0[1359]	2[1344]	CGTAATCAGTAGCGACCATCGTAGTCGCCTGA	32	#888888
0[1391]	2[1376]	AACGTCACCAATGAAAAGCAAATCTACCTTTT	32	#888888
0[1423]	2[1408]	CCAGTAGCACCATTACTCTAAGAAAGGTTTAA	32	#888888
0[1439]	2[1448]	AGAGCCAGGAAAAACGCTCATGGAAATACCTATTGCACGT	40	#f7931e

0[1455]	2[1440]	GAGCCATTTGGGAATTCGACTTGCAAAACAGA	32	#888888
0[1503]	2[1472]	ATTGACGGAAATTATTCATTAAAGGTGAATTAAGATTAGTTAGAACCT	48	#888888
0[1511]	2[1488]	AGGTAAATTTTATCCTGTTTGGATTATACTTCTGAATAAT	40	#1700de
0[1551]	2[1536]	CAAAGACAAAAGGGCGTCTTTCCAGATGATGG	32	#888888
0[1583]	2[1568]	ATCAATAGAAAATTCATAAACAGCGAGCGGAA	32	#888888
0[1615]	2[1600]	AAGACACCACGGAATAAAGAAACGATCATTTT	32	#888888
0[1631]	2[1640]	ATATAAAAATGCGCGAACTGATAGCCCTAAAATTGCCCGA	40	#f7931e
0[1647]	2[1632]	ACATAAAGGTGGCAACAAAATAGCACGTTATT	32	#888888
0[1695]	2[1664]	ATTAAGACTCCTTATTACGCAGTATGTTAGCAAAAACAGGATTCGACA	48	#888888
0[1703]	2[1680]	CTGGCATGACTGAACATGAGGATTTAGAAGTATTAGACTT	40	#1700de
0[1743]	2[1728]	AAACCGAGGAAACGCATGAGCGCTAATAGATT	32	#888888
0[1775]	2[1760]	TAAGCAGATAGCCGAAAATTGAGTTATCTAAA	32	#888888
0[1807]	2[1792]	AGCTATCTTACCGAAGACAATGAACAAATCAA	32	#007200
1[5]	3[31]	CGGAGATTTGTATCATCGCCTGATAAATTATACCAACAACCCG	43	#57bb00
1[48]	3[71]	GACCTGCTCCATGTTAACACTAAAGCGGATTGACCGTAAT	40	#f7931e
1[104]	3[127]	CCGAACTGACCAACTTTGAAAGAGAAACGGGTCCAGTTTG	40	#888888
1[176]	3[191]	TCAAGAGTAATCTTGACGAGGGTAACCGCTTC	32	#1700de
1[208]	3[223]	ATTACCCAAATCAACGGTCACCCTCCATTCGC	32	#888888
1[240]	3[263]	TCAGTGAATAAGGCTTTGCAGGGAAAGGGCGATCGGTGCG	40	#f7931e
1[296]	3[319]	TGAGATGGTTTAATTTCAACTTTAAGTTGCGCGCGATTAA	40	#888888
1[368]	3[383]	AGTCAGGACGTTGGGACTTTAATTAAGCTTGC	32	#1700de
1[400]	3[415]	ATAAAACGAACTAACGAAAATCTCATCCCCGG	32	#888888
1[432]	3[455]	GGTAGAAAGATTCATCAAGGAATTTGGTCATAGCTGTTTC	40	#f7931e
1[488]	3[511]	CATAACGCCAAAAGGAATTACGAGGTATGGGAGAAGCATA	40	#888888
1[560]	3[575]	AAAAACCAAAATAGCGCTCATAGTCTCACTGC	32	#1700de
1[592]	3[607]	GAAGTTTTGCCAGAGGACTACAACCGTGCCAG	32	#888888
1[624]	3[647]	TTTAGACTGGATAGCGTACCGTAAGCGGGGAGAGGCGGTT	40	#f7931e
1[680]	3[703]	CCTCAAATGCTTTAAACAGTTCAGGAACCGCCAACAGCTG	40	#888888
1[752]	3[767]	TATAGTCAGAAGCAAACGGAATAGGCCCCAGC	32	#1700de
1[784]	3[799]	AGATTAAGAGGAAGCCGTGCCGTCGTTCCGAA	32	#888888
1[816]	3[839]	TCGCGTTTTAATTCGATAGCGGGGAAAGAATAGCCCGAGA	40	#f7931e

1[872]	3[895]	CAGGATTAGAGAGTACACCGACCGAACCTATTACG TGGAC	40	#888888
1[944]	3[959]	CTAGAAAAAGCCTGTTAACGGGGTAGCACTAA	32	#1700de
1[976]	3[991]	ATACAAATTCTTACCAGATGATACGATTTAGA	32	#888888
1[1008]	3[1031]	CAACAGTAGGGCTTAATACCGTTCGTGGCGAGAAA GGAAG	40	#f7931e
1[1064]	3[1087]	GGCAGAGGCATTTTCGAGCCAGTACCTTGATATCAC GCTG	40	#888888
1[1136]	3[1151]	CGACGACAATAAACAAACCAGAACTTGCTTTG	32	#1700de
1[1168]	3[1183]	AGAACGCGCCTGTTTACCACCCTCTCGTTAGA	32	#888888
1[1200]	3[1223]	CCTGAACAAGAAAAATCGCCTCCCGCCGATTAAAG GGATT	40	#f7931e
1[1256]	3[1279]	ATAATCGGCTGTCTTTCCTTATCACCCTTATTGTGAG GCC	40	#888888
1[1328]	3[1343]	AAGCCGTTTTTATTTTAGAATCAAGATTAGTA	32	#1700de
1[1360]	3[1375]	ACCGCGCCCAATAGCACCATCGATGAACTCAA	32	#888888
1[1392]	3[1415]	AAGGCTTATCCGGTATCATTAGCACAGAACAATATT ACCG	40	#f7931e
1[1448]	3[1471]	GGGAGGTTTTGAAGCCTTAAATCATCACCGTCCGCT CAAT	40	#888888
1[1520]	3[1535]	CCAACGCTAACGAGCGACATTCAAAAGGGACA	32	#1700de
1[1552]	3[1567]	TTTGCCAGTTACAAAATATGGTTTTTCTGACC	32	#888888
1[1584]	3[1607]	TTATCCCAATCCAAATAGTTTATTAGACAATATTTTT GAA	40	#f7931e
1[1640]	3[1663]	AGCCTTTACAGAGAGAATAACATAAACGTAGATTA AAAAT	40	#888888
1[1712]	3[1727]	AAAGTCAGAGGGTAATATAATAACCGCCTGCA	32	#1700de
1[1744]	3[1759]	AGAGATAACCCACAAGCAAAGTTAGCAAATGA	32	#888888
1[1776]	3[1791]	ATAATAAGAGCAAGAACCCTTTTTAACCTCAA	32	#f7931e
2[31]	2[11]	GCCAGCTTTCATCAACATTAA	21	#57bb00
2[63]	0[48]	ATCAAAAATAATTCGCAACAAACGACACTCAT	32	#1700de
2[95]	0[80]	AATCAGCTCATTTTTTTCACGTTGCTAAAACG	32	#888888
2[127]	0[112]	ATTTTGTTAAAATTCGTGCATCTGAAAATACG	32	#888888
2[191]	0[168]	TAATCAGAAAAGCCCCTTTCCGGCGCAACGGCTACA GAGG	40	#f7931e
2[223]	0[208]	ACTAGCATGTCAATCAGCAAAGCGCAGCAGCG	32	#888888
2[255]	0[240]	AAACAAGAGAATCGATCTGTTGGGGTTAAAGG	32	#1700de
2[287]	0[272]	GGCTATCAGGTCATTGCGCTATTACCGATATA	32	#888888
2[319]	0[304]	GAGAGGGTAGCTATTTGCTGCAAGCGACAATG	32	#888888
2[383]	0[360]	GCCGGAGACAGTCAAACCAGTGCCGTATCGGTTTAT CAGC	40	#f7931e
2[415]	0[400]	TGTGTAGGTAAAGATTTCTAGAGGCAAAAAAA	32	#888888
2[447]	0[432]	CCTCATATATTTTAAACGTAATCAGCGAATAA	32	#1700de
2[479]	0[464]	TATTTCAACGCAAGGAAATTGTTAAGTGAGAA	32	#888888
2[511]	0[496]	TGACCCTGTAATACTTACGAGCCGTTTTGCTA	32	#888888

2[575]	0[552]	ATTAGCAAAATTAAGCGCGTTGCGTAGCGTAACGATCTAA	40	#f7931e
2[607]	0[592]	ACATCCAATAAATCATAAACCTGTGCCTGTAG	32	#888888
2[639]	0[624]	TGGCATCAATTCTACTGCCAACGCCACTGAGT	32	#1700de
2[671]	0[656]	TATATTTTCATTTGGGGGGCGCCATAGCAAGC	32	#888888
2[703]	0[688]	ACATTTCGCAAATGGTAGACGGGCACCCTCAG	32	#888888
2[767]	0[744]	TTCATTCCATATAACAGCTGGTTTGTGTATCACCGTACTC	40	#f7931e
2[799]	0[784]	AAATATGCAACTAAAGTGATGGTGGAGAGGGT	32	#888888
2[831]	0[816]	GCTGAATATAATGCTGATAAATCATTTTGCTC	32	#1700de
2[863]	0[848]	GGTCATTTTTGCGGATAGTGTTGTACTCCTCA	32	#888888
2[895]	0[880]	TTTGAAATCTTTAATTATTAAAGAATTCTGAA	32	#888888
2[959]	0[936]	GAACGCGAGAAAACTTTGCCGTAACAGTGCCTTGAGTAAC	40	#f7931e
2[991]	0[976]	AAATGCTGATGCAAATGAGCCCCCAGGAGTGT	32	#888888
2[1023]	0[1008]	TCCGGCTTAGGTTGGGCGGCGAACCAGTAAGC	32	#1700de
2[1055]	0[1040]	AATCATAGGTCTGAGAGCGAAAGGAATGGAAA	32	#888888
2[1087]	0[1072]	ACGCTGAGAAGAGTCATGTAGCGGTTCACAAA	32	#888888
2[1151]	0[1128]	AATCGTCGCTATTAATTACTATGGCACCACCAGAGCCGCC	40	#f7931e
2[1183]	0[1168]	AATATATGTGAGTGAATGCTTTCCAGAGCCAC	32	#888888
2[1215]	0[1200]	TTACCTTTTTTAATGGAACAGGAGTCAGAGCC	32	#1700de
2[1247]	0[1232]	AAAATTAATTACATTTGAACGGTACGGAACCA	32	#888888
2[1279]	0[1264]	AAAGAAGATGATGAAATATAATCAAGCGTTTG	32	#888888
2[1343]	0[1320]	TTGCTTTGAATACCAAACTTCTTTGTTTGCCTTTAGCGTC	40	#f7931e
2[1375]	0[1360]	ACATCGGGAGAAACAAGAGTAGAAAGCAGCAC	32	#888888
2[1407]	0[1392]	CGTCAGATGAATATACGTAATATCAGGCCGGA	32	#1700de
2[1439]	0[1424]	AATAAAGAAATTGCGTTGCAACAGCAAAATCA	32	#888888
2[1471]	0[1456]	ACCATATCAAAATTATCATTTTGAACCGACTT	32	#888888
2[1535]	0[1512]	CAATTCATCAATATAAAGTAATAACCGATTGAGGGAGGGA	40	#f7931e
2[1567]	0[1552]	TTATCATCATATTCCTTAGAACCCACCAGCGC	32	#888888
2[1599]	0[1584]	GCGGAACAAAGAAACCCGTGGCACTTGTCACA	32	#1700de
2[1631]	0[1616]	AATTTTAAAAGTTTGAAGTCTTTAGAAACGCA	32	#888888
2[1663]	0[1648]	ACTCGTATTAAATCCTCATCGCCAAAATACAT	32	#888888
2[1727]	0[1704]	AGAGCCGTCAATAGATATTAACACGGAATACCCAAAAGAA	40	#f7931e
2[1759]	0[1744]	ATATCTTTAGGAGCACAGCCAGCACCAGAAGG	32	#888888
2[1791]	0[1776]	CAGTTGAAAGGAATTGCCTTGCTGAAGAAAAG	32	#1700de
2[1812]	1[1807]	TCTGGTCAGTTGGATAGCAAT	21	#007200
3[11]	0[5]	ATGTGAGCGAGTAAGCGCGAAACAAAGTACAA	32	#57bb00
3[32]	1[47]	TCGGATTCTCCGTGGGGTCTGGCCAAATCCGC	32	#888888
3[72]	1[95]	GGGATAGGAACCAATAGAACGAGGCGCAGACGGTCAATCA	40	#1700de

3[128]	1[159]	AGGGGACGACGACAGTAATTGTAAAACGGTGTACA GACCAGGCGCATA	48	#888888
3[144]	1[175]	ATCGGCCTCAGGAAGATCGCACTCCAGCCAGCAAA AACAGGACCTTCA	48	#f7931e
3[192]	1[207]	TGGTGCCGGAAACCAGTATGTACCGGATATTC	32	#888888
3[224]	1[239]	CATTCAGGCTGCGCAAGAACGGTACTGCTCAT	32	#888888
3[264]	1[287]	GGCCTCTTCCTGAGAGGAGAAACACCAGAACGAGT AGTAA	40	#1700de
3[320]	1[351]	GTTGGGTAACGCCAGGTGATAAATGAATTACCTTAT GCGATTTTAAGA	48	#888888
3[336]	1[367]	GTTTTCCCAGTCACGACGTTGTAAAACGACGGTCAC CATCATTATACC	48	#f7931e
3[384]	1[399]	ATGCCTGCAGGTCGACCAAAAGGGCTACGTTA	32	#888888
3[416]	1[431]	GTACCGAGCTCGAATTTGCAATGCTTATTACA	32	#888888
3[456]	1[479]	CTGTGTGATAAAAATTTTTAGGAATACCACATTCAA CTAA	40	#1700de
3[512]	1[543]	AAGTGTAAAGCCTGGGTGTACCAAAGAGCAACACT ATCATAACCCTCG	48	#888888
3[528]	1[559]	GTGCCTAATGAGTGAGCTAACTCACATTAATTAATA AAGCACGACGAT	48	#f7931e
3[576]	1[591]	CCGCTTTCCAGTCGGGACAGGCAATTGCAAAA	32	#888888
3[608]	1[623]	CTGCATTAATGAATCGAATAGTAGGTAAAATG	32	#888888
3[648]	1[671]	TGCGTATTGCGCGAGCTGCGGAATCGTCATAAATAT TCAT	40	#1700de
3[704]	1[735]	ATTGCCCTTCACCGCCAGTTTGACAATGACCATAAA TCAAAAATCAGG	48	#888888
3[720]	1[751]	TGGCCCTGAGAGAGTTGCAGCAAGCGGTCCACGTT GATTCCTGACTAT	48	#f7931e
3[768]	1[783]	AGGCGAAAATCCTGTTTACGGTGTCATCAAAA	32	#888888
3[800]	1[815]	ATCGGCAAAATCCCTTTAGCTCAATTCAAATA	32	#888888
3[840]	1[863]	TAGGGTTGGGCTTAGAGCGAACCAGACCGGAAGCA AACTC	40	#1700de
3[896]	1[927]	TCCAACGTCAAAGGGCGACCTAAAATAAGGCGTTA AATAAGAATAAAC	48	#888888
3[912]	1[943]	GAAAAACCGTCTATCATTTTTTGGGGTCGAGGTTTC AAATCATAATTA	48	#f7931e
3[960]	1[975]	ATCGGAACCCTAAAGGCCAATCGCTATGCGTT	32	#888888
3[992]	1[1007]	GCTTGACGGGGAAAGCTTATATAACCAACGCT	32	#888888
3[1032]	1[1055]	GGAAGAAAGACTACCTCGCCATATTTAACAACGCC AACAT	40	#1700de
3[1088]	1[1119]	CGCGTAACCACCACACGATAGCTTATATAAAGTACC GACAAAAGGTAA	48	#888888
3[1104]	1[1135]	CCGCCGCGCTTAATGCGCCGCTACAGGGCGCGTAAT TTTCTGTCCAGA	48	#f7931e
3[1152]	1[1167]	ACGAGCACGTATAACGTAACCTTGGCTAATGC	32	#888888
3[1184]	1[1199]	ATCAGAGCGGGAGCTAAAACAGTAAGATAAGT	32	#888888

3[1224]	1[1247]	TTAGACAGAACAATTTATCCTAATTTACGAGCATGT AGAA	40	#1700de
3[1280]	1[1311]	ACCGAGTAAAAGAGTCTTCAATTAACGGGTATTAA ACCAAGTACCGCA	48	#888888
3[1296]	1[1327]	TGTCCATCACGCAAATTAACCGTTGTAGCAATGTTA CAAAGAACAAGC	48	#f7931e
3[1344]	1[1359]	ATAACATCACTTGCCTTAACGGATGAATCATT	32	#888888
3[1376]	1[1391]	ACTATCGGCCTTGCTGAGTAACAGAGATATAG	32	#888888
3[1416]	1[1439]	CCAGCCATAGATTTTCCGCGAGGCGTTTTAGCGAAC CTCC	40	#1700de
3[1472]	1[1503]	CGTCTGAAATGGATTAGGAAGGGTTGCTATTTTGCA CCCAGCTACAAT	48	#888888
3[1488]	1[1519]	TTTACATTGGCAGATTCACCAGTCACACGACCTCCT GATTGAATCTTA	48	#f7931e
3[1536]	1[1551]	TTCTGGCCAACAGAGAGATTATCAGAGCCTAA	32	#888888
3[1568]	1[1583]	TGAAAGCGTAAGAATAACCAGAAGCATATTAT	32	#888888
3[1608]	1[1631]	TGGCTATTGTAACATTATTTTTTGTTTAACGTCAAAA ATG	40	#1700de
3[1664]	1[1695]	ACCGAACGAACCACCATACAAACAGAAGCGCATTA GACGGGAGAATTA	48	#888888
3[1680]	1[1711]	GCAGAAGATAAAACAGAGGTGAGGCGGTCAGTAAT ACATTCCCTGAAC	48	#f7931e
3[1728]	1[1743]	ACAGTGCCACGCTGAGTAACAACTAATATCAG	32	#888888
3[1760]	1[1775]	AAAATCTAAAGCATCAAGGAAGGTTAAGCCCA	32	#888888
3[1792]	3[1812]	ATATCAAACCCTCAATCAATA	21	#007200

APPENDIX B

Example Procedure for Preparation of DNA conjugated Gold Nanoparticles

Five Nanometer DNA Conjugated (3'cSB, 5'cSA) Gold Nanoparticle (AuNP) Samples as Prepared by Nathan Robinson, Department of Chemistry, Boise State University

A.1: Laboratory Supplies and Equipment

Reagents:

1. $HAuCl_4 \cdot 3H_2O$ (tetrachloroauric acid)*
2. $HOC(COONa)(CH_2COONa)_2 \cdot 2H_2O$ (trisodium citrate trihydrate)*
3. $NaBH_4$ (sodium borohydride)*
4. $NaH_2PO_4 \cdot H_2O$ (monosodium phosphate)*
5. $Na_2HPO_4 \cdot 7H_2O$ (disodium hydrogen phosphate heptahydrate)*
6. $CH_3(CH_2)_{11}OSO_3Na$ (sodium dodecyl sulfate, SDS)*
7. $HSCH_2CH(OH)CH(OH)CH_2SH$ (DL-dithiothreitol, DTT)*
8. NaCl (sodium chloride)**

*Sigma-Aldrich (www.sigmaaldrich.com)
**Fisher Scientific (www.fishersci.com)

Single stranded DNA oligonucleotides were purchased from Integrated DNA

Technologies (www.idtdna.com) with a dithiol modification

GE Healthcare illustra™ NAP™-10 columns were purchased from GE Healthcare

(www.gehealthcare.com)

All water used during experimentation was 18.2 MΩ

Instrumentation:

1. Thermo Scientific Barnstead NANOpure® Diamond™ water purifier
2. Beckman TL-100 ultracentrifuge
3. Varian Cary® 100 UV/Vis.

A2: Procedure

Preparation of Colloidal Gold:

1. Colloidal gold was prepared in an Erlenmeyer flask (1 L), by dissolving $HAuCl_4$ (99.6 mg, 0.250 mmol) and trisodium citrate (74.8 mg, 0.250 mmol) in water (1 L).
    a. The chloroauric acid was chilled over ice, and vigorously stirred.
2. Into a vial, $NaBH_4$ (11.4 mg, 3 mmol) was dissolved in water (30 mL), and then chilled over ice.
3. Upon reaching ice-cold temperatures, the $NaBH_4$ solution was rapidly injected into the chloroauric acid solution, resulting in a rust-red colored solution, which was then continually stirred over ice (20 min).
4. The colloidal gold solution was placed into a plastic storage container, and incubated (2 h, 4 °C) to remove any excess hydride.

5. The concentration of colloidal gold solution was measured (62 nM) using UV-Vis. The absorption at 509 nm was measured and the concentration was calculated using Beer's law (extinction coefficient = 1.1×10^7, path length = 1 cm).

DNA Surface Functionalization

1. The preparation of 5'cSA-AuNP, and 3'cSB-AuNP was done in two batches of each oligonucleotide strand.
2. 5'cSA was prepared by placing the diluted strand (550 µL, ~60 nmol) into each of two micro-centrifuge tubes (1.5 mL) with DTT (150 µL, 15 µmol).
3. 3'cSB was prepared by placing the diluted strand (660 µL, ~75 nmol) into each of two micro-centrifuge tubes (1.5 mL) with DTT (175 µL, 17.5 µmol).
4. The samples were incubated (90 min, 22 °C) and then purified using a NAP-10 desalting column.
    a. The de-salting columns were prepared by eluting with water (15 mL)
    b. Upon sample insertion, 15 drops were drained, uncollected
    c. The next 15 fractions, (~200 µL, 5 drops) were collected in micro-centrifuge tubes (1.5 mL).
    d. The fractional DNA solutions were then quantized by measuring the absorbance at 260 nm using UV absorption spectroscopy, and the fractions containing DNA were combined.
5. Each DNA strand was then combined with AuNP in 50:1 DNA:AuNP ratio and incubated (24 h, 22ºC) in the dark
    a. Batch #1
        i. 5'cSA (1.58 mL, 45.7 nmol):AuNP (14.8 mL, 914 pmol)
        ii. 3'cSB (1.56 mL, 78.9 nmol):AuNP (25.5 mL, 1.58 nmol)
    b. Batch #2
        i. 5'cSA (1.47 mL, 42.7 nmol):AuNP (13.8 mL, 854 pmol)
        ii. 3'cSB (1.60 mL, 73.1 nmol):AuNP (23.6 mL, 1.46 nmol)
1. Following incubation:
    a. DNA conjugated AuNP solutions were adjusted to:
        i. pH 7.4
        ii. 100 mM phosphate buffer concentration
        iii. 0.01 % SDS (wt/wt) concentration
        iv. 300 mM NaCl concentration (Step iv. in four increments over 2 h).
2. Samples were then purified via centrifugation (3X, 50k RPM, 15 min) and re-suspended in solution of pH 7.4, 100 mM phosphate buffer, 0.01 % SDS (wt/wt), and 300 mM NaCl.
3. Sample concentration
    a. Batch #1
        i. 5'cSA (495 nM)
        ii. 3'cSB (785 nM)
    b. Batch #2
        i. 5'cSA (568 nM)
        ii. 3'cSB (718 nM)